# INVESTIGATION OF FLOW AROUND SIMPLE BODIES IN HYPERSONIC FLOW

Thesis by

Toshi Kubota

In Partial Fulfillment of the Requirements

For the Degree of

Doctor of Philosophy

California Institute of Technology

Pasadena, California

1957

## ACKNOWLEDGMENTS

The author wishes to express deep appreciation to Professor Lester Lees for his guidance throughout the investigation. He would like to thank the members of the Aeronautics machine shop for constructing various pieces of equipment; the staff of the Hypersonic group for their assistance in the course of experiment; Mrs. Charlotte Willmarth and Mrs. Nell Kindig for their assistance with the computation and preparation of graphs; and Mrs. Geraldine Van Gieson for typing the manuscript. The author should also like to acknowledge the assistance given by Dr. John Christopher of ElectroData Corporation with the numerical integration of the differential equations.

## ABSTRACT

A theoretical analysis of the flow around slender blunt-nosed bodies was made by applying the flow similarity concept to the hypersonic small-disturbance equations. The flow field around a class of bodies of the form $r_b \sim x^m$ exhibits a certain similarity in the sense that the pressure, density and transverse velocity are described by relations of the form $Q(x, r)/Q(R) = f(r/R)$, where R is the distance from the axis to the shock wave. This similarity holds when the Mach number is infinitely large, and when the exponent in the equation defining the body shape lies in the range $\frac{1}{2} < m \leqq 1$ for axially-symmetric bodies and in the range $2/3 < m \leqq 1$ for two-dimensional bodies. For large but finite Mach numbers a second approximation was obtained by expanding solutions in series of powers of $x^{2(1-m)}/M_\infty{}^2 \delta^2$.

An experimental investigation of the flow around "similar-flow" bodies of revolution was conducted at Mach number 7.7 in the GALCIT hypersonic wind tunnel. The surface pressure distributions agreed closely with the theoretical predictions, after a simplified correction was made for the boundary-layer displacement effect. The results indicated that the boundary layer interaction effect needs a further investigation.

TABLE OF CONTENTS

## LIST OF FIGURES

# LIST OF SYMBOLS

| | |
|---|---|
| $a$ | speed of sound |
| $a_1$ | coefficient in expression for shock shape |
| $c_v$ | specific heat at constant volume |
| $C_D$ | drag coefficient, $D/\left[\frac{1}{2}\rho_\infty u_\infty^2 (\pi/4)^k d^{1+k}\right]$ |
| $C_p$ | pressure coefficient, $(p - p_\infty)/(\frac{1}{2}\rho_\infty u_\infty^2)$ |
| $d$ | diameter, or thickness |
| $D$ | drag |
| $E$ | energy |
| $f, F, f_1$ | function of z appearing in expression for pressure |
| $k$ | geometric index, 0 for two-dimensional flow<br>1 for axially-symmetric flow |
| $L$ | body length |
| $m$ | exponent, $r_b \sim x^m$ |
| $M$ | Mach number |
| $p$ | pressure |
| $Q$ | any physical quantity |
| $r$ | distance normal to body axis or chord line (x- axis) |
| $R$ | distance of shock wave from x- axis |
| $Re_L$ | Reynolds number, $\rho_\infty u_\infty L/\mu_\infty$ |
| $s$ | distance along body surface measured from forward stagnation point |
| $\tilde{s}$ | distorted distance $= \int_0^s \rho_e \mu_e u_e r^{2k}\, ds$ |
| $t$ | time |
| $T$ | absolute temperature |
| $u, v$ | velocity components parallel and normal to x- axis |
| $x$ | distance along body axis or chord line measured from forward stagnation point |

| | |
|---|---|
| $y$ | $r - r_b$ |
| $z$ | $\bar{r}/\bar{x}^m$ |
| $\alpha$ | exponent, $(1 - m)/m$ |
| $\beta$ | shock wave angle |
| $\bar{\beta}$ | pressure gradient parameter, $\frac{2\tilde{s}}{M_e}\frac{dM_e}{d\tilde{s}}$ |
| $\gamma$ | ratio of specific heats |
| $\delta$ | thickness ratio of body; or shock shape parameter |
| $\delta^*$ | viscous boundary layer displacement thickness |
| $\varepsilon$ | $(x/L)^{2(1-m)}/M_\infty{}^2\,\delta^2$ |
| $\theta$ | angle between x- axis and tangent to body surface; also flow deflection |
| $\theta_c$ | semi-vertex angle of cone |
| $\theta_w$ | shock wave angle |
| $\mu$ | viscosity coefficient |
| $\rho$ | density |
| $\varphi, \Phi, \varphi_1$ | functions of z appearing in expression for velocity |
| $\psi, \psi_1$ | functions of z appearing in expression for density |
| $\omega$ | $= (\mu/T)_e/(\mu/T)_\infty$ |
| $()_b$ | quantity evaluated at body surface |
| $()_e$ | quantity evaluated at edge of boundary layer |
| $()_s$ | quantity evaluated at shock wave |
| $()_\infty$ | quantity evaluated at free stream |
| $\bar{()}$ | non-dimensionalized quantity |

# I. INTRODUCTION

The flow around a slender body traveling in a stream of a gas at a uniform very high speed may be adequately described by the hypersonic small disturbance theory. The basic idea of this approximation is that the flow perturbation along the stream caused by the body is an order of magnitude smaller than that transverse to the stream. This fact may be deduced from a study of shock wave relations.

The relation between Mach number M, wave angle $\beta$, and deflection angle $\theta$ for an oblique shock wave may be written in the form

$$M^2 \sin^2 \beta - 1 = \frac{\gamma + 1}{2} M^2 \frac{\sin \beta \sin \theta}{\cos (\beta - \theta)}$$

For small values of $\theta$, and large values of M, such that $M\theta \gtrsim 1$, $\beta$ is also the same order of magnitude as $\theta$ for a branch of the solution usually called that for weak waves (the part of the shock polar curve lying outside the sonic circle), and hence the above relation reduces to

$$M^2 \beta^2 - 1 = \frac{\gamma + 1}{2} M^2 \beta \theta$$

or

$$\frac{\beta}{\theta} = \frac{\gamma + 1}{4} + \sqrt{\left( \frac{\gamma + 1}{4} \right)^2 + \frac{1}{(M\theta)^2}}$$

The components u, v of the velocity behind the wave are related to the upstream velocity $u_1$ by

$$\frac{u}{u_1} = 1 - \frac{2(M^2 \sin^2 \beta - 1)}{(\gamma + 1) M^2}$$

$$\frac{v}{u_1} = \frac{2(M^2 \sin^2 \beta - 1)}{(\gamma + 1) M^2} \cot \beta$$

which, for small values of $\beta$ and large values of M, reduce to

$$\frac{u - u_1}{u_1} = - \frac{2}{\gamma + 1} \beta^2 \left( 1 - \frac{1}{M^2 \beta^2} \right)$$

$$\frac{v}{u_1} = \frac{2}{\gamma + 1} \beta \left( 1 - \frac{1}{M^2 \beta^2} \right)$$

This clearly indicates that the perturbation $u - u_1$ is order of $\theta^2$ while v is order of $\theta$.

When the approximation based on this fact is introduced, the equations of motion of an inviscid gas reduce to the equations of the hypersonic small-disturbance theory, which are, as pointed out by Hayes[1], identical with the equations of unsteady motion in the transverse plane. Although the equations are very much simplified, they are still nonlinear and, in general, cannot be solved.

Cole[2] applied an expansion in powers of $(\gamma - 1)/(\gamma + 1)$ to these equations and obtained a general solution of the first approximation, which is valid when $(\gamma - 1)/(\gamma + 1)$ is small and $(\gamma + 1)/\left[(\gamma - 1) M_\infty^2 \delta^2\right]$ is order of unity or smaller. In particular the formula for the surface pressure distribution agrees with the Newtonian formula[3, 4] which includes the centrifugal force correction.

As Lees[5, 6] pointed out, for a class of slender blunt-nosed bodies of the form $r_b \sim x^m$ in hypersonic stream, the flow field exhibits similarity of the type originally found by G. I. Taylor[7] in his analysis of a constant-energy flow behind an intense spherical shock wave. In Taylor's analysis, the pressure, density, and transverse velocity are

described by relations of the form

$$Q(r)/Q(R) = f(r/R)$$

This similarity holds only in the intermediate zone not too close to the origin, yet not so far away that the shock strength has decayed to a level where the strong shock approximations are no longer applicable. For bodies of the form $r_b \sim x^m$, the flow in a transverse plane is analogous to flow generated by an expanding cylinder ($r_b \sim t^m$) or a moving plane wall in the two-dimensional case.

This similitude reduces the partial differential equations of the hypersonic small disturbance theory to a system of non-linear ordinary differential equations which is capable of solution by numerical methods of integration. A detailed analysis of the equations in Part II shows that, for the similar flow to exist, the exponent m of $r_b \sim x^m$ must lie in the range $2/3 < m \leq 1$ for two-dimensional bodies, and in the range $\frac{1}{2} < m \leq 1$ for axially-symmetric bodies.

To extend the solution for similar flow bodies to large but finite Mach numbers, the pressure, density, and transverse velocity are expanded in series of the form

$$\frac{Q(x, r)}{Q(R_o)} = \sum_{n=0}^{\infty} q_n (r/R_o)/(M_\infty{}^2 R_o'^2)^n$$

where $R_o(x)$ is the shock wave shape from the first approximation. Sakurai[8, 9] analyzed not-so-strong blast waves by constructing solutions in series of similar form. This analysis may be carried out for any value of $\gamma$, and the solution serves to investigate the dependence of flow fields on the values of $\gamma$.

The Newtonian flow theory and the similar flow theory for

"power" bodies give the surface pressure depending only on the local body slope. A solution of this form is obviously not applicable on the afterbody of a blunt-nosed cylinder in axially-symmetric flow, since it gives $C_p = 0$ on the afterbody. On these bodies, the drag is concentrated at the nose, and the flow in a transverse plane behind the nose resembles the flow generated by the explosion of a long, highly concentrated cylindrical charge. S. C. Lin[10], by extending Taylor's analysis to the case of a cylindrical blast wave, found that, in this case, the radius of the shock wave is given by

$$R \sim (E/\rho_\infty)^{1/4} \quad t^{1/2}$$

Hence by identifying the time with $x/u_\infty$ and the energy of explosion with the nose drag, the shock shape for a blunt-nosed cylinder is described by

$$R \sim (D_N/\rho_\infty)^{1/4} \quad (x/u_\infty)^{1/2}$$

or

$$R/d \sim (C_{D_N})^{1/4} \quad (x/d)^{1/2}$$

and the pressure on the afterbody is given by

$$p/(\tfrac{1}{2} \rho_\infty u_\infty^2) \sim (C_{D_N})^{1/2} \quad (x/d)^{-1}$$

This analogy is readily extended to a flat-plate with blunt leading edge at zero angle of attack. In this case, the analogy with the plane blast wave analyzed by Sakurai[8, 9] gives

$$R/d \sim (C_{D_N})^{1/3} \quad (x/d)^{2/3}$$

$$p/(\tfrac{1}{2}\rho_\infty u_\infty^2) \sim (C_{D_N})^{2/3} \quad (x/d)^{-2/3}$$

This particular analogy was also noticed by Cheng and Pallone.[11]

In Part II, the equations of motion are analyzed in detail for both classes of flow. It is shown that the constant-energy solution is a singular limit of the solution for bodies of the form $r_b \sim x^m$ as $m \longrightarrow 2/3$ in two-dimensional flow and $m \longrightarrow 1/2$ in axially-symmetric flow.

Since no measurements were available for these classes of bodies at hypersonic speeds, an experimental investigation was carried out in the GALCIT M = 7.8 wind tunnel to check the accuracy and limitations of theoretical analyses and to study what parameters are important in determining the flow field.

The surface pressure distributions on, and the shock waves and the impact pressure profiles about a hemisphere-cylinder, "3/4-power" bodies, "2/3-power" bodies, and "1/2-power" bodies of revolution were measured, and profiles of static pressure, density, and velocity, etc. were computed from the measured data.

The description and results of the experiment are presented in Part III.

# II. THEORETICAL INVESTIGATION

## A. Equations of Hypersonic Small Disturbance Theory for Two-Dimensional and Axially-Symmetric Flow

Consider a slender body placed in a steady uniform stream of an inviscid gas. As shown in the introduction, when $M_\infty >> 1$, $\delta << 1$ such that $M_\infty \delta \gtrsim 1$, the flow perturbations are

$$(u-u_\infty)/u_\infty \sim \delta^2 \qquad \text{and} \qquad v/u_\infty \sim \delta$$

and

$$p/p_\infty \sim M_\infty{}^2 \delta^2$$

where $\delta$ is the parameter determining the order of magnitude of the flow deflection angle in the disturbed region. For "power" bodies of finite length, $\delta$ is chosen to be $r_{b_{max}}/L$ or $(r_b/L)/(x/L)^m$, and in the "constant-energy" case, $\delta = (R/d)/(x/d)^{2/(3+k)}$. For $m < 1$, however, the flow deflection angle is much larger than $\delta$ near the nose of the body, and the small-disturbance assumption is not fulfilled in the nose region. On the other hand, far downstream from the body, the flow deflection approaches zero because of the decay of the shock wave, and the assumption (Mach number) x (deflection) $\gtrsim 1$ is violated. Hence, the hypersonic small disturbance theory is valid only in some intermediate zone, and not uniformly valid throughout the region except for the case $m = 1$ (cone and wedge).

The consideration of the order of magnitude of perturbations suggests the following change of variables:

$$\bar{x} = x/L, \quad \bar{r} = r/(L\delta)$$

$$\bar{u} = (u - u_\infty)/(u_\infty \delta^2), \quad \bar{v} = v/(u_\infty \delta)$$

$$\bar{p} = p/(M_\infty^2 p_\infty \delta^2), \quad \bar{\rho} = \rho/\rho_\infty$$

$$\bar{R}(\bar{x}) = R(x)/(L\delta), \quad \bar{r}_b(\bar{x}) = r_b(x)/(L\delta)$$

When this transformation of variables is introduced into the full equations of motion of an inviscid gas, and terms which contain $\delta^2$ explicitly are discarded, the differential equations reduce to

x- momentum $$\bar{\rho}\left(\frac{\partial \bar{u}}{\partial \bar{x}} + \bar{v}\frac{\partial \bar{u}}{\partial \bar{r}}\right) + \frac{\partial \bar{p}}{\partial \bar{x}} = 0$$

continuity $$\frac{\partial \bar{\rho}}{\partial \bar{x}} + \frac{\partial \bar{\rho}\bar{v}}{\partial \bar{r}} + k\frac{\bar{\rho}\bar{v}}{\bar{r}} = 0$$

r- momentum $$\bar{\rho}\left(\frac{\partial \bar{v}}{\partial \bar{x}} + \bar{v}\frac{\partial \bar{v}}{\partial \bar{r}}\right) + \frac{\partial \bar{p}}{\partial \bar{r}} = 0$$

energy $$\left(\frac{\partial}{\partial \bar{x}} + \bar{v}\frac{\partial}{\partial \bar{r}}\right)\left(\frac{\bar{p}}{\bar{\rho}^\gamma}\right) = 0$$

where k = 0 for two-dimensional flow and k = 1 for axially-symmetric flow. The boundary conditions become

tangency $$\bar{v} = \frac{d\bar{r}_b}{d\bar{x}}$$

upstream $$\bar{u} = \bar{v} = 0$$

$$\bar{p} = 1/(\gamma M_\infty^2 \delta^2)$$

$$\bar{\rho} = 1$$

and the conditions at the shock become

velocity $$\bar{V}_s = \frac{2}{\gamma+1} \frac{\bar{R}'^2 - 1/(M_\infty^2 \delta^2)}{\bar{R}'^2}$$

pressure $$\bar{p}_s = \frac{2}{\gamma+1} \left( \bar{R}'^2 - \frac{\gamma-1}{2\gamma M_\infty^2 \delta^2} \right)$$

density $$\bar{\rho}_s = \frac{\gamma+1}{\gamma-1} \frac{\bar{R}'^2}{\bar{R}'^2 + \frac{2}{\gamma-1} \frac{1}{M_\infty^2 \delta^2}}$$

A significant feature of the reduced equations is that the axial velocity $\bar{u}$ is absent from the equations governing $\bar{v}$, $\bar{p}$, and $\bar{\rho}$. After $\bar{v}$, $\bar{p}$, and $\bar{\rho}$ are obtained, $\bar{u}$ can be determined from Bernoulli's equation

$$\bar{u} + \frac{\bar{V}^2}{2} + \frac{\gamma}{\gamma-1} \frac{\bar{p}}{\bar{\rho}} = \frac{1}{\gamma-1} \frac{1}{M_\infty^2 \delta^2}$$

As pointed out by Hayes[1], if $x/u_\infty$ is identified with time, these equations of motion are exactly those of unsteady flow in the transverse plane.

## B. First Approximation: Similar Flow

### 1. Similar Flow Field

A solution of the hypersonic small disturbance equations is sought which exhibits flow similarity in the sense that

$$\bar{v}(\bar{x}, \bar{r}) = \bar{v}_s(\bar{x})\, \varphi(z)$$
$$\bar{p}(\bar{x}, \bar{r}) = \bar{p}_s(\bar{x})\, f(z)$$
$$\bar{\rho}(\bar{x}, \bar{r}) = \bar{\rho}_s(\bar{x})\, \psi(z)$$

where $z = r/R$.

By utilizing the above expressions, the operator $\frac{\partial}{\partial x} + v \frac{\partial}{\partial r}$ ,

which appears in the differential equations of motion, becomes

$\frac{\partial}{\partial \bar{x}} + \frac{\bar{R}'}{\bar{R}} \left( \frac{\bar{v}_s}{\bar{R}'} \varphi - z \right) \frac{\partial}{\partial z}$ . Therefore, if the similar solution is to exist, $\bar{v}_s/\bar{R}'$ must be independent of $\bar{x}$. From the shock relation, this condition is satisfied either when

$$M_\infty \longrightarrow \infty \qquad (I)$$

or when $\bar{R}'$ = const. (wedge or cone) for arbitrary M.

For $M_\infty \longrightarrow \infty$, the flow variables become

$$\bar{v}(\bar{x}, \bar{v}) = \frac{2}{\gamma + 1} \bar{R}'(\bar{x}) \varphi(z) \equiv \bar{R}'(\bar{x}) \Phi(z)$$

$$\bar{p}(\bar{x}, \bar{r}) = \frac{2}{\gamma + 1} \bar{R}'^2(x) \cdot f(z) \equiv \bar{R}'^2(\bar{x}) F(z)$$

$$\bar{\rho}(\bar{x}, \bar{v}) = \psi(z)$$

In terms of $\Phi$ , F, $\psi$ , and $\bar{R}$

$$\frac{\partial}{\partial \bar{x}} + \bar{v} \frac{\partial}{\partial \bar{r}} = \frac{\partial}{\partial \bar{x}} + \frac{\bar{R}'}{\bar{R}} (\Phi - z) \frac{\partial}{\partial z}$$

and the equations of motion become

Continuity

$$\frac{\bar{R}'}{\bar{R}} \left[ (\Phi - z) \psi' + \psi \Phi' + k \frac{\psi \Phi}{z} \right] = 0$$

Momentum

$$(\Phi - z) \Phi' + \frac{F'}{\psi} + \frac{\bar{R} \bar{R}''}{\bar{R}'^2} \Phi = 0$$

Energy

$$(\Phi - z) \left( \frac{F'}{F} - \gamma \frac{\psi'}{\psi} \right) + 2 \frac{\bar{R} \bar{R}''}{\bar{R}'^2} = 0$$

Hence the assumption of flow similarity is satisfied when

$$\bar{R}\,\bar{R}''/\bar{R}'^{2} = \text{const.} = -a, \quad \text{or}$$

$$\bar{R}^{a}\,\bar{R}' = \text{const.} = A, \quad \text{and hence} \quad \bar{R} = (A/m)\,x^{m} \qquad \text{(II)}$$

where $m = 1/(1 + a)$.

Also the boundary condition on the body requires

$$\bar{V}(\bar{r}_b) = \frac{d\bar{r}_b}{d\bar{x}} = z_b\,\bar{R}' + \bar{R}\cdot z_b'$$

Therefore, $z'_b = 0$, or

$$r_b \sim x^{m} \qquad \text{(III)}$$

and the shock wave and the body shape are similar.

When the conditions (I), (II), and (III) are satisfied, the flow field in a transverse plane is governed by the following set of ordinary, non-linear, first-order differential equations:

"Continuity"

$$(\Phi - z)\,\psi' + \psi\,\Phi' + k\,\frac{\psi\Phi}{z} = 0 \qquad (1)$$

"Momentum"

$$(\Phi - z)\,\Phi' + F'/\psi - a\,\Phi = 0 \qquad (2)$$

"Energy"

$$(\Phi - z)\left[(F'/\Gamma) - \gamma\,(\psi'/\psi)\right] - 2a = 0 \qquad (3)$$

where $a = (1/m) - 1$.

The conditions at the shock become

$$\Phi(1) = F(1) = \frac{2}{\gamma+1}, \quad \Psi(1) = \frac{\gamma+1}{\gamma-1} \tag{4}$$

and the boundary condition on the body becomes

$$\Phi(z_b) = z_b \tag{5}$$

## 2. Drag and Energy

Consider a symmetric body at zero angle of attack in a uniform flow, and take a volume enclosed by a surface shown in the sketch.

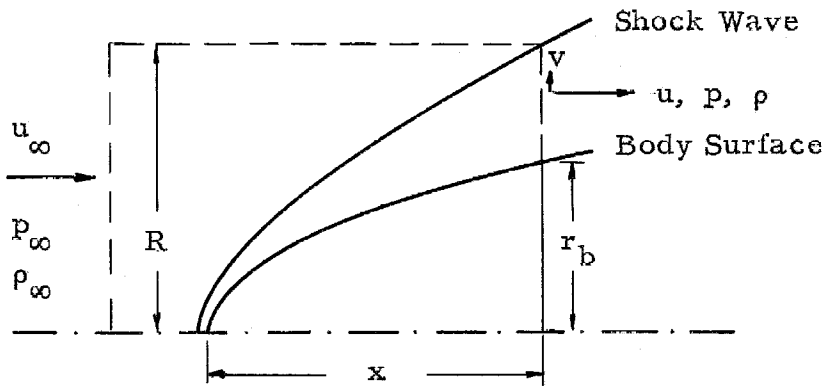


For steady flow, the momentum of the gas in the volume remains unchanged with time. Hence by Newton's second law applied to the axial component of the momentum and force

$$2\pi^k \int_{r_b}^{R} \rho u^2 r^k dr - \frac{2\pi^k}{k+1} R^{k+1} \rho_\infty u_\infty^2$$

$$= -D(x) - 2\pi^k \int_{r_b}^{R} p r^k dr + \frac{2\pi^k}{k+1} R^{k+1} p_\infty$$

where D(x) is the drag acting on the body. Rearranging terms and using the integral form of the continuity of mass

$$2\pi^k \int_{r_b}^{R} \rho u r^k dr - \frac{2\pi^k}{k+1} R^{k+1} \rho_\infty u_\infty = 0$$

one obtains

$$D(x) = -2\pi^k \int_{r_b}^{R} \left[ p + \rho u (u - u_\infty) \right] r^k dr + \frac{2\pi^k}{k+1} R^{k-1} p_\infty \qquad (6)$$

For inviscid flow, the conservation of energy gives

$$2\pi^k \int_{r_b}^{R} \rho u \left[ \frac{1}{2}(u^2+v^2) + c_v T \right] r^k dr + 2\pi^k \int_{r_b}^{R} p u r^k dr$$

$$- \frac{2\pi^k}{k+1} R^{k+1} \left[ \rho_\infty u_\infty \left( \frac{1}{2} u_\infty^2 + c_v T_\infty \right) + p_\infty u_\infty \right] = 0$$

By utilizing the continuity of mass, this may be written as

$$-2\pi^k u_\infty \int_{r_b}^{R} \left[ \rho (u - u_\infty) + p \right] r^k dr + \frac{2\pi^k}{k+1} R^{k+1} p_\infty u_\infty$$

$$= 2\pi^k \int_{r_b}^{R} \rho u \left[ \frac{1}{2} v^2 + c_v T + \frac{1}{2}(u - u_\infty)^2 \right] r^k dr$$

$$+ 2\pi^k \int_{r_b}^{R} p (u - u_\infty) r^k dr - \frac{2\pi^k}{k+1} R^{k+1} \rho_\infty u_\infty c_v T_\infty$$

Therefore, by combining the equations (6) and (7),

$$D(x) = \frac{2\pi^k}{u_\infty} \int_{r_b}^{R} \rho u \left[ \frac{1}{2} v^2 + c_v T + \frac{1}{2}(u - u_\infty)^2 \right] r^k dr$$

$$+ \frac{2\pi^k}{u_\infty} \int_{r_b}^{R} p (u - u_\infty) r^k dr - \frac{2\pi^k}{k+1} R^{k+1} \rho_\infty c_v T_\infty \qquad (7)$$

When the hypersonic small disturbance approximation is introduced, the last formula becomes

$$D(x) = 2\pi^k \rho_\infty u_\infty^2 L^{k+1} \delta^{3+k} \bar{R}^{k+1} \int_{z_b}^{1} \left( \frac{1}{2} \bar{\rho} \bar{v}^2 + \frac{1}{\gamma - 1} \bar{p} \right) z^k dz \qquad (8)$$

in the limit of $M_\infty \longrightarrow \infty$ .

It is interesting to note that in this approximation the energy of the transverse flow is the drag acting on the body from the nose to that transverse plane.

Since the drag is also given by

$$D(x) = 2\pi^k \rho_\infty u_\infty^2 L^k \delta^{3+k} \int_0^{\bar{x}} \bar{p}_b \frac{d\bar{r}_b}{d\bar{x}} \bar{r}_b^k d\bar{x}$$

the rate of increase of drag with x is

$$dD/dx = 2\pi^k \rho_\infty u_\infty^2 L^k \delta^{3+k} p_b v_b r_b^k \qquad (9)$$

In terms of similarity variables, eq. (8) becomes

$$D(x) = 2\pi^k \rho_\infty u_\infty^2 L^{k+1} \delta^{3+k} A^2 \left[\bar{R}(\bar{x})\right]^{1+k-2a} \int_{z_b}^{1} \left( \frac{1}{2} \psi \Phi^2 + \frac{1}{\gamma - 1} F \right) z^k dz \qquad (10)$$

where $A = \bar{R}^a \cdot \bar{R}' =$ const. for similar flow.

Evidently from eq. (10) the drag is constant when $2a = 1 + k$ or $m = 2/(3+k)$, and by eq. (9) $v_b = 0$ everywhere except right at the nose. This corresponds to the case of a blunt-nose followed by a cylindrical or flat-plate afterbody, and for two-dimensional flow

$m = 2/3$ and $R \sim x^{2/3}$, and for axially-symmetric flow $m = \frac{1}{2}$ and $R \sim x^{\frac{1}{2}}$. When $2a < 1 + k$, or $m > 2/(3+k)$, then $dD/dx > 0$, and $v_b > 0$, $z_b > 0$; and similar solutions exist, if at all, only for these values of m.

For this constant-drag case, eq. (10) becomes

$$D = 2\pi^k \rho_\infty u_\infty^2 \left[R^\alpha R'(x)\right]^2 \int_0^1 \left(\frac{1}{2}\psi\Phi^2 + \frac{1}{\gamma-1}F\right) z^k dz$$

Hence, this case is analogous to the constant-energy flow behind a blast-wave produced by a strong explosion if the energy E of the explosion is identified with the drag $D/2^{1-k}$ and the time t is identified with $x/u_\infty$.

In this case the shock shape is described by

$$\frac{R}{d} = \left[\frac{(3+k)^2}{4^{2+k}} \frac{C_D}{I(k,\gamma)}\right]^{\frac{1}{3+k}} \left(\frac{x}{d}\right)^{\frac{2}{3+k}} \tag{11}$$

and the pressure on the afterbody, not too close to the nose, is given by

$$\frac{p}{p_\infty} = \gamma M_\infty^2 \frac{4}{(3+k)^2} \left[\frac{(3+k)^2}{4^{2+k}} \frac{C_D}{I(k,\gamma)}\right]^{\frac{2}{3+k}} F(0) \left(\frac{x}{d}\right)^{-2\frac{1+k}{3+k}} \tag{12}$$

where

$$C_D = \frac{D}{\frac{1}{2}\rho_\infty u_\infty^2 (\pi/4)^k d^{1+k}}$$

d = nose diameter, or thickness of blunt leading-edge

and $$I(k,\gamma) = \int_0^1 \left(\frac{1}{2}\psi\Phi^2 + \frac{1}{\gamma-1}F\right) z^k dz$$

As the study of the mathematical properties of the solution shows (Section 2), the special constant-drag solution with $m = 2/(3+k)$ is a singular limit of solutions for bodies of the form $r_b \sim x^m$. The similar-flow solution yields a shock wave that lies farther and farther away from the body surface as m tends to $2/(3+k)$, and the small disturbance approximation must become poorer as this critical value of m is approached.

## 3. Mathematical Study of Similarity Solution

The criterion $m \geq 2/(3+k)$ is a necessary condition for the existence of a similarity solution, but a study of the mathematical properties of the equations of motion is required to determine whether this condition is also a sufficient one.

Since Eqs. (1), (2), and (3) are invariant under the transformation ( $\Phi \longrightarrow a\Phi$ , $z \longrightarrow az$ , $F \longrightarrow a^2 F$ , $\psi \longrightarrow \psi$ ), these equations are reducible to a single non-linear first-order equation in the new variables $t = d\Phi/dz$ and $s = \Phi/z$. This reduction is accomplished by first eliminating F' and $\psi'$ to obtain the relation

$$t = \frac{2\alpha - k\gamma s + \alpha s(1-s) z^2 \psi/F}{\gamma - (1-s)^2 z^2 \psi/F} \tag{13}$$

The quantity $\psi/F$ is then eliminated by differentiating Eq. (13) and utilizing Eqs. (2), (3), and (14). By employing the identity

$$z \frac{d}{dz} \equiv (t-s) \frac{d}{ds} \tag{14}$$

the following equation is finally obtained

$$\frac{dt}{ds} = \frac{N(s,t)}{(1-s)\left[\alpha\gamma s + (1-s)(2\alpha - k\gamma s)\right](s-t)} \tag{15}$$

where

$$N(s,t) = (\gamma t - 2\alpha + k\gamma s)\left\{(\gamma+1)(1-s)t^2 + \left[(\alpha\gamma + 3\alpha + 2)s - (3\alpha+2)\right.\right.$$
$$\left.\left. + k(\gamma-1)(1-s)s\right]t - \alpha(2\alpha+1)s + k\alpha(\gamma-1)s^2\right\}$$
$$- k\gamma(1-s)\left[(1-s)t + \alpha s\right](s-t)$$

At the shock wave z = 1, $\Phi = F = 2/(\gamma+1)$, $\psi = (\gamma+1)/(\gamma-1)$. Hence, from eq. (14), the shock wave corresponds to

$$s = \Phi/z = \frac{2}{\gamma+1}$$
$$t = \frac{6\alpha}{\gamma+1} - k\frac{4\gamma}{(\gamma+1)^2} \tag{16}$$

in the s - t plane.

At the body surface $\Phi = z$,

$$s = 1$$
$$t = 2\alpha/\gamma - k \qquad \text{for } 2\alpha < 1 + k \tag{17}$$

For the case $2\alpha = 1 + k$, both $\Phi$ and z approach zero, and hence $s \longrightarrow t$ near z = 0. Therefore,

$$s = t = 1/\gamma \qquad \text{for} \qquad 2\alpha = 1 + k \tag{17a}$$

Except for the special case $2\alpha = 1 + k$, near the body

$$\Phi = z_b + \left(\frac{2\alpha}{\gamma} - k\right)(z - z_b) + \ldots$$

and from eq. (1)

$$\psi \cong \text{const.}\ (z - z_b)^n$$

where

$$n = \frac{2\alpha}{(1+k)\gamma - 2\alpha} = \frac{2(1-m)}{m[(1+k)\gamma+2]-2}$$

Thus n must be positive if the density is to be finite at the surface, or

$$\frac{2}{2 + (1 + k)\gamma} \leq m \leq 1$$

In fact the density is zero at the surface, exactly as in Taylor's case, unless m takes one of these extreme values in which case the density has non-zero value on the body. But for any real gas the lower limit is always less than or equal to the value $2/(3 + k)$ imposed by the drag considerations (Article 2), so that actually m is confined to the range $2/(3 + k) \leq m \leq 1$ for a body with a positive slope.

For two-dimensional flow k = 0*

$$\frac{dt}{ds} = \frac{N(s,t)}{\alpha(1-s)[1-(2-\gamma)s](t-s)} \tag{15a}$$

$$N(s,t) = (\gamma t - 2\alpha)\left\{(\gamma+1)(1-s)t^2 + [(\alpha\gamma+3\alpha+2)s - (3\alpha+2)]t - \alpha(2\alpha+1)s\right\}$$

$$= \gamma(\gamma+1)\left(t - \frac{2\alpha}{\gamma}\right)(1-s)[t - t_1(s)][t - t_2(s)]$$

where $t = t_1(s)$ and $t = t_2(s)$ are the upper and lower branches of the curve defined by the relation

---

* The analysis for axially-symmetric flow is similar, but the algebra is more extensive.

$$(\gamma+1)(1-s)t^2+\left[(\alpha\gamma+3\alpha+2)s-(3\alpha+2)\right]t-\alpha(2\alpha+1)s=0$$

and

$$t_1(s) > \frac{2\alpha}{\gamma} > t_2(s) \qquad \text{for } 0 < s < 1 \text{ and } \quad \alpha < \frac{2\gamma}{2-\gamma}$$

There are nine singular points of Eq. (15a), but only four of these are relevant to the present discussion. These four singular points are (Figure 7):

(1) $s = 1$, $t = 2\alpha/\gamma$ , a node (point B)

(2) $s = t = 2\alpha/\gamma$ , a saddle point (point A)

(3) $s = 1$, $t = (1 + 2\alpha)/\gamma$ (point C), a node when $\alpha > (\gamma - 1)/2$, or a saddle point when $\alpha < (\gamma - 1)/2$

(4) $s = t = 2(1 + \alpha)/(\gamma + 1)$, a saddle point when $\alpha > (\gamma - 1)/2$, or a node when $\alpha < (\gamma - 1)/2$

In the region $s \leq 1$, $t \geq 2\alpha/\gamma$ the slope dt/ds is negative below the line $t = s$, while above this line dt/ds is positive, provided that $t < t_1(s)$. Along the line $t = s$ the slope dt/ds is infinite, except at the saddle point A, and the integral curves must behave as shown in Figure 7. Every integral curve contained in the "triangular" region ABC passes through the body surface point, and the shock point $s = 2/(\gamma + 1)$, $t = 6\alpha/(\gamma + 1)$ lies within this region so long as $\alpha < \frac{1}{2}$; therefore, analytic solutions exist in the s-t plane for $0 < \alpha < \frac{1}{2}$. The fact that dt/ds becomes infinite at $t = s$ for $1/3 < \alpha < \frac{1}{2}$ does not lead to any singularity in the physical plane.

To summarize: similarity solutions exist in the entire range $2/3 < m \leq 1$ for axially-symmetric flows. From the present point of view the constant-drag (or energy) solution $m = 2/(3 + k)$ is a singular

solution passing through the saddle point (Figure 7 ) with a slope $d\Phi/dz = t = 1/\gamma$ at $s = 1/\gamma$ .

Included within the admissible range of values of m are of course the wedge and cone (m = 1), and also the "hypersonic optimum shape" $r_b \sim x^{3/4}$, or body of revolution of minimum zero-lift drag for a given slenderness ratio, as determined from Newtonian impact theory, neglecting centrifugal force, by Eggers, Dennis, and Resnikoff[12]. J. D. Cole[2] obtained m = 2/3 for this optimum shape by including centrifugal force. For two-dimensional flow Cole obtained an optimum shape with m = 0.87; both of his cases also lie within the similar flow range.

## 4. Solution for Constant-Energy Case

For the case of a strong spherical blast wave Latter[13] obtained the solution in a closed form. This result can be extended to include axially-symmetric and two-dimensional flow.

For this case, $\alpha = (k + 1)/2$ and the equations become

$$(\Phi - z)\Phi' + (F'/\psi) - (k + 1)/2\ \Phi = 0 \tag{18}$$

$$(\Phi - z)\psi' + \psi\Phi' + k(\psi\Phi/z) = 0 \tag{19}$$

$$(\Phi - z)\left(\frac{F'}{F} - \gamma\frac{\psi}{\psi}\right) - (k + 1) = 0 \tag{20}$$

where the prime indicates differentiation with respect to z. Eq. (20) may be rewritten with the help of eq. (19) as

$$(\Phi - z)(F'/F) + \gamma\left(\Phi' + k\frac{\Phi}{z}\right) - (k + 1) = 0 \tag{20'}$$

By multiplying eq. (18) by $z^k\psi\Phi$, eq. (19) by $z^k\Phi^2/2$ and adding the

results, one obtains

$$\left[z^k\,(\Phi - z)\,\psi\Phi^2/2\right]' + z^k\Phi F' = 0 \quad .$$

By multiplying eq. (20') by $z^k F$ and rearranging terms, one also obtains

$$\left[z^k\,(\Phi - z)\,F\right]' + (\gamma - 1)\,F\,(z^k\Phi)' = 0 \quad .$$

By adding the two results, one obtains finally

$$\left[z^k\left\{(\Phi - z)\left(\frac{1}{\gamma - 1}\,F + \frac{\psi\Phi^2}{2}\right) + F\Phi\right\}\right]' = 0$$

which can be integrated readily and upon determination of the integration constant by the condition at the shock

$\{\Phi = F = 2/(\gamma + 1),\ \psi = (\gamma + 1)/(\gamma - 1)$ at $z = 1\}$ yields

$$(\Phi - z)\left(\frac{1}{\gamma - 1}\,F + \frac{\psi\Phi^2}{2}\right) + F\Phi = 0 \qquad (21)$$

By putting $2a = 1 + k$ in eq. (14), one obtains

$$\Phi' = \frac{(k+1)\,z - \gamma k\Phi + \frac{1}{2}(k+1)\,z\Phi(z - \Phi)\,\psi/F}{z\left\{\gamma - (z - \Phi)^2\,\psi/F\right\}}$$

From eq. (21)

$$\psi/F = \frac{2}{(z - \Phi)\,\Phi} - \frac{2}{(\gamma - 1)\Phi^2}$$

Hence, finally

$$\Phi' = \frac{2(k+1)(\gamma - 1)\,z\Phi^2 - k\gamma(\gamma - 1)\Phi^3 - (k+1)(z - \Phi)\,z\Phi}{z\left\{\gamma(\gamma - 1)\Phi^2 - 2(\gamma - 1)(z - \Phi)\Phi + 2(z - \Phi)^2\right\}}$$

Let $t = \Phi'$ and $s = \Phi/z$, and then

$$t = \frac{-k\gamma(\gamma-1)\,s^3 + (k+1)(2\gamma-1)\,s^2 - (k+1)\,s}{\gamma(\gamma+1)\,s^2 - 2(\gamma+1)\,s + 2}$$

Also

$$dz/ds = z/(t-s)$$

or

$$\log z = \int_s^{2/(\gamma+1)} ds/(s-t)$$

After the integration, the result is in a parametric form

$$\left.\begin{aligned} z &= \left(\frac{\gamma+1}{2}\,s\right)^n \left[\frac{\gamma+1}{\gamma-1}(\gamma s - 1)\right]^p \left[\frac{(\gamma+1)\{k+3-[(1+k)\gamma+(1-k)]\,s\}}{1+3k+(1-k)\gamma}\right]^q \\ \Phi &= sz \\ \text{for } 1/\gamma &\leq s \leq \frac{2}{\gamma+1} \end{aligned}\right\} \quad (22)$$

where

$$n = -2/(3+k), \quad p = (\gamma-1)/(2\gamma-1+k),$$

$$q = -\frac{(5+2k+k^2)\gamma^2 + (1+2k-3k^2)\gamma - 4(1-k^2)}{(3+k)(2\gamma-1+k)[(1+k)\gamma+1-k]}$$

By dividing eq. (19) by $-\Psi(\Phi-z)/(\gamma-1)$ and eq. (20') by $(\Phi-z)$ and adding the results, one obtains

$$F'/F - (\gamma-1)\,\Psi'/\Psi + (\Phi'-1)/(\Phi-z) + k/z = 0$$

which yields after determining the integration constant by the condition at z = 1*

---

* Also in general case, an integral of this form may be obtained which reads

$$z^{\frac{2\alpha k}{1+k}} F\,(z-\Phi)^{\frac{2\alpha}{1+k}} \Psi^{-(\gamma-\frac{2\alpha}{1+k})} = 2(\gamma-1)^{\gamma}/(\gamma+1)^{\gamma+1}$$

$$z^k F (z-\Phi)\ \psi^{-(\gamma-1)} = 2(\gamma-1)^\gamma/(\gamma+1)^{\gamma+1} \tag{23}$$

From eqs. (13) and (15)

$$\left.\begin{aligned} F &= \left[\frac{2^\gamma(\gamma-1)}{(\gamma+1)^{\gamma+1}}\right]^{\frac{1}{2-\gamma}} \left[\frac{(\gamma\Phi - z)^{\gamma-1}}{z^k (z-\Phi)^\gamma \Phi^{2(\gamma-1)}}\right]^{\frac{1}{2-\gamma}} \\ \psi &= \left[\frac{4(\gamma-1)^{\gamma-1}}{(\gamma+1)^{\gamma+1}}\right]^{\frac{1}{2-\gamma}} \left[\frac{\gamma\Phi - z}{z^k (z-\Phi)^2 \Phi^2}\right]^{\frac{1}{2-\gamma}} \end{aligned}\right\} \tag{24}$$

Thus F and $\psi$ are expressed in terms of z and $\Phi$, and the solution is completed.

## 5. Solutions by Numerical Integration

For the cases other than the constant-energy case, the solutions were obtained by integrating the equations in the physical plane rather than in the s - t plane.

Equations (1), (2), and (3) are integrated by means of a numerical method. The procedure is to start the integration from the shock wave where $\Phi$, F, and $\psi$ are known and integrate numerically towards small values of z. Near the body surface, a singular point of the equations, power series representations of the solution are matched to the numerical solution at some value of z close to $z_b$.

The results of integration for the axially symmetric case are shown in Figures 9 through 13 together with results from Cole's[2] approximation for comparison.

Similarity solutions give the surface pressure distribution as

$$C_p = \frac{2F(z_b)}{z_b^2} m^2 \delta^2 \left(\frac{x}{L}\right)^{2(m-1)}$$

or

$$\frac{C_p}{(dr_b/dx)^2} = \frac{2F(z_b)}{z_b^2} \tag{25}$$

As shown in Figure 13, the result from Cole's Newtonian flow theory[2] agrees fairly well with the more exact present solution when m is close to unity, but the agreement becomes poorer as m approaches the critical value of $\frac{1}{2}$. Cole's result for the surface pressure in first approximation is

$$C_p = 2\left(\frac{dr_b}{dx}\right)^2 + \frac{2}{1+k} r_b \frac{d^2 r_b}{dx^2}$$

which is identical with Busemann's expression. But the first term implies that $\gamma \cong 1$ and that the shock wave coincides with the body surface. Actually for $\gamma$ not too close to unity the inclination of the shock with respect to the body surface is responsible for an increase in surface pressure that almost counterbalances the "relieving" effect of the centrifugal force term.

The tangent-cone (or wedge) approximation replaces $2F(z_b)/z_b^2$, which varies with m, by the value at m = 1 for all m's, and for these bodies it overestimates the pressure by an appreciable amount. However, the variation of this parameter with m is rather slow, and for bodies slightly different from $r_b \sim x^m$ it may be possible to approximate the pressure distribution by the formula $C_p = (2F/z_b^2)(dr_b/dx)^2$, using the actual body slope and the value of $2F/z_b^2$ at some average value of m. This approximation is used later to estimate the effect of the boundary layer on the surface pressure distributions on similar-flow bodies.

## C. Successive Approximations

### 1. Expansion Procedure

In the similarity solution of the previous section, Mach number was assumed to be infinitely large. When Mach number is not infinite, the examination of the shock relations suggest a scheme of expansion. For example, the density ratio across the shock

$$\frac{\rho}{\rho_\infty} = \frac{\gamma+1}{\gamma-1}\,\frac{1}{1+N} \qquad \text{where} \quad N = \frac{2}{\gamma-1}\,\frac{1}{M_\infty^2 R'^2}$$

may be expanded as

$$\frac{\rho}{\rho_\infty} = \frac{\gamma+1}{\gamma-1}\sum_{n=0}^{\infty}(-1)^n N^n \qquad \text{when } N > 1 .$$

This fact suggests an expansion of the form

$$Q(x, r) = Q(R)\sum_{n=0}^{\infty} q_n\,(r/R)/(M_\infty{}^2\,R'^2)^n$$

In fact, Sakurai[8, 9] used this form of expansion in his analysis of constant-energy flow produced by a blast wave.

In the case of "power" bodies, however, this form of expansion will result in some difficulty, since the body surface is not given by $r/R$ = constant in the higher approximations, and since the solutions of the first approximation have singularities at the body surface. In order to avoid this difficulty, the physical quantities are expanded in inverse powers of $M^2 R_o'^2$, where $R_o(x)$ is the shock shape obtained from the first approximation. The coefficients of the series are functions of $r/R_o$, so that the body surface is always given by $r/R_o$ = const.

The transverse velocity, pressure and density are expanded in the following series:

$$\bar{v}(\bar{x}, \bar{r}) = m\bar{x}^{m-1} \sum_i \varphi_i(z)\,\varepsilon^i$$

$$\bar{p}(\bar{x}, \bar{r}) = m^2 \bar{x}^{2(m-1)} \sum_i f_i(z)\,\varepsilon^i$$

$$\bar{\rho}(\bar{x}, \bar{r}) = \sum_i \psi_i(z)\,\varepsilon^i$$

The shock wave shape is expanded as

$$\bar{R}(\bar{x}) = \bar{x}^m \sum_i a_i\,\varepsilon^i, \qquad a_o = 1$$

where $z = r/x^m$ and $\varepsilon = x^{2(1-m)}/M_\infty^2\,\delta^2$.

By substituting these expressions into the hypersonic small disturbance equations of motion, and equating the sum of coefficients of powers of $\varepsilon$ to zero separately, one obtains a sequence of equations for $(\varphi_o, f_o, \psi_o)$, $(\varphi_1, f_1, \psi_1)$, . . . . . , where $\varphi_o$, $f_o$, $\psi_o$ are identical with $\Phi$, F, $\psi$ studied previously, and the equations of higher approximations are linear.

The conditions at the shock are satisfied approximately by expanding physical quantities about the shock location of the first approximation $M_\infty \longrightarrow \infty$. For example

$$\bar{V}(\bar{R}) = \bar{V}(\bar{R}_o) + \left(\frac{\partial \bar{V}}{\partial \bar{r}}\right)_{\bar{R}_o} (\bar{R} - \bar{R}_o) + \cdots$$

$$= m\,\bar{x}^{m-1}\left[\varphi_o(1) + \{\varphi_1(1) + \varphi_o'(1)\}\varepsilon + \cdots\right]$$

On the shock, on the other hand,

$$\bar{V}(\bar{R}) = \frac{2}{\gamma+1}\left(\bar{R}' - \frac{1}{M_\infty^2 \delta^2 \bar{R}'^2}\right)$$

$$\bar{V}(\bar{R}) = \frac{2}{\gamma+1}\left[1 + \left\{\left(\frac{2}{m} - 1\right) a_1 - \frac{1}{m^2}\right\}\varepsilon + \cdots\right]$$

Hence

$$\varphi_0(1) = \frac{2}{\gamma+1}$$

$$\varphi_1(1) + a_1 \varphi_0'(1) = \frac{2}{\gamma+1}\left[\left(\frac{2}{m} - 1\right) a_1 - \frac{1}{m^2}\right]$$

The tangency condition on the body becomes

$$\varphi_0(z_b) = z_b$$

$$\varphi_i(z_b) = 0, \qquad i \geq 1.$$

## 2. Second Approximation

The equations for the second approximation are

Continuity

$$\varphi_1' + (\varphi_0 - z)\frac{\psi_1'}{\psi_0} + \left(\frac{\psi_0'}{\psi_0} + \frac{k}{z}\right)\varphi_1 + \left[2\alpha - (\varphi_0 - z)\frac{\psi_0'}{\psi_0}\right]\frac{\psi_1}{\psi_0} = 0$$

Momentum

$$(\varphi_0 - z)\varphi_1' + \frac{f_1}{\psi_0} + (\varphi_0' + \alpha)\varphi_1 + \left[(\varphi_0 - z)\varphi_0' - \alpha\varphi_0\right]\frac{\psi_1}{\psi_0} = 0$$

Energy

$$\gamma\varphi_1' + (\varphi_0 - z)\frac{f_1'}{f_0} + \left(\frac{f_0'}{f_0} + k\frac{\gamma}{z}\right)\varphi_1 + \gamma\left(\varphi_0' + k\frac{\varphi_0}{z}\right)\frac{f_1}{f_0} = 0$$

(26)

The conditions at the shock are as follows:

$$\left.\begin{aligned}
\varphi_1(1) &= \frac{2}{\gamma+1}\left[-(1+\alpha)^2 + a_1\left\{1+2\alpha-\frac{\gamma+1}{2}\varphi_0'(1)\right\}\right] \\
f_1(1) &= \frac{2}{\gamma+1}\left[-\frac{\gamma-1}{2\gamma}(1+\alpha)^2 + a_1\left\{2+4\alpha-\frac{\gamma+1}{2}f_0'(1)\right\}\right] \\
\psi_1(1) &= -2\frac{\gamma+1}{(\gamma-1)^2}(1+\alpha)^2 - a_1\psi_0'(1)
\end{aligned}\right\} \quad (27)$$

where $\alpha = (1-m)/m$ as before. On the body

$$\varphi_1(z_b) = 0 \quad (28)$$

The conditions at the shock contain an unknown constant $a_1$, and the differential equations can not be integrated directly by a numerical method. An obvious method is to integrate the equations by assuming several values of $a_1$ and to obtain the value of $a_1$ satisfying the boundary conditions. However, as Sakurai[9] noted, since the equations are linear with respect to the functions to be solved, $\varphi_1$, $f_1$, $\psi_1$ may be split into two parts as

$$\begin{aligned}
\varphi_1 &= \varphi_1^{(1)} + a_1\varphi_1^{(2)} \\
f_1 &= f_1^{(1)} + a_1 f_1^{(2)} \\
\psi_1 &= \psi_1^{(1)} + a_1\psi_1^{(2)}
\end{aligned}$$

Then the differential equations satisfied by $\varphi_1^{(1)}$, $f_1^{(1)}$, $\psi_1^{(1)}$ and $\varphi_1^{(2)}$, $f_1^{(2)}$, $\psi_1^{(2)}$ are identical with the original equations 26, with the conditions at $z = 1$

$$\left.\begin{aligned} \varphi_1^{(1)} &= -\frac{2}{\gamma+1}\,(1+a)^2 \\ f_1^{(1)} &= -\frac{\gamma-1}{\gamma(\gamma+1)}\,(1+a)^2 \\ \psi_1^{(1)} &= -\frac{2(\gamma+1)}{(\gamma-1)^2}\,(1+a)^2 \end{aligned}\right\} \quad (29a)$$

and

$$\left.\begin{aligned} \varphi_1^{(2)} &= \frac{2}{\gamma+1}\,(1+2a) - \varphi_o' \\ f_1^{(2)} &= \frac{4}{\gamma+1}\,(1+2a) - f_o' \\ \psi_1^{(2)} &= -\psi_o' \end{aligned}\right\} \quad (29b)$$

After these two sets of functions are obtained, $a_1$ is determined by the boundary condition on the body

$$\varphi_1(z_b) = \varphi_1^{(1)}(z_b) + a_1\,\varphi_1^{(2)}(z_b) = 0$$

Numerical integrations have been carried out for axially-symmetrical flow with $\gamma = 5/3,\ 1.4,\ 1.15$, and $m = \frac{1}{2},\ 4/7,\ 2/3,\ 3/4$, and 1. The results are tabulated in Table I.

For bodies of revolution $r_b/L = \delta(x/L)^m$, the formula for shock location is

$$\frac{R(x)}{r_b(x)} = \frac{1}{z_b}\left\{1 + \frac{a_1 z_b^2}{M_\infty^2 \delta^2}\left(\frac{x}{L}\right)^{2(1-m)}\right\}$$

and the surface pressure coefficient is given by

$$\frac{C_p}{(dr_b/dx)^2} = \frac{2F(z_b)}{z_b^2}\left\{1 + \frac{z_b^2}{m^2\gamma F(z_b)}\left\{m^2\gamma f_1(z_b) - 1\right\}\frac{(x/L)^{2(1-m)}}{M_\infty^2\delta^2}\right\}$$

For example, the formulae for shock location and pressure coefficient on the surface of a cone are, up to the second approximation:

$$\theta_w/\theta_c = 1.092\left(1 + \frac{0.332}{M_\infty^2\,\theta_c^2}\right)$$

$$C_p/\theta_c^2 = 2.090 + \frac{0.402}{M_\infty^2\,\theta_c^2}$$

The present result is compared with that from a numerical integration[21] of the exact equations for flow around a cone (Table II). It is seen that the present approximation agrees very well with the exact value for $M \tan\theta_c > 1$.

According to the first approximation of Cole's Newtonian flow theory, the shock location for bodies of revolution $r_b/L = \delta(x/L)^m$ is given by

$$\frac{R(x)}{r_b(x)} = 1 + \frac{\gamma-1}{\gamma+1}\,\frac{m}{1-m}\int_0^1 \frac{dy}{\left(y + \frac{3m-1}{1-m}\right)y^{(1-m)/m}}$$

$$+ \frac{\log\left[2m/(3m-1)\right]}{m(1-m)} \cdot \frac{(x/L)^{2(1-m)}}{M_\infty^2\,\delta^2}$$

This result is compared with the present solution in the following table. ($\gamma = 1.40$)

| | Present Approximation | | Cole's 1st Approximation | |
|---|---|---|---|---|
| m | A | B | A | B |
| 1 | 1.092 | 0.332 | 1.083 | 0.461 |
| 3/4 | 1.143 | 0.518 | 1.123 | 0.866 |
| 2/3 | 1.192 | 0.558 | 1.202 | 1.077 |
| 4/7 | 1.379 | 0.457 | 1.439 | 1.333 |

where

$$R(x)/r_b(x) = A\left[1 + B\,(x/L)^{2(1-m)}/M_\infty^2\,\delta^2\right]$$

The agreement between the present results and Cole's first approximation is fair for m close to unity, but it becomes poorer as m decreases. However, the agreement would be improved if Cole's calculation were carried out further to include terms of higher powers of $(\gamma - 1)/(\gamma + 1)$.

# III. EXPERIMENTAL STUDY

An experiment was conducted to determine the surface pressure distribution, shock wave shape, and flow quantity profiles such as static pressure and density profiles about simple bodies of revolution. The tests were designed to permit a check on the accuracy of the predictions of the similarity solution developed in Part II.

On these models the surface pressure distributions were measured by means of small orifices distributed in the surface; the shock wave shapes from schlieren photographs of the flow; the impact pressure profiles by means of a small probe. The flow quantity profiles were computed from the shock wave and impact pressure data.

## A. Description of the Experiment

### 1. Models and Equipment

The experiment was conducted in the GALCIT hypersonic wind tunnel leg no. 2, which is of the continuous-flow, closed-return type using air as a working medium. A semi-flexible nozzle — solid throat blocks and flexible-plate nozzle liners — of five inches by six and a half inches test section was installed in the circuit and adjusted to produce uniform flow at Mach number 7.8 in the test section.* With this nozzle in the circuit, the compressor plant supplied the maximum reservoir pressure of 350 psig at the maximum supply temperature of 800 deg. F. which is obtained by means of an electric resistance heater.

---

* The original nozzle used in the experiment was later replaced by an improved nozzle.

The reservoir pressure was held constant within $\pm$ 0.04 psi during the operation of the tunnel by means of a differential pressure controller. The supply temperature was maintained within $\pm$ 3 deg. F. by means of a pneumatic controller, using standard thermocouple input, regulating the power to the electric heater.

All tests were made with a reservoir pressure of 300 psig and a supply temperature of 700 deg. F. Under this condition Mach number and Reynolds number per inch in the test section were 7.7 and $1.73 \times 10^5$, respectively, and a preliminary test showed that the air was free of condensation in the test section, and that the static pressure was constant within $\pm$ 4 per cent along the centerline of the tunnel.

The stainless-steel hemisphere cylinder model was 10 in. long and 0.75 in. diameter, and was supported from the rear by a sting of 0.5 inch diameter. For the measurement of the pressures there were fifteen orifices along the surface. Four orifices were located at $45^\circ$ from the nose, spaced equally around the axis, on the hemisphere cap, and these were used to align the model with the flow direction.

The "power-law" models were made of brass, and their shape and dimensions were

(1) "3/4-power" bodies, $r/r_{max} = (x/L)^{3/4}$

(1-a) $r_{max} = 0.75$ in., $L = 1.545$ in.

(1-b) $r_{max} = 0.75$ in., $L = 3.19$ in.

(2) "2/3-power" bodies, $r/r_{max} = (x/L)^{2/3}$

(2-a) $r_{max} = 0.75$ in., $L = 1.442$ in.

(2-b) $r_{max} = 0.75$ in., $L = 3.19$ in.

(3) "1/2-power" bodies, $r/r_{max} = (x/L)^{1/2}$

(3-a) $r_{max} = 0.75$ in., $L = 1.236$ in.

(3-b) $r_{max} = 0.75$ in., $L = 3.19$ in.

Pressure orifices of 0.013 in. diameter were located at distances of every tenth of the total length from the nose. At the last station three orifices were provided, equally spaced about the axis, for aligning the model to the flow direction. Figure 14 shows the construction of these models.

A total pressure probe, of the type commonly used in boundary layer surveys, with a frontal height of 0.005 inch, was used in the survey of the flow about the models.

The surface pressures were measured by means of a multi-tube vacuum-referenced silicone oil manometer. The total pressures were measured by a vacuum-referenced mercury micromanometer.

The shock wave shapes were obtained from the schlieren photographs of the flow by means of the Kodak Contour Projector optical comparator.

## 2. Test Procedure

A preliminary test was made to determine the minimum supply temperature for condensation-free flow in the test section. The test consisted of measuring the impact pressure and the static pressure at a fixed location as the supply temperature was varied. When the components of the air condense, the static pressure increases above its value without condensation. On the other hand, the impact pressure is affected little by the condensation. Therefore, when the Mach

number computed from the ratio of the static pressure to the reservoir pressure using the dry isentropic relation agrees with the Mach number computed from the impact pressure and the reservoir pressure, it is assumed that the air in the test section is in one phase. Thus it was found that the minimum temperature was 700°F. at the supply pressure of 315 psia. and Mach number 7.7 (Figure 15). All subsequent tests were made under these conditions.

All models were tested at zero yaw and positioned on the tunnel axis. After the pressure leads were connected to the manometer, the system was tested for leaks. The tunnel was operated for at least three hours to allow the equilibrium condition to establish before taking readings. Surface pressure measurements were taken with a model in three rotational positions 120° apart around the axis of revolution and mean values were taken to eliminate some of the effects of the flow non-uniformity in the test section. The impact pressure surveys were made in the plane normal to the axis of revolution at stations 0.3, 0.5, 0.7, 0.9 of the total length from the nose of "power law" models and at a station three diameters downstream from the nose of the hemisphere-cylinder model.

### 3. Data Reduction

Because of the mounting mechanism employed, it was difficult to align the model perfectly with the flow, and a correction was applied to the surface pressure data in the following manner: By assuming that the surface pressure is proportional to the square of the cosine of the angle between the free stream direction and the normal to the surface, the misalignment angle was computed from the three pressures measured at the last station and the corrections of the order of 5 per

cent were made accordingly to other pressure readings.

The shock wave coordinates were measured from the schlieren photographs of the flow by means of an optical comparator. The accuracy of the instrument was within 0.0001 inch, and the repeatability of the shock wave measurement was within 0.002 inch, depending largely on the sharpness of the image. The coordinates of the body profile were measured at the same time to check distortions of the images and they were found to be not discernible within the accuracy of measurement. From the measured coordinates the local inclination of the shock wave and the local strength of the shock were computed. In order to improve the accuracy of the results, the following procedure was used: First, an analytic expression which fitted the shock shape best was obtained by the least-square method, and the differences between the measurement and the calculation were obtained and plotted with ordinates stretched. A smooth curve was faired in the last plot, and its slope was obtained graphically. The shock wave slope was the sum of the slope computed from the best-fit analytical expression and the small correction ($\sim$10 per cent) obtained graphically. It is believed that by this means the shock slope was computed within a couple of per cent.

From the impact pressure data and the shock strength, the flow quantities were computed by the following method:

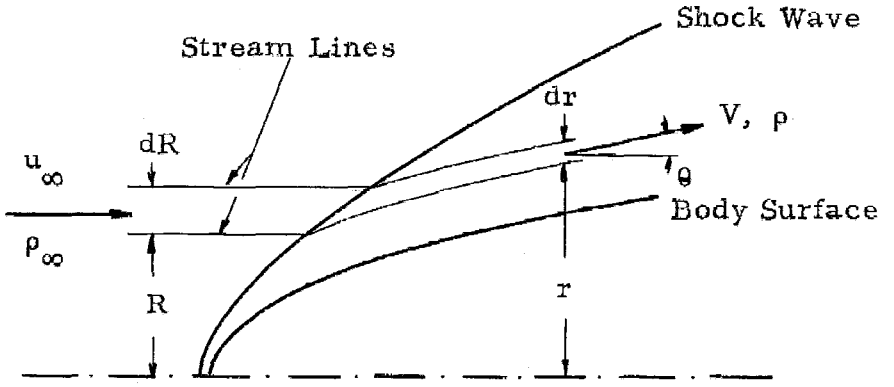


From the continuity of the mass flow

$$\rho_\infty u_\infty \cdot 2\pi R\, dR = \rho V \cos\theta \cdot 2\pi r\, dr$$

and by rearranging the factors

$$\frac{dr}{dR} = \frac{\rho_\infty}{\rho_{0\infty}} \frac{u_\infty}{a^*} \frac{R/r}{(p_0/p_{0\infty})(\rho/\rho_0)(V/a^*)\cos\theta}$$

where $\rho/\rho_0$, $V/a^*$ are obtained by the isentropic relations using Mach number computed from the ratio of the local impact pressure $p_0'$ to the local stagnation pressure $p_0$. From the measured shock shape, the stagnation pressure $p_0$ was computed as a function of R. From the survey of the flow in the transverse plane, $p_0'$ was known as a function of r. Since the flow direction immediately behind the shock was almost equal to the slope of the body surface, the flow direction was assumed to be constant from the body to the shock. Then, the above equation became the differential equation relating r and R.

The equation was integrated numerically step-by-step starting

from the shock, where $p_o$ and M were known and also r = R. In the course of the integration the profiles of Mach number and stagnation pressure were obtained, from which other flow variables were computed.

### 4. Discussion of Accuracy

The surface pressures were measured with less than one per cent error.

The total pressure profile may contain errors due to (a) probe location (b) probe error. The probe locations were accurate within 0.001 inch. Since the flow behind the bow shock is not uniform, the total pressure probe was not always perfectly aligned with the flow direction. The misalignment was, however, not more than $5^o$, and the error caused by misalignment in the measured pressure was less than 0.5 per cent.[14] The probe errors due to velocity gradient and low Reynolds number effect were very small except in viscous boundary layers.

The errors contained in the computed profiles were difficult to estimate quantitatively, since they were caused not only by errors in the data from which the profiles were computed, but also by the error of step-by-step integration. It is felt that the computed profiles were accurate to within five per cent.

## B. Results and Discussion

### 1. Hemisphere-Cylinder

The surface pressure distribution on the hemisphere-cylinder model is presented in Figure 16 as a plot of $p/p_{max}$ versus s/d where

s is the length along the surface of the model measured from the axis of symmetry, and d is the diameter of the cylinder. Also plotted in the figure are the modified Newtonian approximation and the Prandtl-Meyer expansion over the hemispherical part and the pressure predicted by the analogy with the axially-symmetric blast wave theory.

According to the blast wave theory[8, 9, 10], the surface pressure on the cylindrical afterbody for $M_\infty = 7.7$, $\gamma = 1.40$ is given by

$$p/p_\infty = 0.394/(x/d)$$

in the first approximation, and by

$$p/p_\infty = 0.394/(x/d) + 0.405$$

in the second approximation.[9] The slow decay of the pressure over the afterbody is predicted closely by the second approximation.

For this case the shock wave shape given by the strong blast wave theory is found to be for $M_\infty = 7.7$, $\gamma = 1.4$

$$R/d = 0.78\,(x/d)^{\frac{1}{2}}$$

and the second approximation gives the result

$$R/d = 0.78\,(x/d)^{\frac{1}{2}}\left[\,1 + 0.027\,(x/d)\,\right]$$

In Figure 17 these predicted shock shapes are compared with the shock shape determined from schlieren photographs. Evidently the local slope of the shock is closely reproduced by the blast wave analogy; in fact the experimental and theoretical shock wave ordinates differ by an almost-constant amount of 0.3 d. A better agreement between the theory and the experiment can be obtained by choosing an "effective origin" at about 0.5 diameter upstream of the stagnation

point of the body.* A further study, however, is necessary to account properly for the effect of the finite diameter of the body.

The modified Newtonian approximation $C_p/C_{p_{max}} = \cos^2 \theta$ predicts the pressure over the nose portion with good accuracy, but starts deviating from the measured values as the junction of the hemispherical nose and the cylindrical afterbody is approached. In this region an attempt was made to predict the pressure by the Prandtl-Meyer expansion $dp/p = -(\gamma M^2/\sqrt{M^2-1})\, d\theta$ matched to the Newtonian approximation at the point where both the pressure and the pressure gradient given by these two formulae are equal.

From the Newtonian approximation

$$p = (p_{max} - p_\infty) \cos^2 \theta + p_\infty$$

By differentiating with respect to $\theta$

$$dp/d\theta = -2 (p_{max} - p_\infty) \cos \theta \sin \theta$$

By equating this value of $dp/d\theta$ and the Prandtl-Meyer expansion and using the value of p given by the Newtonian formula, one obtains

$$\frac{2(p_{max} - p_\infty) \cos \theta \sin \theta}{(p_{max} - p_\infty) \cos^2 \theta - p_\infty} = \frac{\gamma M^2}{\gamma \sqrt{M^2 - 1}}$$

where Mach number is computed by the isentropic relation from $p/p_{max}$ using $p_{max}$ as the stagnation pressure. At Mach number of 7.7, the matching is effected at $s/d = 0.485$ (or $\theta = 66.2^\circ$), where the

---

* This idea was suggested by W. Chester of Bristol University (Visiting Research Fellow, California Institute of Technology, 1956-57).

local Mach number is 1.37. This approximation is seen to agree very well with the experiment up to the junction of the nose and the afterbody.

The impact pressure profile at x/d = 3 is shown in Figure 18. The other profiles shown in Figure 19 were computed from the experimental data on the impact pressure and the shock wave. The local-stagnation-pressure gradient is quite large, as expected for the flow behind a highly curved shock wave in high Mach number flow. Outside the viscous boundary layer the flow may be regarded as isoenergetic, and the stagnation pressure gradient is related to the vorticity by Crocco's vortex theorem

$$|\Omega| = (1/V) \left| \text{grad } H - T \text{ grad } S \right| = \{V/(\gamma M^2 p_o)\} \left| \text{grad } p_o \right|$$

It was found that, immediately outside the viscous boundary layer, the vorticity is less than one per cent of the vorticity in the boundary layer, and its effect may not be important. However, at Reynolds number much lower than the present experiment, or at stations further downstream from the nose, the boundary layer emerges from the wake of the nearly normal part of the bow shock wave and grows into a region of large entropy gradient, and the vorticity at the edge of the boundary layer becomes larger, and its effect on the boundary layer may become appreciable.

In Figure 20 the static pressure profile is compared with that computed by the blast-wave analogy. The close agreement between the experiment and the second approximation is rather surprising since the blast-wave theory does not take into account the presence of the afterbody of finite diameter.

## 2. "3/4- and 2/3- Power Bodies"

The surface pressure distributions on "3/4-power" and "2/3-power" bodies of revolution are plotted in Figures 21a and 21b in the form $C_p$ versus x/L. Also plotted in the figures are the values given by

Newtonian flow theory (with centrifugal force correction)

Similar-flow solution

It is seen that the Newtonian flow theory prediction is consistently lower than the experiment. For slender bodies the similarity solution predicts the pressure distribution quite closely when the effect of the viscous boundary layer is taken into account (B. 5). The agreement is poor for thicker bodies because of the fact that the similarity solution is based on the hypersonic small disturbance equations.

The shock wave locations for these bodies are presented in Figures 22a and 22b. In these plots solid lines drawn through shock points represent curves similar to the body shape. For thicker models the shock waves are seen to be similar to the body shapes, but for the slender models the bow shocks are not quite similar to the body shapes. The best-fit expressions for the experimental data are

$$r_b \sim x^{3/4}; \quad R/r_b = 1.27 \text{ for } \delta = 0.485$$

$$R/r_b = 1.29\left[1 + 0.081\,(x/L)^{\frac{1}{2}}\right] \text{ for } \delta = 0.235$$

$$r_b \sim x^{2/3}; \quad R/r_b = 1.28 \text{ for } \delta = 0.520$$

$$R/r_b = 1.31\left[1 + 0.113\,(x/L)^{2/3}\right] \text{ for } \delta = 0.235$$

On the other hand the similarity solution predicts

$$r_b \sim x^{3/4}; \quad R/r_b = 1.143 \left[1 + 0.037 (x/L)^{\frac{1}{2}}\right] \text{ for } \delta = 0.485$$

$$R/r_b = 1.143 \left[1 + 0.158 (x/L)^{\frac{1}{2}}\right] \text{ for } \delta = 0.235$$

$$r_b \sim x^{2/3}; \quad R/r_b = 1.192 \left[1 + 0.035 (x/L)^{2/3}\right] \text{ for } \delta = 0.520$$

$$R/r_b = 1.192 \left[1 + 0.170 (x/L)^{2/3}\right] \text{ for } \delta = 0.235$$

The causes of the discrepancy between the theory and the experiment are:

(a) As shown by the total pressure profiles (Figure 23) the viscous boundary layer thickness is an appreciable fraction of the distance between the shock and the body, and the effective body shape is considerably altered from the geometrical shape by the displacement thickness.

(b) Strictly speaking, the theory is applicable only for very strong shock waves or $(\gamma - 1) M_\infty^2 \delta^2/2 >> 1$. When this parameter is close to or less than one, a large error occurs in the predicted density distribution (Figure 24). However, the computed pressure profile shows a relatively small variation with the parameter, as seen in Figure 25, and the pressure field is predicted quite accurately even by the first approximation ($M_\infty \longrightarrow \infty$).

Figure 26 shows the profiles of flow variables computed from experimental data at the nine-tenth station of the "2/3-power" slender body. One important feature of this flow is that the local stagnation pressure gradient is quite high at the edge of the boundary layer. In boundary layer calculations one ordinarily assumes that every flow variable is known outside the viscous layer, either from inviscid flow calculations or from surface pressure measurements. However, around a body which produces a shock wave with large curvature, the

stagnation pressure changes rapidly with normal distance near the surface. The actual stagnation pressure, and in turn the Mach number and temperature at the edge of the boundary layer, depend on the mass flow in the layer, which determines where the streamline at the edge of the layer crossed the bow shock. For example, with the model tested, if the stagnation pressure at the edge is assumed to be the value behind a normal shock the Mach number at the edge is 2.7, while the measured value is 5.1. This result suggests the necessity for further study of this interaction effect.

### 3. Paraboloids of Revolution

The similar flow solution investigated in Part II and also the Newtonian flow theory of Cole* break down for paraboloids of revolution. Both theories are based on the hypersonic small-disturbance theory. Evidently the nose of paraboloid is too blunt, and its effect is felt throughout the disturbed flow field. (It is interesting to note that the radius of curvature at the nose is zero for $m > \frac{1}{2}$ but finite for $m = \frac{1}{2}$, and that the supersonic small-perturbation theory for slender bodies of revolution breaks down also as $m \longrightarrow \frac{1}{2}$.) At the present time, no theory is available which is capable of accurately predicting the flow around bodies with round nose.

The surface pressure distributions measured on two paraboloid models are presented in Figure 27 as a plot of pressure coefficients versus x/L. Also plotted in the figure are the modified Newtonian

---

* This fact was not pointed out in Cole's paper, but the shock distance from the body computed by his formula becomes infinite for paraboloids of revolution.

approximation $C_{p_{max}} \cos^2 \theta$ and the Newtonian flow approximation including centrifugal force correction. The latter approximation[3, 4, 15] is

$$C_p = \frac{(1/4)\delta^2}{\bar{x} + 1/4\,\delta^2} + \frac{(\frac{1}{2}\delta)^4}{\bar{x}^{\frac{1}{2}}(\bar{x} + 1/4\,\delta^2)^{3/2}} \ln \frac{\bar{x}^{\frac{1}{2}} + \sqrt{\bar{x} + (1/4)\delta^2}}{\frac{1}{2}\delta}$$

for arbitrary values of $\delta$ and reduces to

$$C_p = (1/4)\delta^2/\bar{x}$$

for small $\delta$ as given by Cole.[2]

The modified Newtonian approximation agrees with the experiment on the blunt model, but the agreement is poor on the slender model, where boundary layer effects may be important. The Newton-Busemann flow theory seems to overestimate the effect of centrifugal force.

The shock locations for the two models are presented in Figure 28, where $(r/L)^2$ is plotted against $(x/L)$. For the model of $\delta = 0.60$, the shock wave is also parabolic near the nose, and the stand-off distance and the radius of curvature at the nose are 0.178 and 1.72, respectively, in terms of the radius of curvature of the model at the nose. A theoretical analysis has been made by W. Chester[18] to predict the flow around a paraboloid in hypersonic flow. His analysis gives the shock stand-off distance and the radius of curvature as 0.12 and 1.25 of the body radius at the nose. The analysis of Li and Geiger[19], which also assumes a very large density ratio across the shock and incompressible flow behind the shock, gives a value of 0.115 of the nose-radius for the shock stand-off distance. Their analysis makes no

distinction between the shock curvature and the body curvature.

When the stand-off distance is normalized by the shock radius, the experimental value agrees closely with theoretical predictions.

The measured shock wave of the slender model was not parabolic and the best-fit expression is

$$R/L = 0.317\,(x_s/L)^{\frac{1}{2}}\left[1 + 0.238\,(x_s/L)\right]$$

where $x_s$ is the distance measured along the axis from the vertex of the shock.

The flow quantity profiles at the nine-tenth station of the slender body are shown in Figure 30. They are seen to be similar to those for the "2/3-power" model. The static pressure outside the boundary layer is lower than the measured surface pressure. A similar phenomenon was observed on a flat plate at Mach number 5.8 by Kendall[14], but in the present case it may have been caused by the accumulation of errors.

## 4. Foredrag Coefficient

The foredrag coefficients in Figure 23, which were obtained by integrating the pressure distributions, are presented as the ratio of the drag of the test body to the drag of a cone of the same slenderness versus the exponent in the equation defining the body profile. It shows that the drags of the "3/4-power" and "2/3-power" bodies are less than that of a cone, and at the same time it shows that the experimental points lie appreciably above the theoretical prediction. A large part of the difference can be accounted for by including the boundary layer interaction effect. The modified impact theory of

Eggers, Dennis, and Resnikoff[12] gives the trend of the drag increase with decreasing exponents where the small disturbance theories fail, and the measured drag on paraboloids compares favorably with the prediction.

## 5. Boundary Layer Effect

The survey of the flow field between the shock wave and the body revealed that the boundary layer thickness is appreciable compared with the body radius, and an attempt was made to estimate its effect by using the local similarity concept of Lees[17].

In Reference 17 the displacement thickness is given by

$$\delta^* = \frac{(2\tilde{s})^{1/2}}{r_b \rho_e u_e} \int_0^\infty \left( \frac{\rho_e}{\rho} - \frac{u}{u_e} \right) d\eta$$

where

$$\tilde{s} = \int_0^s \rho_e \mu_e u_e r_b^2 \, ds = \omega \rho_\infty \mu_\infty u_\infty \int_0^s (p_e/p_\infty) \, r_b^2 \, ds$$

assuming $\mu_e/T_e = \text{const.} = \omega \, \mu_\infty/T_\infty$ and $u_e = u_\infty$.

With the additional assumptions

Prandtl number = 1

insulated surface

$$p_e/p_\infty = \gamma M_\infty^2 \frac{F(z_b)}{z_b^2} \left( \frac{dr_b}{dx} \right)^2$$

$s = x$

The growth of the displacement thickness on a body of revolution $r_b \sim x^m$ is described by

$$\frac{\delta^*}{L} = \frac{Z_b}{\sqrt{\gamma F(Z_b)}} \left[ I_1 + \frac{(\gamma-1) M_e^2}{2 + (\gamma-1) M_e^2} I_2 \right] \frac{2 + (\gamma-1) M_\infty^2}{2 M_\infty \delta} \sqrt{\frac{2\omega}{Re_L}} \frac{m}{\sqrt{4m-1}} \left( \frac{x}{L} \right)^{\frac{3}{2} - m}$$

where

$$I_1 = \int_0^\infty \left( 1 - \frac{u}{u_e} \right) d\eta$$

$$I_2 = \int_0^\infty u/u_e \left( 1 - \frac{u}{u_e} \right) d\eta$$

The values of $I_1$ and $I_2$ are obtained from the similar flow solution of an incompressible boundary layer, corresponding to the pressure gradient parameter $\bar{\beta} = \frac{2\tilde{s}}{M_e} \frac{dM_e}{d\tilde{s}}$ (See, for example, Table I, Reference 18.)

The parameter $\bar{\beta}$ is given approximately by the relation

$$\bar{\beta} = \frac{2 + (\gamma - 1) M_e^2}{2 \gamma M_e^2} \frac{4(1 - m)}{4m - 1}$$

by using the same assumptions as before.

When Mach number is much larger than unity everywhere, the above expressions reduce to

$$\frac{\delta^*}{L} = \frac{\gamma - 1}{\sqrt{2\gamma}} \frac{Z_b}{\sqrt{F(Z_b)}} \frac{M_\infty}{\delta} \sqrt{\frac{\omega}{Re_L}} \frac{m}{\sqrt{4m-1}} \left( \frac{x}{L} \right)^{\frac{3}{2} - m}$$

$$\bar{\beta} = \frac{\gamma - 1}{\gamma} \frac{2(1 - m)}{4m - 1}$$

The surface pressure distribution is corrected for the boundary layer approximately by

$$C_p = \frac{2F(Z_b)}{Z_b^2} \left( \frac{dr_b}{dx} + \frac{d\delta^*}{dx} \right)^2$$

where the value of $2F(z_b)/z_b^2$ corresponds to the value of m for the geometrical shape.

For $\gamma = 1.40$, $M_\infty = 7.7$, $Re_L = 5.5 \times 10^5$, $\delta = 0.235$

m = 2/3: $C_p = 0.0424\,(x/L)^{-2/3}\left[1 + 0.204\,(x/L)^{\frac{1}{2}}\right]$

m = 3/4: $C_p = 0.0637\,(x/L)^{-\frac{1}{2}}$

From the equation for $\delta^*/L$ it is seen that $\delta^* \sim x^{3/4}$ for $r_b \sim x^{3/4}$, i.e., the boundary layer growth is similar to the body shape, and in this case the transverse flow field exhibits complete similarity as pointed out by Stewartson[19] for the two-dimensional case and by Yasuhara[20] for the axially-symmetric case.

From the expression for $\delta^*/L$, the ratio of the displacement thickness to the body radius is given by the relation

$$\frac{\delta^*}{r_b} = \frac{(\gamma-1)\,z_b\sqrt{\omega}}{\sqrt{2\gamma F(z_b)}}\,\frac{M_\infty}{\delta^2\sqrt{Re_L}}\,\frac{m}{\sqrt{4m-1}}\left(\frac{x}{L}\right)^{\frac{3}{2}-2m}$$

which is proportional to $1/\delta^2$, and the interaction of the boundary layer becomes more important as the body becomes more slender.

# IV. SUMMARY OF RESULTS

## A. Theoretical Investigation

(1) A similar flow field is possible for $M_\infty \longrightarrow \infty$ and for slender bodies of the form $r_b \sim x^m$ provided $m' < m \leq 1$ where $m' = 2/3$ for two-dimensional case and $m' = 1/2$ for axially-symmetric case. In these cases, the shock wave is similar to the body shape, and the surface pressure is given by a relation of the form

$$C_p = f(m, \gamma) \cdot (dr_b/dx)^2$$

(2) In the case of a blunt-nosed circular cylinder (or a flat plate with a blunt leading-edge) at zero angle of attack, the energy of the transverse flow is constant with respect to the distance from the nose. The solution for this case is a singular limit of the solutions for a class of bodies of the form $r_b \sim x^m$ as $m \longrightarrow m'$, and the shock shape and the pressure on the afterbody are described by the relations of the form

$$R/d \sim (C_{D_N})^{1/(3+k)} \; (x/d)^{2/(3+k)}$$

and

$$C_p \sim (C_{D_N})^{2/(3+k)} \; (x/d)^{-2(1+k)/(3+k)}$$

(3) The results from the similarity theory agree closely with those from the Newtonian flow theory for m close to unity, but the agreement becomes poorer as $m \longrightarrow m'$.

## B. Experimental Investigation

### 1. Hemisphere-Cylinder

(a) The slope of the shock wave and the pressure distribution on the afterbody agreed closely with the prediction of the blast-wave analogy. However, the difference between the measured location of the shock and the predicted location indicates the necessity for further study of the effect of finite diameter of the afterbody.

(b) The pressure distribution on the hemisphere agreed very closely with the modified Newtonian approximation plus Prandtl-Meyer expansion.

### 2. "Power-law" Bodies

(a) The pressure distributions on the slender models agreed with theoretical predictions with the boundary layer correction. The pressures on the thicker models were proportional to the square of sine of local slope of the body and agreed closely with the modified Newtonian approximation.

(b) The shock wave was found to be similar to the body shape for the thicker models, but for the slender models the decay of the bow shock was not as rapid as the similar-flow theory predicted.

(c) The total pressure profile was found to possess a large gradient near the boundary layer, which suggests the need for a critical examination of the boundary layer calculation for these bodies.

3. Paraboloids of Revolution

(a) The surface pressure distributions agreed closely with the modified Newtonian approximation, and they were markedly higher than the prediction of the Newtonian flow theory which includes the centrifugal force effect.

(b) The shock wave was also parabolic around the nose, but its stand-off distance and radius of curvature at the nose were considerably larger than theoretical predictions.

These results suggest that it would be worthwhile to investigate further the following:

(1) The inviscid flow around "similar-flow" bodies at small angle of attack.

(2) The behavior of the solution for $\gamma \cong 1$ and $m \cong m'$.

(3) The effect of the finite diameter of the cylindrical afterbody and a proper procedure for joining the solution around the nose to the solution in the downstream region.

(4) The boundary layer interaction including the effects of vorticity outside the boundary layer, and also including the effects of transverse curvature for slender bodies of revolution.

## REFERENCES


1. Hayes, W. D.: On Hypersonic Similitude. Quarterly of Applied Mathematics, Vol. 5, No. 1, pp. 105-106, April, 1947.

2. Cole, J. D.: Newtonian Flow Theory for Slender Bodies. RAND Corporation, RM-1633, 13 February 1956.

3. Busemann, A.; Flüssigkeits-und-Gasbewegung. Handwörterbuck der Naturwissenschaften, pp. 275-277, Zweite Auflage (Gustav Fischer, Jena), 1933.

4. Ivey, H. R.; Klunker, E. G.; and Bowen, E. N.: A Method for Determining the Aerodynamic Characteristics of Two- and Three-Dimensional Shapes at Hypersonic Speeds. NACA TN 1613, 1948.

5. Lees, L.: Inviscid Hypersonic Flow over Blunt-Nosed Slender Bodies. GALCIT Hypersonic Research Project, Memorandum No. 31, February 1, 1956.

6. Lees, L. and Kubota, T.: Inviscid Hypersonic Flow over Blunt-Nosed Slender Bodies. Journal of the Aeronautical Sciences, Vol. 24, No. 3, pp. 195-202, March, 1957.

7. Taylor, G. I.: The Formation of a Blast Wave by a Very Intense Explosion. Part I. Theoretical Discussion. Part II. The Atomic Explosion of 1945. Proc. Roy. Soc. (A), Vol. 201, No. 1065, pp. 159-186, March, 1950.

8. Sakurai, A.: On the Propagation and Structure of the Blast Wave, I. Journal of the Physical Society of Japan, Vol. 8, No. 5, pp. 662-669, September-October, 1953.

9. Sakurai, A.: On the Propagation and Structure of the Blast Wave, II. Journal of the Physical Society of Japan, Vol. 9, No. 2, pp. 256-266, March-April, 1954.

10. Lin, S. C.: Cylindrical Shock Waves Produced by Instantaneous Energy Release. Journal of Applied Physics, Vol. 25, No. 1, pp. 54-57, January, 1954.

11. Cheng, H. K. and Pallone, A. J.: Inviscid Leading-Edge Effect in Hypersonic Flow. Readers' Forum, Journal of the Aeronautical Sciences, Vol. 23, No. 7, pp. 700-702, July, 1956.

12. Eggers, A. J.; Dennis, D. H.; and Resnikoff, M. M.: Bodies of Revolution Having Minimum Drag at High Supersonic Airspeeds. NACA TN 3666, February, 1956.

13. Latter, R.: Similarity Solution for a Spherical Shock Wave. Journal of Applied Physics, Vol. 26, No. 8, pp. 954-960, August, 1955.

14. Kendall, J. M., Jr.: An Experimental Investigation of Leading Edge Shock Wave Boundary Layer Interaction. Thesis, California Institute of Technology. Also, Journal of the Aeronautical Sciences, Vol. 24, No. 1, pp. 47-56, January, 1957.

15. Chester, W.: Supersonic Flow Past a Bluff Body with a Detached Shock, Part II. Axisymmetrical Body. Journal of Fluid Mechanics, Vol. 1, Part 5, pp. 490-496, November, 1956.

16. Li, T. Y. and Geiger, R. E.: Stagnation Point of a Blunt Body in Hypersonic Flow. Journal of the Aeronautical Sciences, Vol. 24, No. 1, pp. 25-32, January, 1957.

17. Lees, L.: Laminar Heat Transfer over Blunt-Nosed Bodies at Hypersonic Flight Speeds. Jet Propulsion, Vol. 26, No. 4, pp. 259-269, April, 1956.

18. Smith, A. M. O.: Rapid Laminar Boundary-Layer Calculations by Piecewise Application of Similar Solutions. Journal of the Aeronautical Sciences, Vol. 23, No. 10, pp. 901-912, October, 1956.

19. Stewartson, K.: On the Motion of a Flat Plate at High Speed in a Viscous Compressible Fluid. II. Steady Motion. Journal of the Aeronautical Sciences, Vol. 22, No. 5, pp. 303-309, May, 1955.

20. Yasuhara, M.: On the Hypersonic Viscous Flow Past Slender Bodies of Revolution. Journal of the Physical Society of Japan, Vol. 11, No. 8, pp. 878-886, August, 1956.

21. Staff of the Computing Section, Center of Analysis (under the direction of Zdenek Kopal): Tables of Supersonic Flow Around Cones. Technical Report No. 1, Massachusetts Institute of Technology, Department of Electrical Engineering, Center of Analysis, 1947.

# TABLE I

## SUMMARY OF RESULTS OF INTEGRATION FOR AXIALLY-SYMMETRIC FLOW

$\gamma = 1.67$

| m | $z_b$ | $F(z_b)$ | $a_1$ | $f_1(z_b)$ |
|---|---|---|---|---|
| 1/2 | 0 | 0.241 | 0.826 | 0.90 |
| 4/7 | 0.652 | 0.403 | 0.732 | 1.76 |
| 2/3 | 0.776 | 0.544 | 0.663 | 1.93 |
| 3/4 | 0.819 | 0.634 | 0.575 | 1.61 |
| 1 | 0.870 | 0.811 | 0.350 | 0.78 |

$\gamma = 1.40$

| m | $z_b$ | $F(z_b)$ | $a_1$ | $f_1(z_b)$ |
|---|---|---|---|---|
| 1/2 | 0 | 0.311 | 0.937 | 1.07 |
| 4/7 | 0.725 | 0.467 | 0.870 | 2.36 |
| 2/3 | 0.839 | 0.607 | 0.793 | 2.38 |
| 3/4 | 0.875 | 0.696 | 0.677 | 1.93 |
| 1 | 0.915 | 0.875 | 0.396 | 0.92 |

$\gamma = 1.15$

| m | $z_b$ | $F(a_b)$ | $a_1$ | $f_1(z_b)$ |
|---|---|---|---|---|
| 1/2 | 0 | 0.411 | 1.07 | 1.35 |
| 4/7 | 0.845 | 0.553 | 1.15 | 3.53 |
| 2/3 | 0.924 | 0.688 | 0.982 | 3.05 |
| 3/4 | 0.945 | 0.775 | 0.829 | 2.43 |
| 1 | 0.965 | 0.948 | 0.455 | 1.10 |

TABLE II

SHOCK WAVE AND SURFACE PRESSURE OF A CONE

Shock Wave Angle $\theta_w/\theta_c$

| $M \tan \theta_c$ | Present Approx. $\gamma = 1.40$ | Exact $\gamma = 1.405$ | |
|---|---|---|---|
| | | $\theta_c = 5^\circ$ | $\theta_c = 10^\circ$ |
| 0.660 | 1.919 | 1.815 | 1.849 |
| 1.150 | 1.364 | 1.378 | 1.390 |
| 2.469 | 1.149 | 1.163 | 1.168 |
| 3.988 | 1.113 | 1.121 | 1.124 |
| $\infty$ | 1.092 | 1.094 | 1.095 |

Pressure Coefficient $C_p/\theta_c^2$

| $M \tan \theta_c$ | Present Approx. $\gamma = 1.40$ | Exact $\gamma = 1.405$ | |
|---|---|---|---|
| | | $\theta_c = 5^\circ$ | $\theta_c = 10^\circ$ |
| 0.660 | 3.012 | 2.642 | 2.659 |
| 1.150 | 2.395 | 2.330 | 2.320 |
| 2.469 | 2.156 | 2.148 | 2.138 |
| 3.988 | 2.115 | 2.110 | 2.097 |
| $\infty$ | 2.090 | 2.085 | 2.070 |

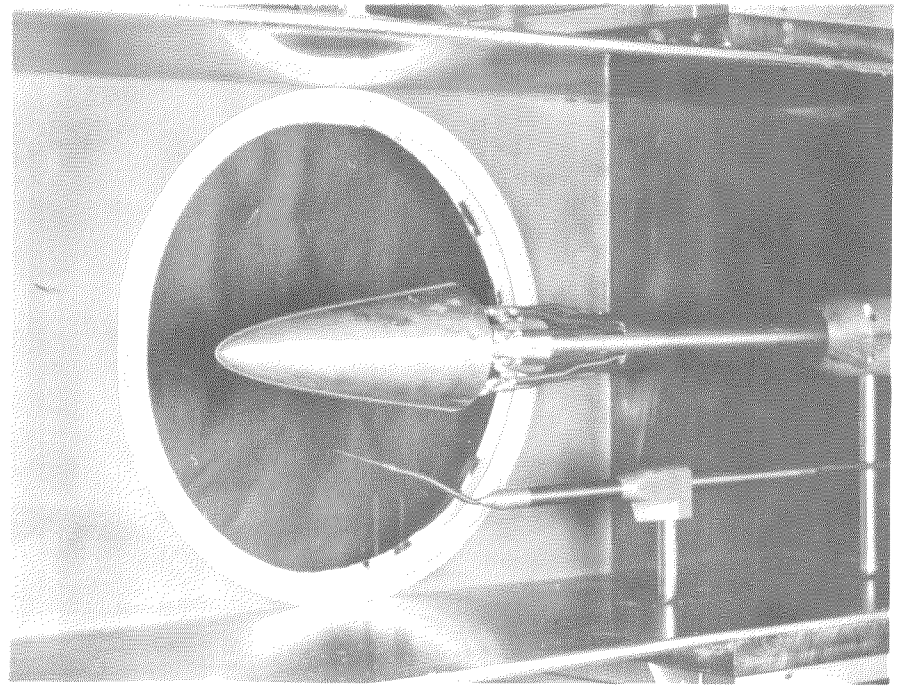

FIG. 1 TYPICAL MODEL INSTALLATION

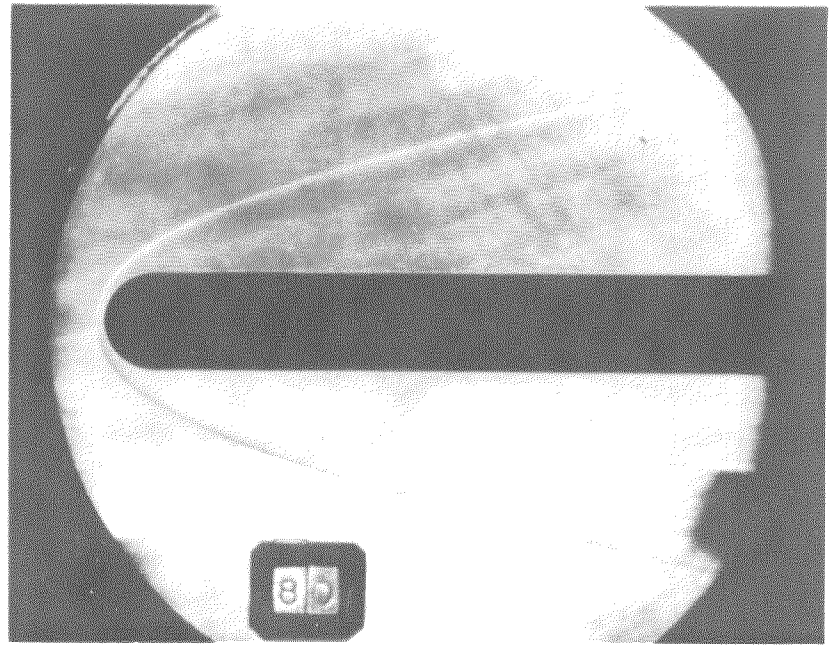

FIG. 2 SCHLIEREN PHOTOGRAPH OF HEMISPHERE CYLINDER

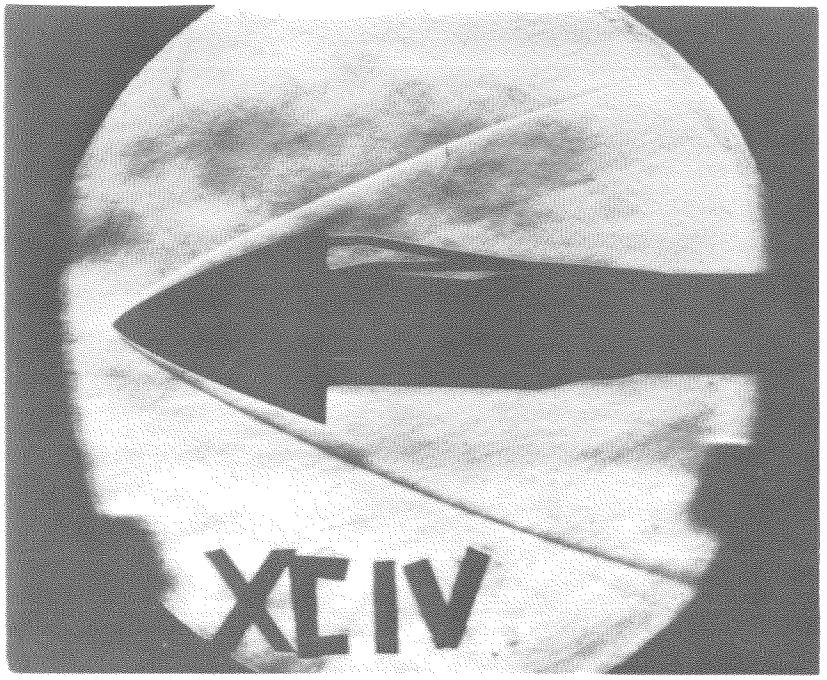


$\delta = 0.485$

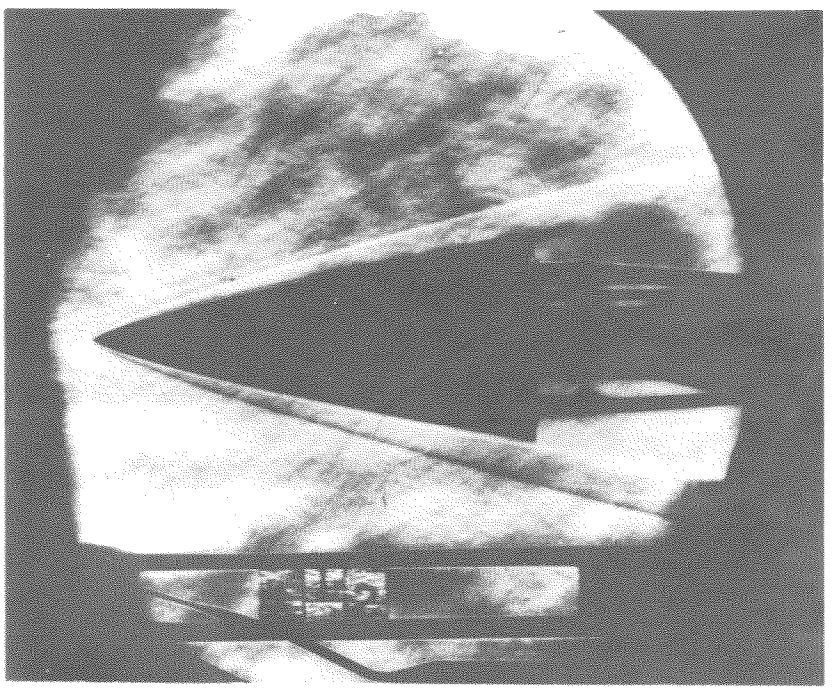

$\delta = 0.235$

FIG. 3 SCHLIEREN PHOTOGRAPH OF "3/4 — POWER" BODY

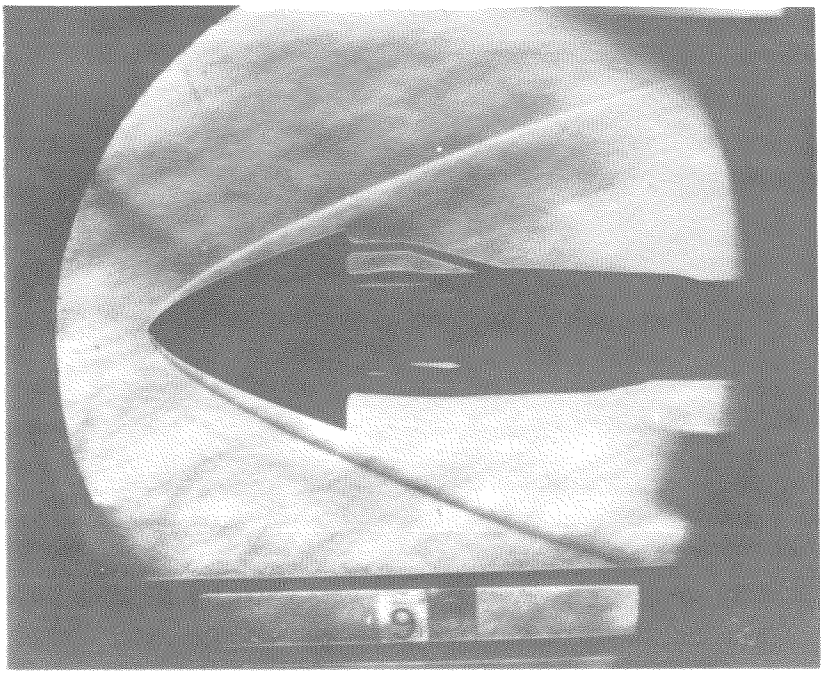

$\delta = 0.520$

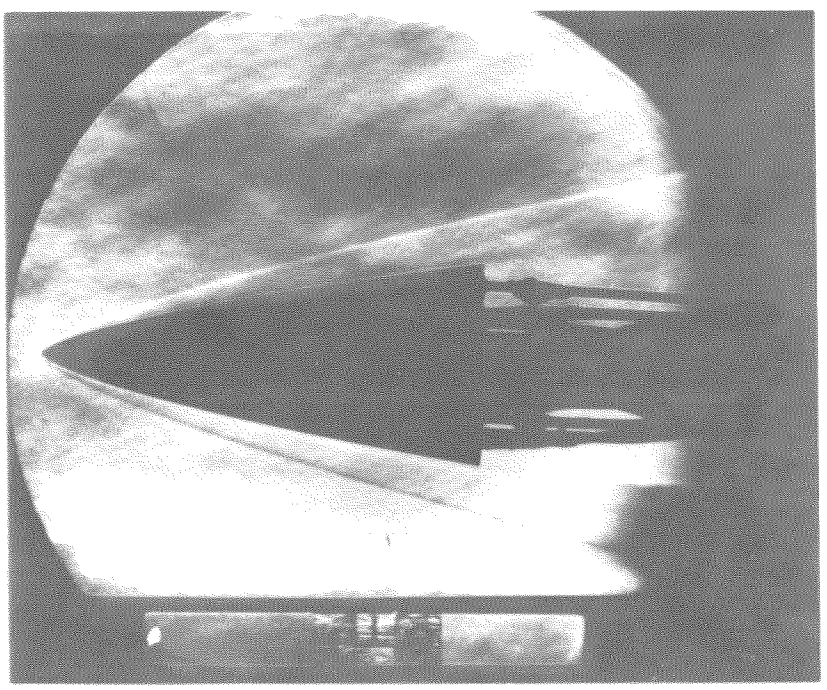

$\delta = 0.235$

FIG. 4 SCHLIEREN PHOTOGRAPH OF "2/3 — POWER" BODY

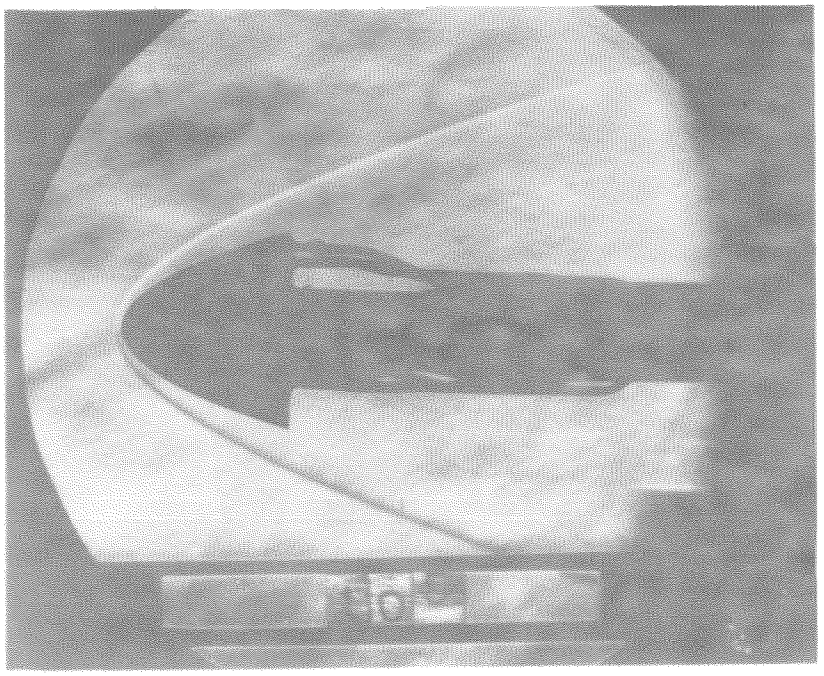

$\delta = 0.607$

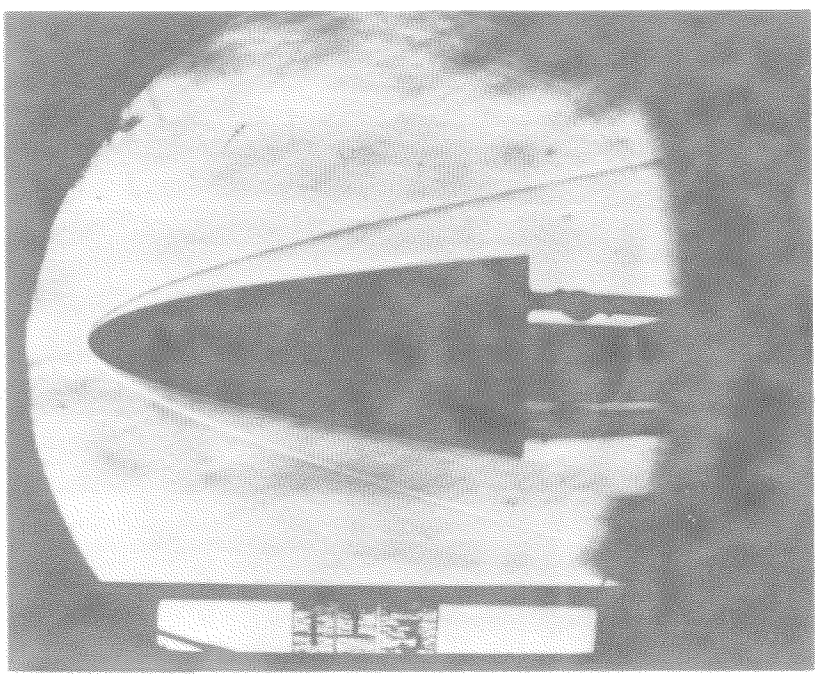

$\delta = 0.235$

FIG. 5 SCHLIEREN PHOTOGRAPHS OF "1/2 – POWER" BODY

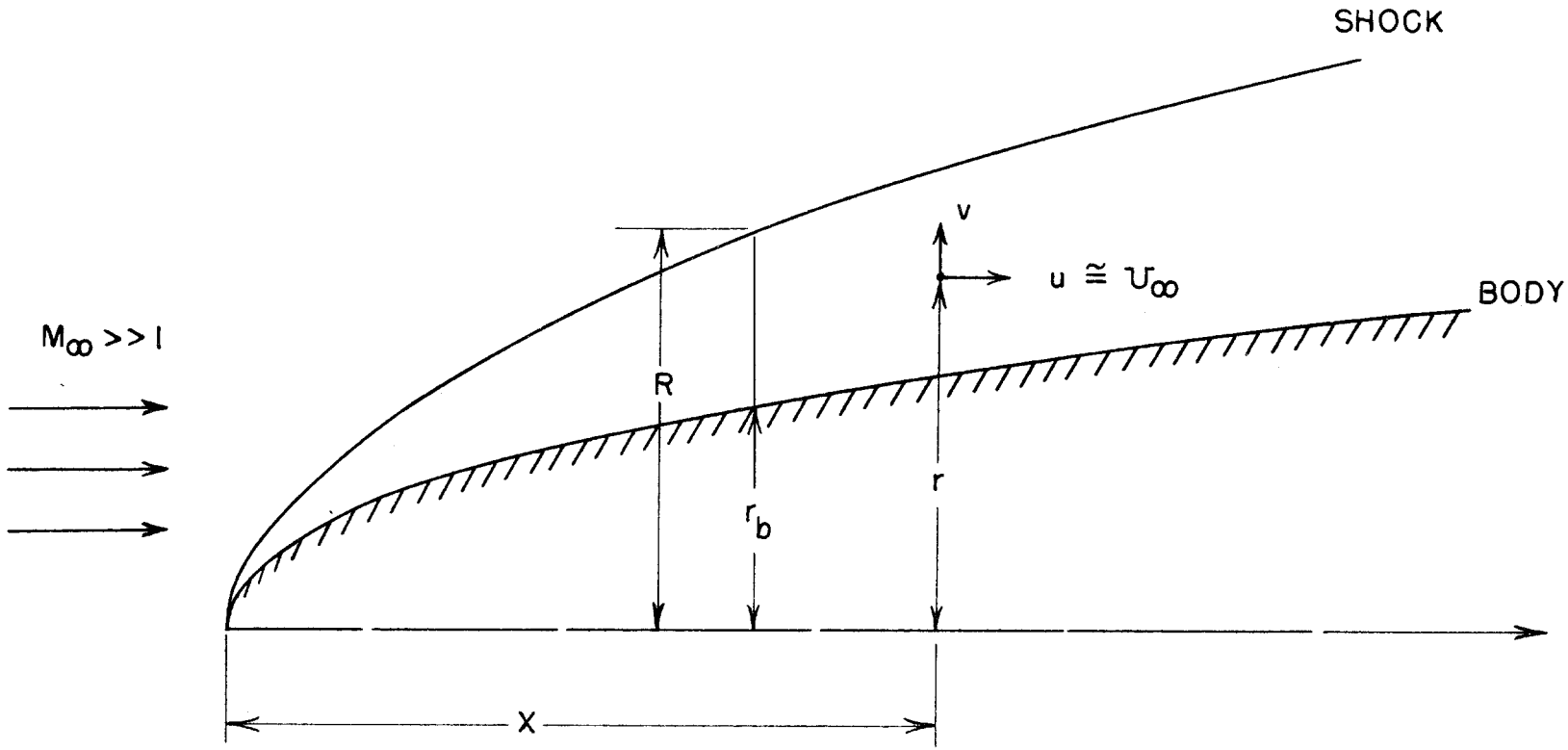


FIG.6- HYPERSONIC INVISCID FLOW OVER A BLUNT-NOSED SLENDER BODY

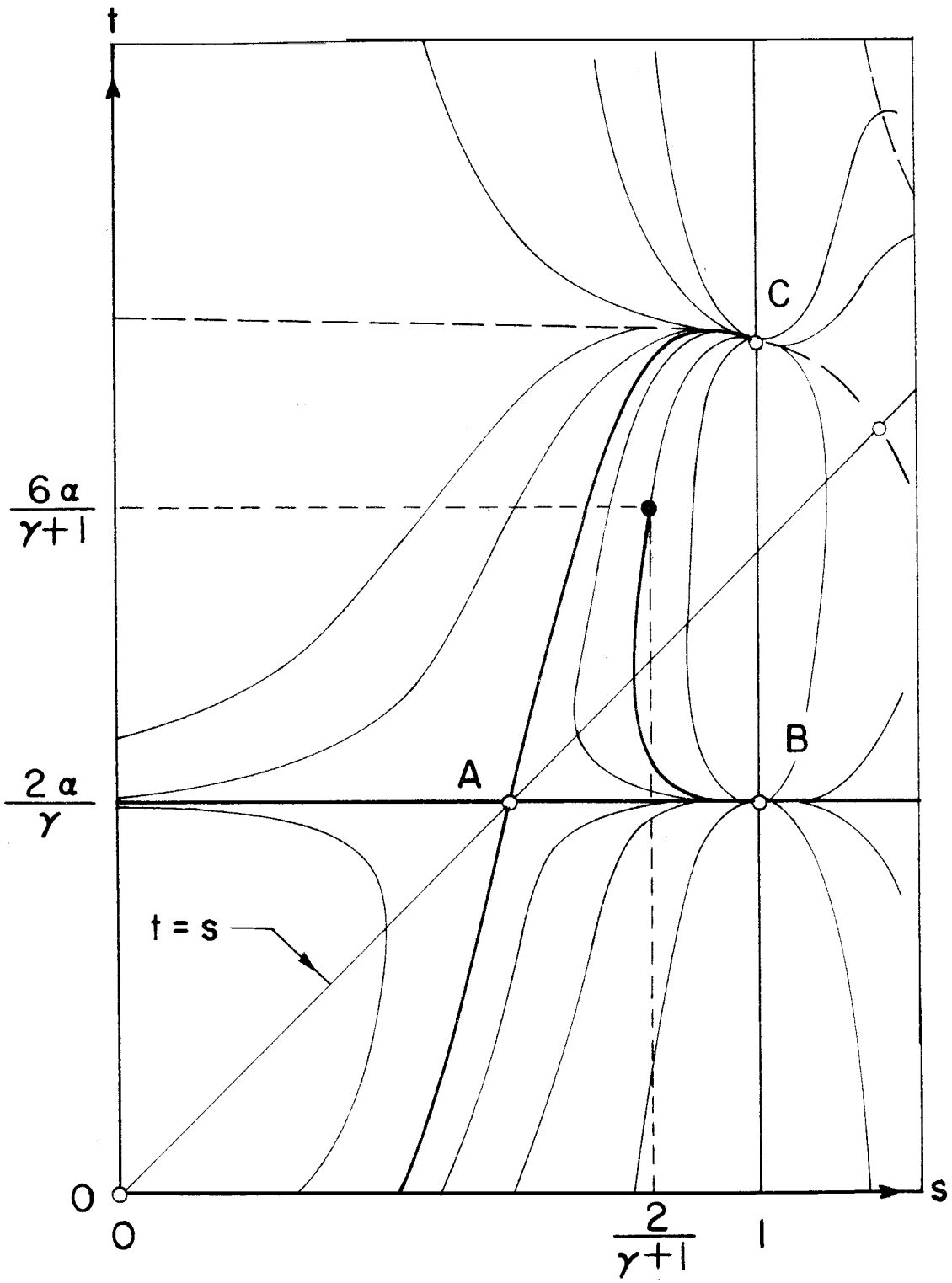


FIG. 7 INTEGRAL CURVES IN s-t PLANE, k = 0

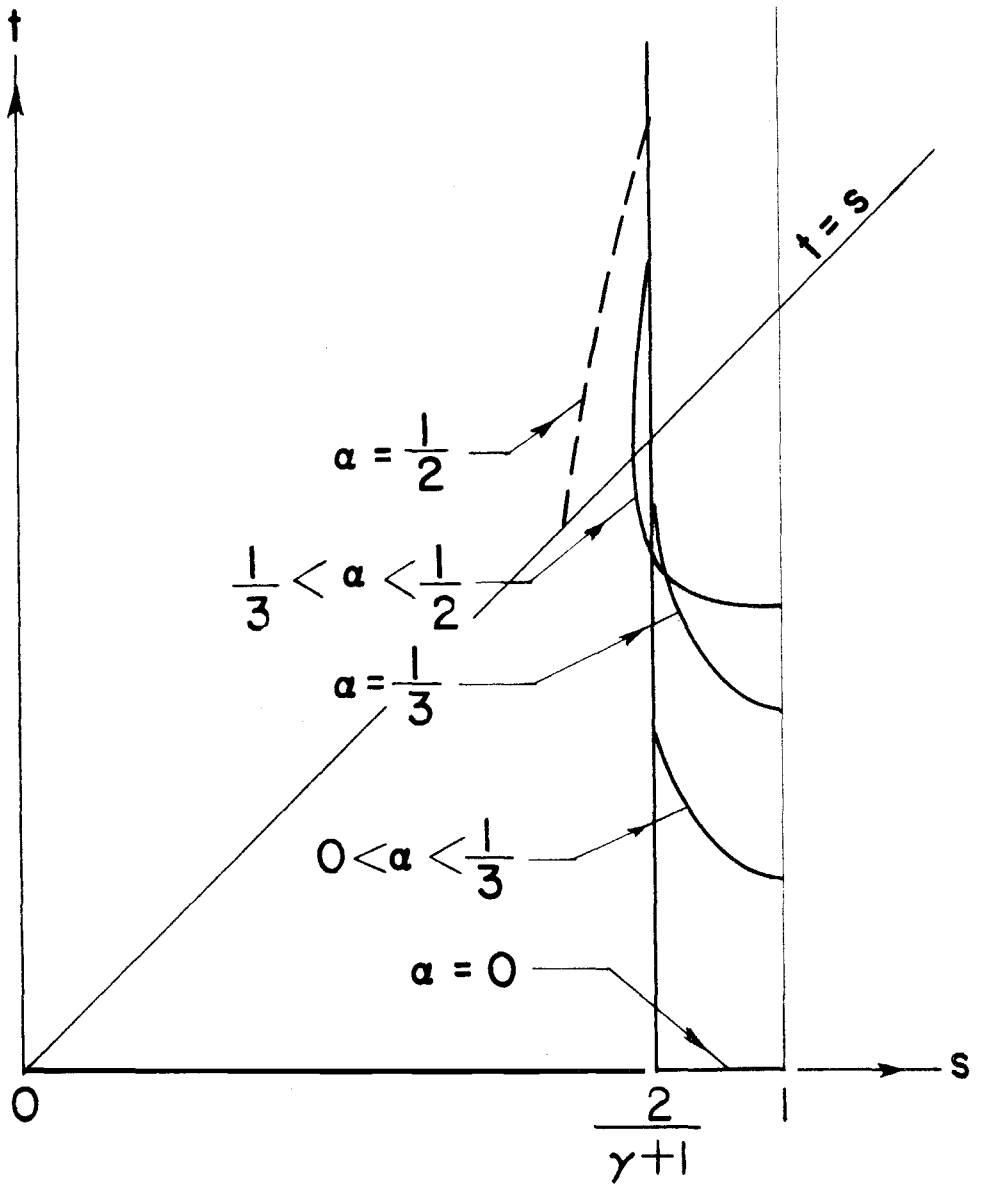


FIG. 8a SOLUTIONS IN s-t PLANE, k=0 (SCHEMATIC)

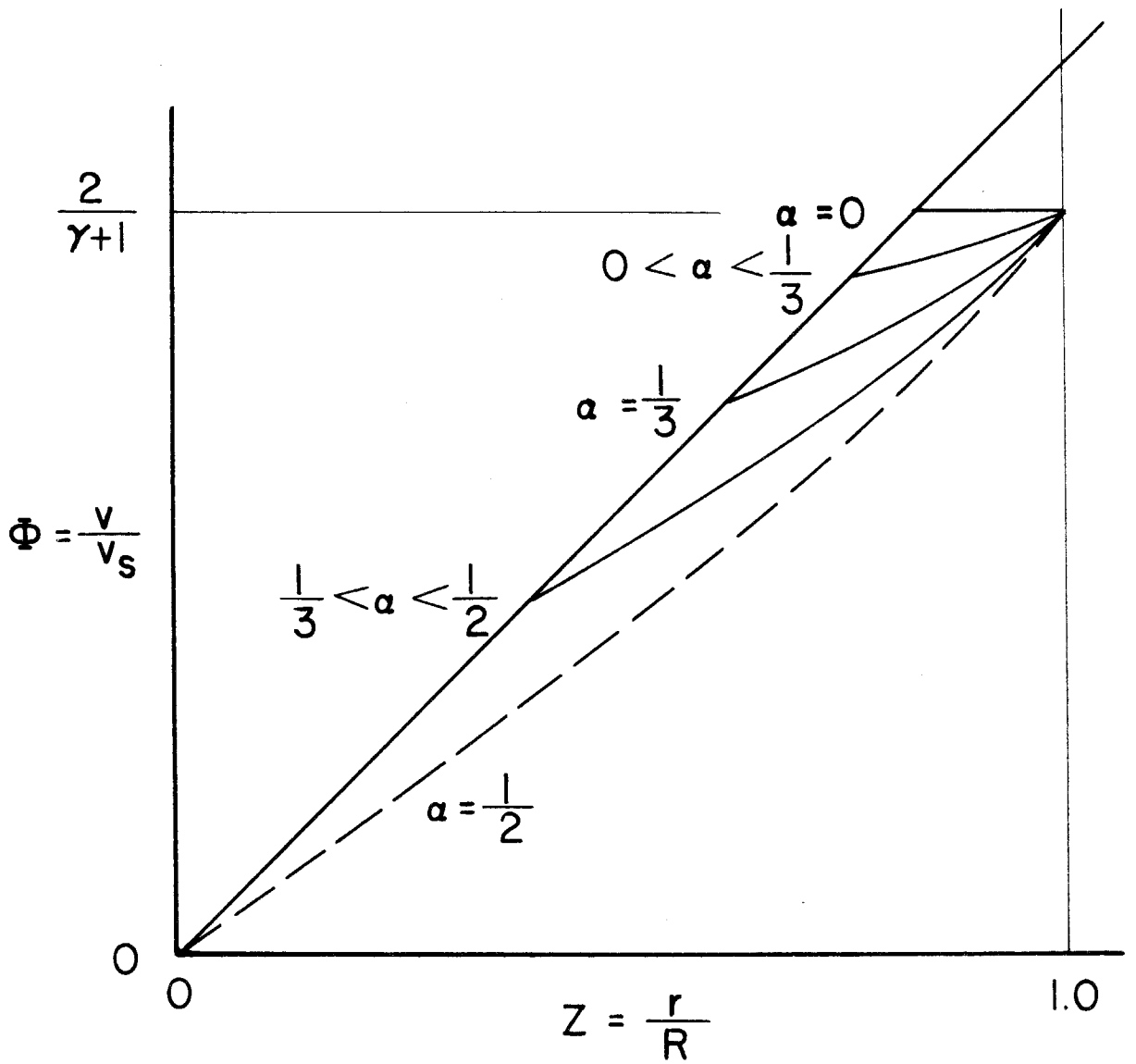


FIG. 8b SOLUTIONS IN THE PHYSICAL PLANE, k=0 (SCHEMATIC)

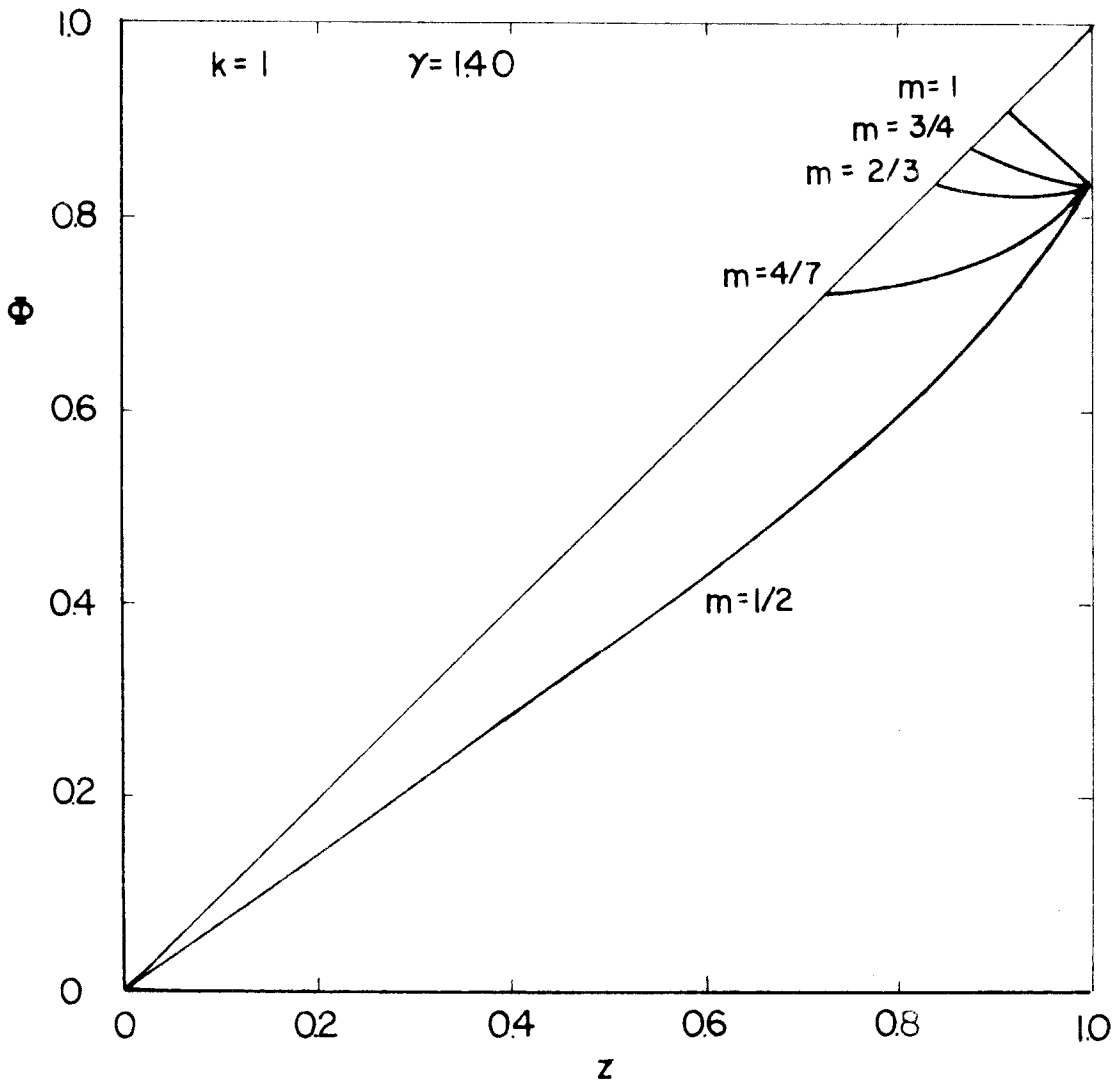


FIG. 9 – VELOCITY FUNCTION

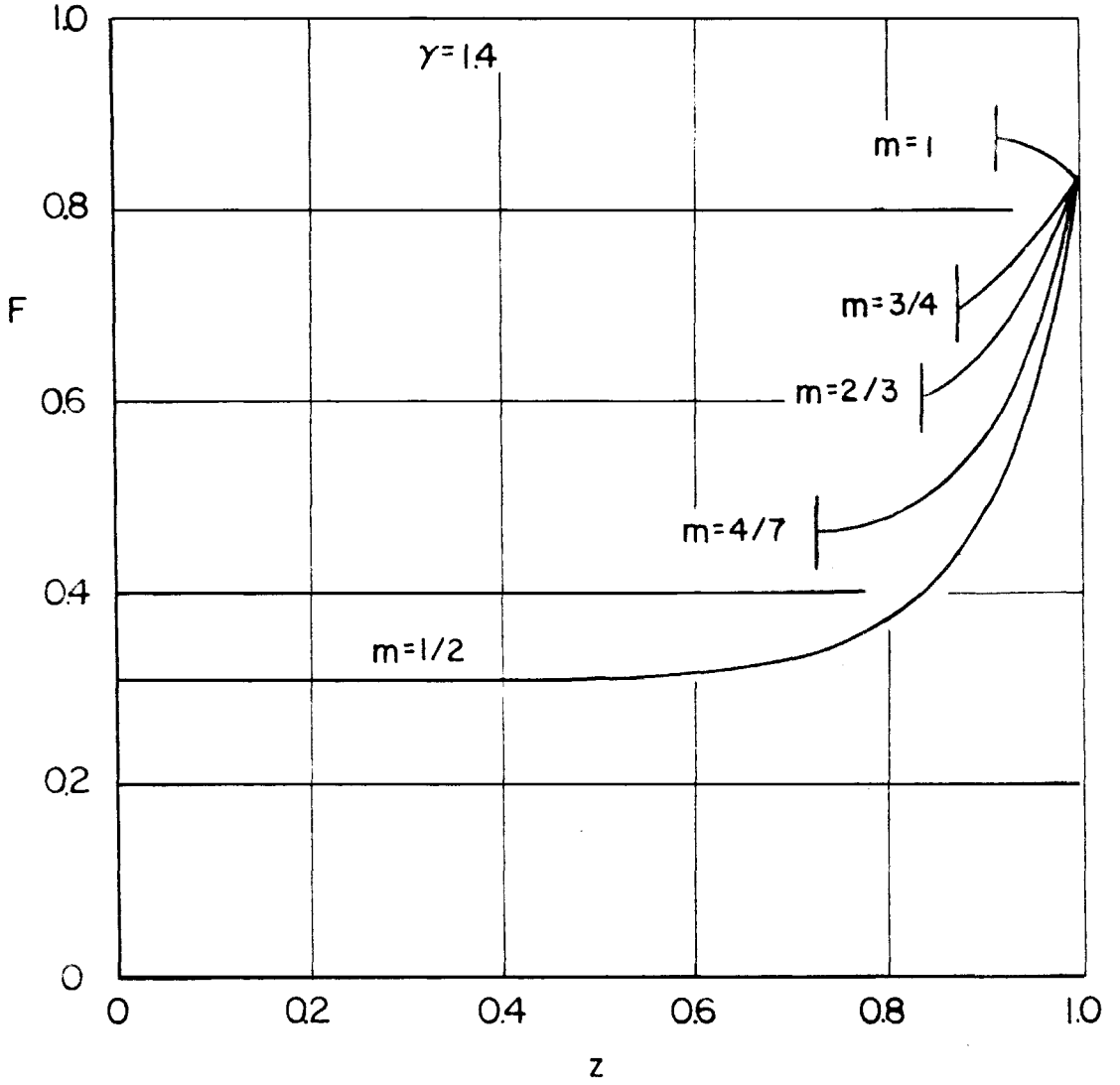


FIG. 10 - PRESSURE FUNCTION

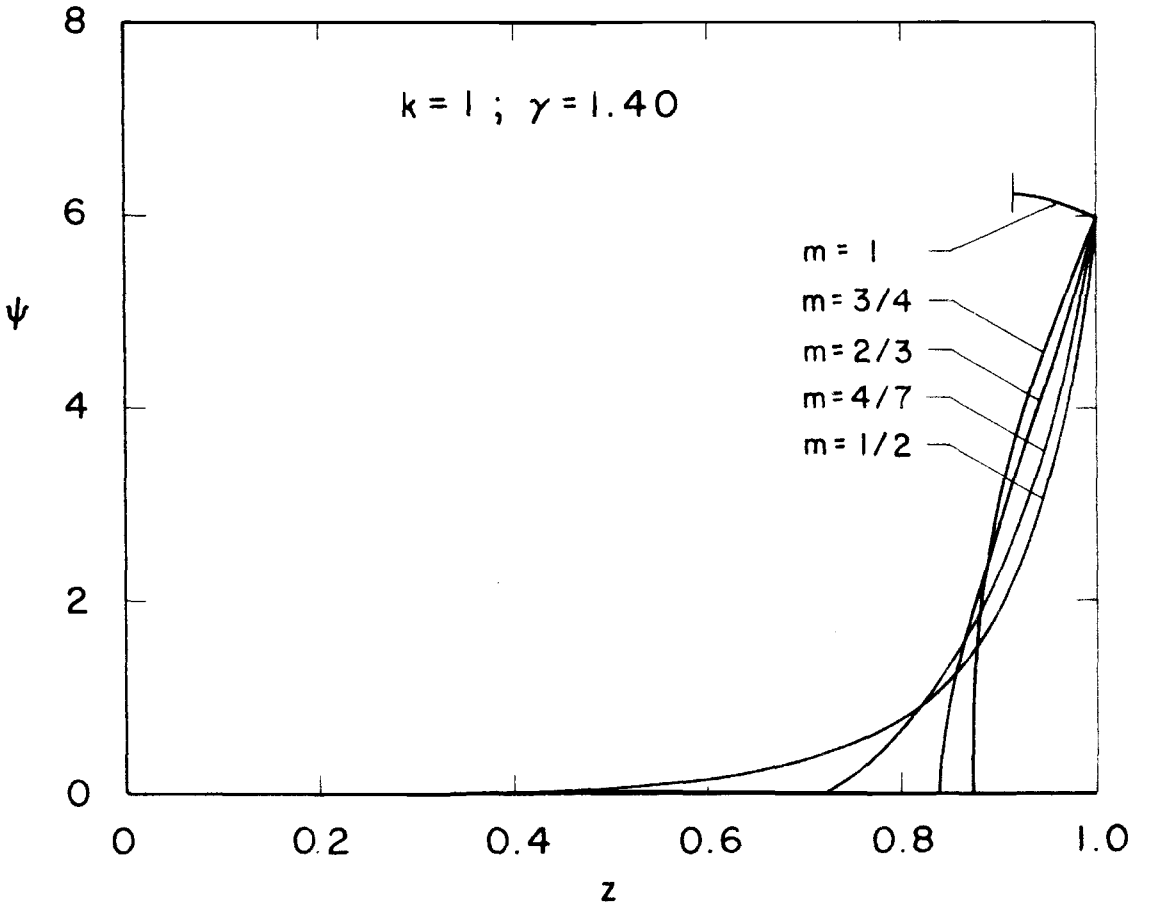


FIG. II - DENSITY FUNCTION

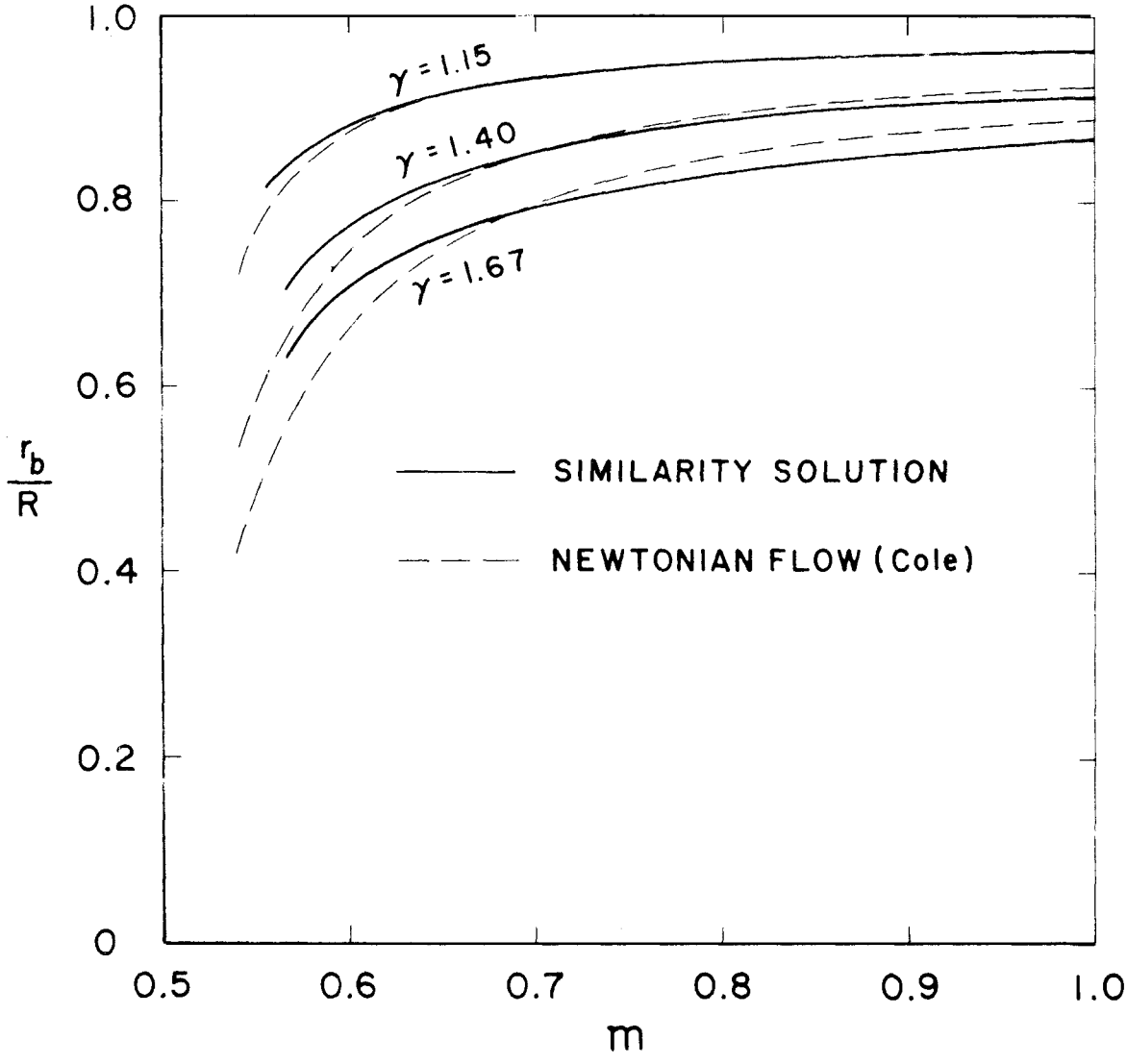


FIG. 12a – SHOCK LOCATION

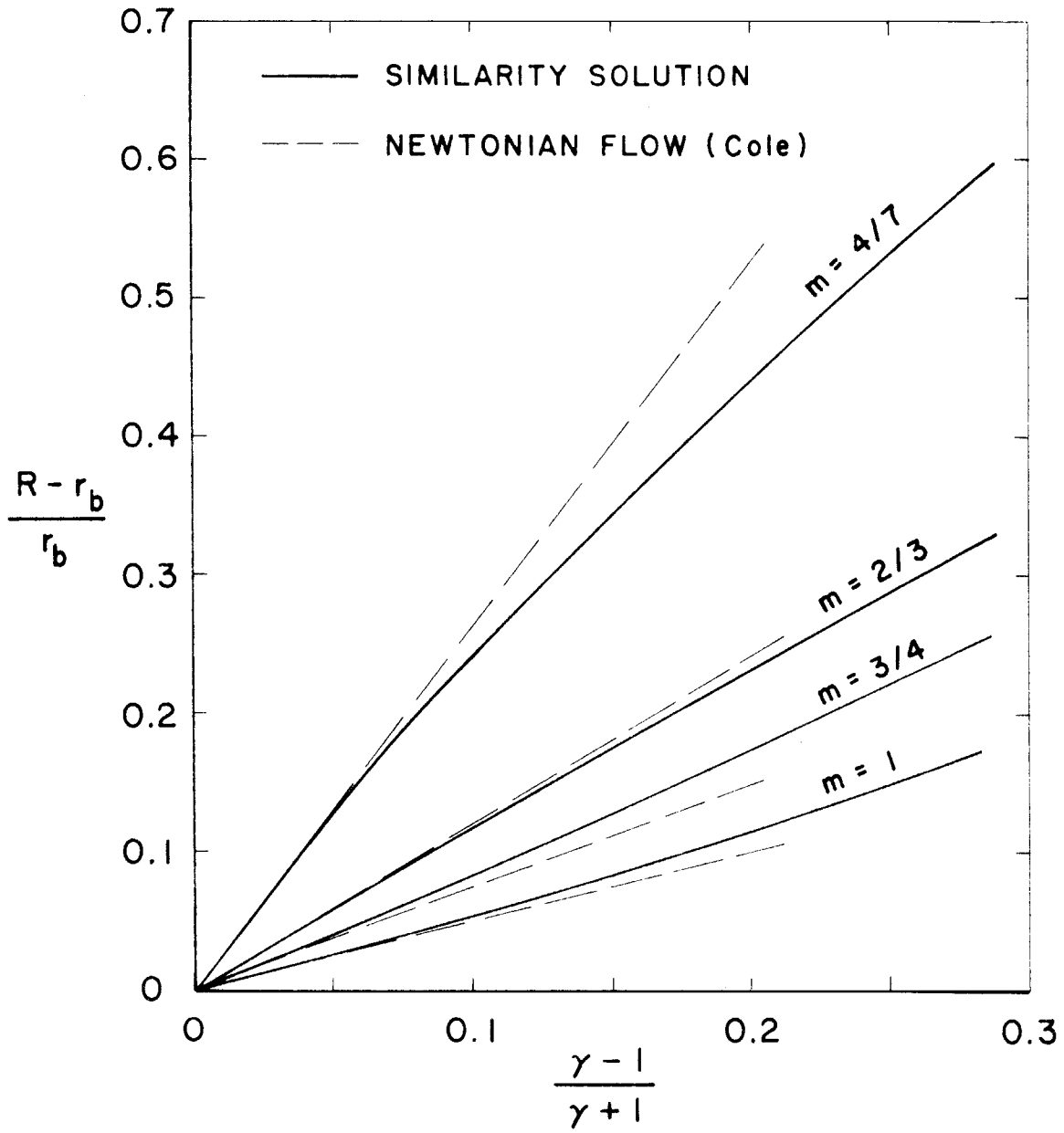


FIG. 12b – SHOCK LOCATION

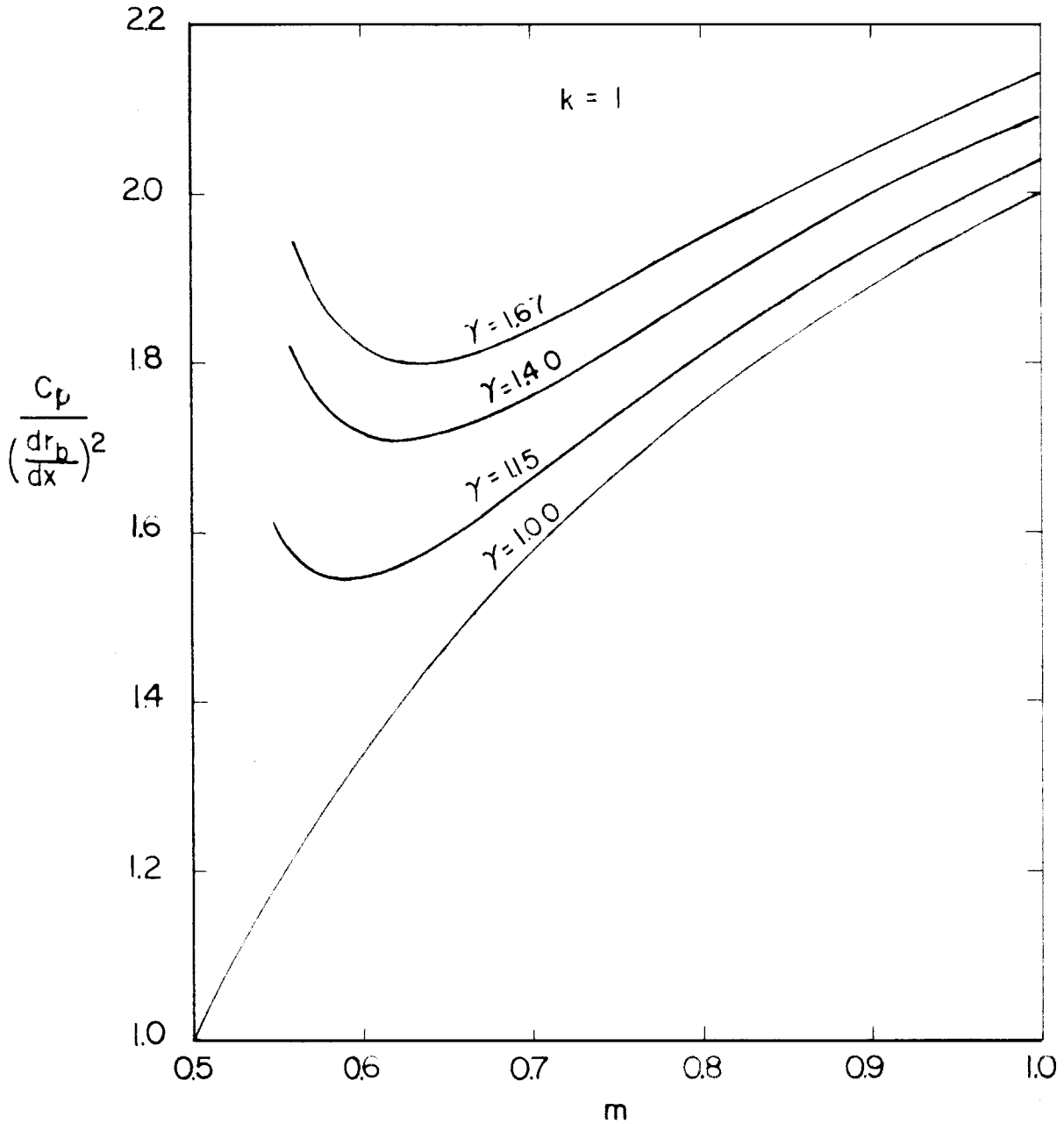


FIG. 13a – PRESSURE COEFFICIENT

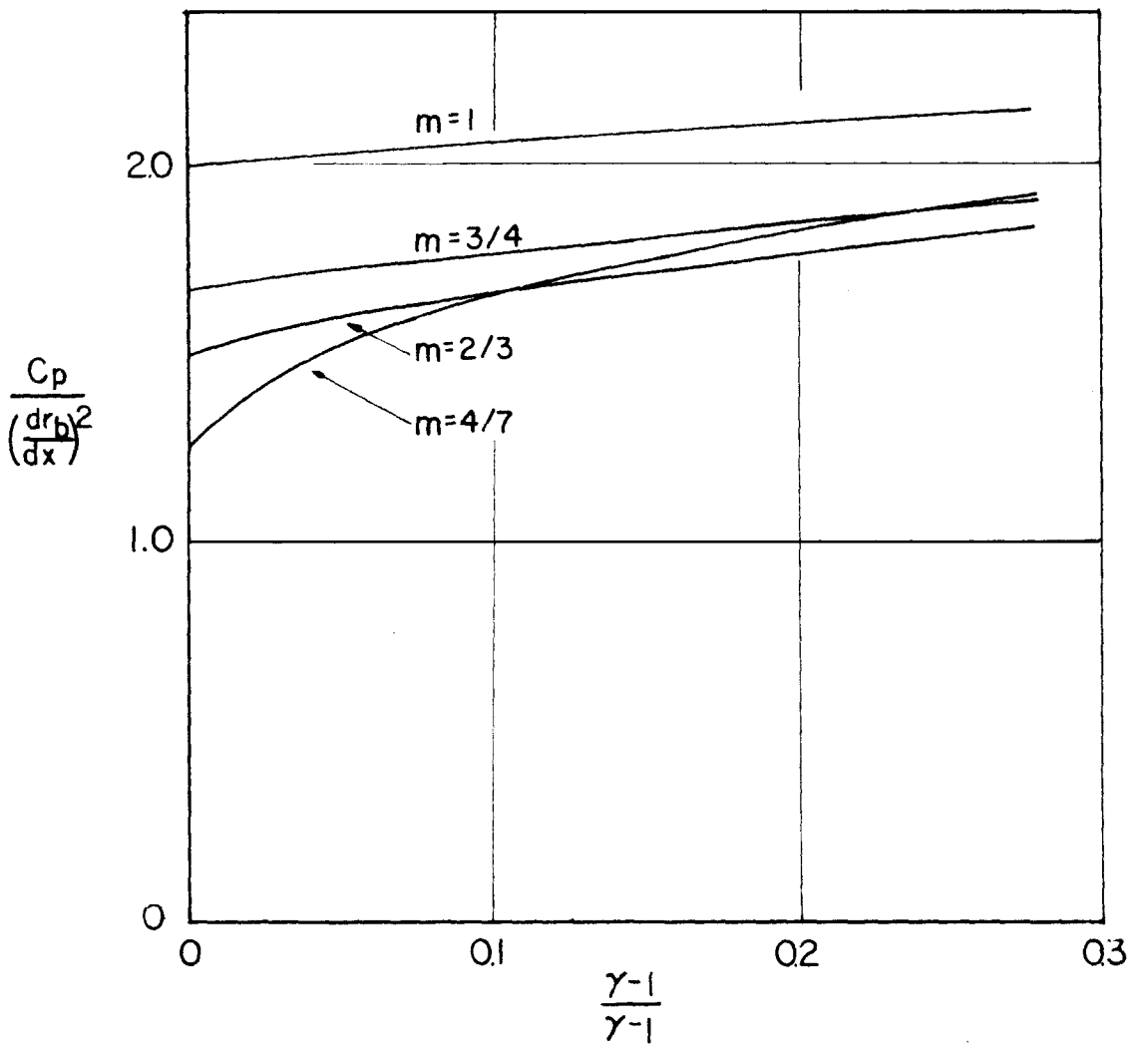


FIG. 13 b – PRESSURE COEFFICIENT

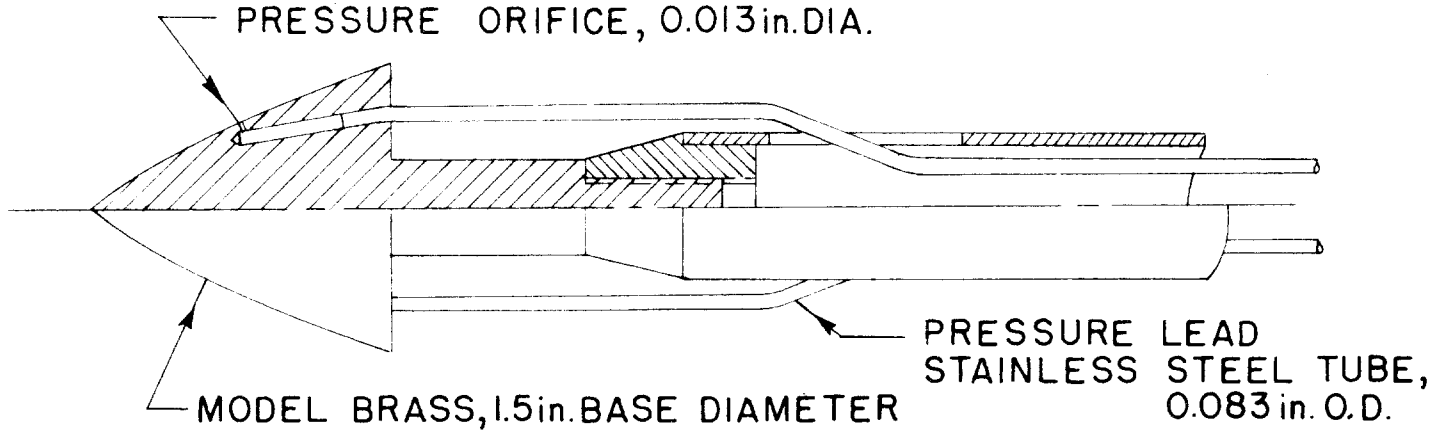


SIDE VIEW

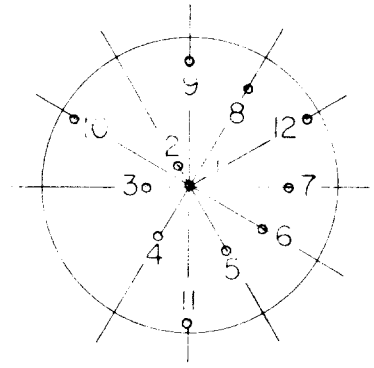


FRONT VIEW

FIG. 14 – DETAILS OF TYPICAL MODEL CONSTRUCTION

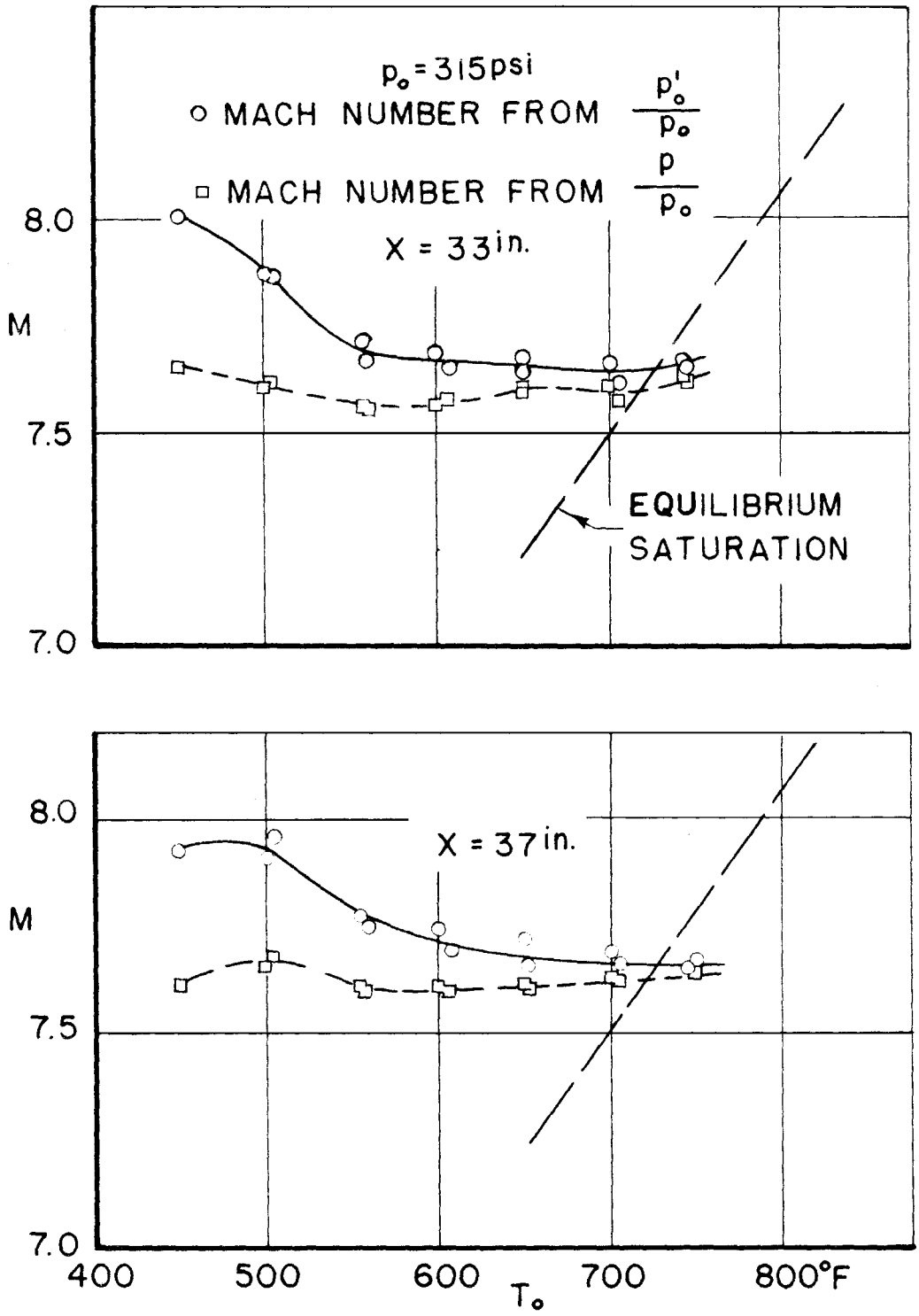


FIG. 15 — TEST SECTION MACH NUMBER AS FUNCTION OF SUPPLY TEMPERATURE

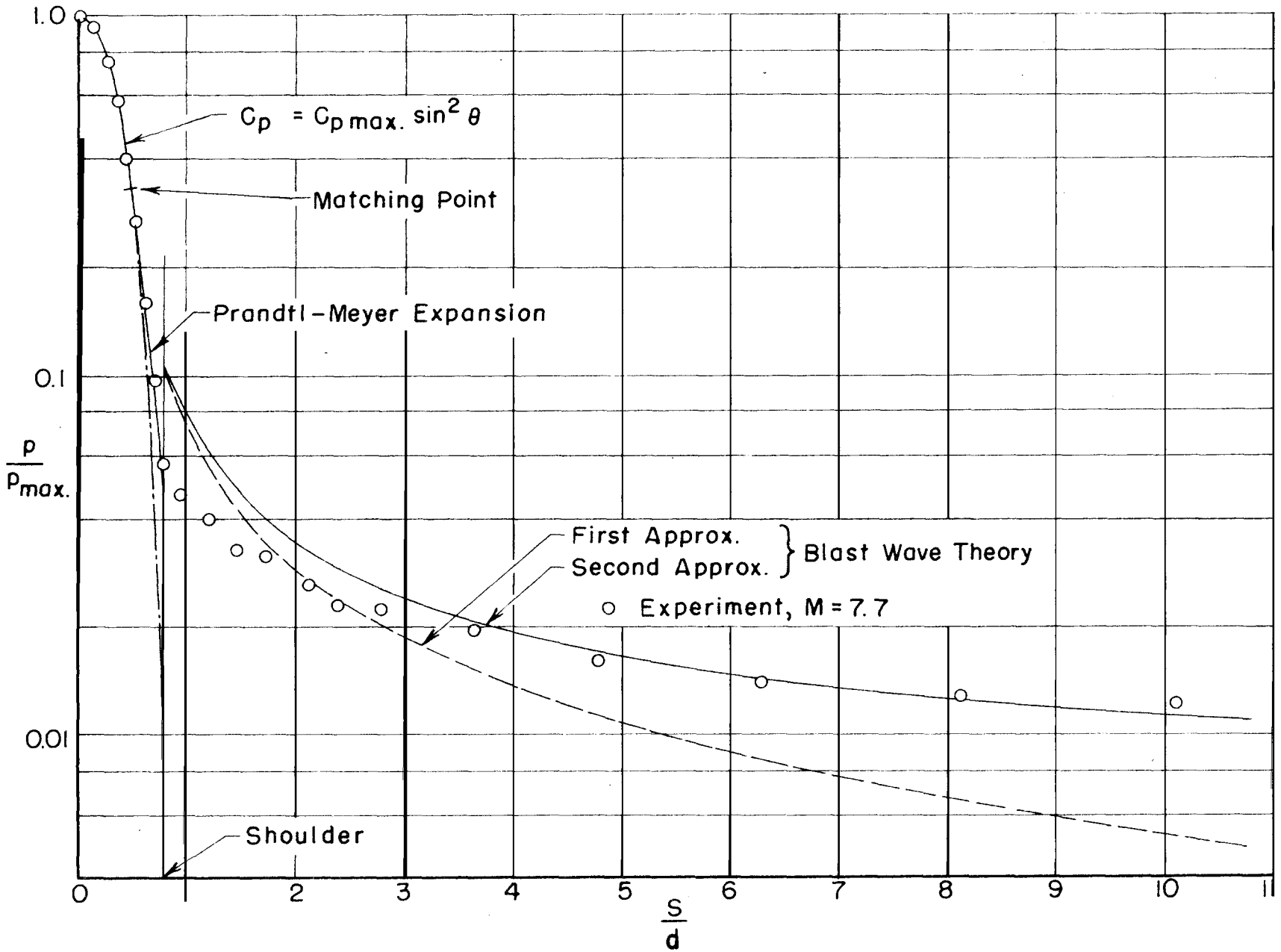


FIG. 16 - PRESSURE ON HEMISPHERE-CYLINDER

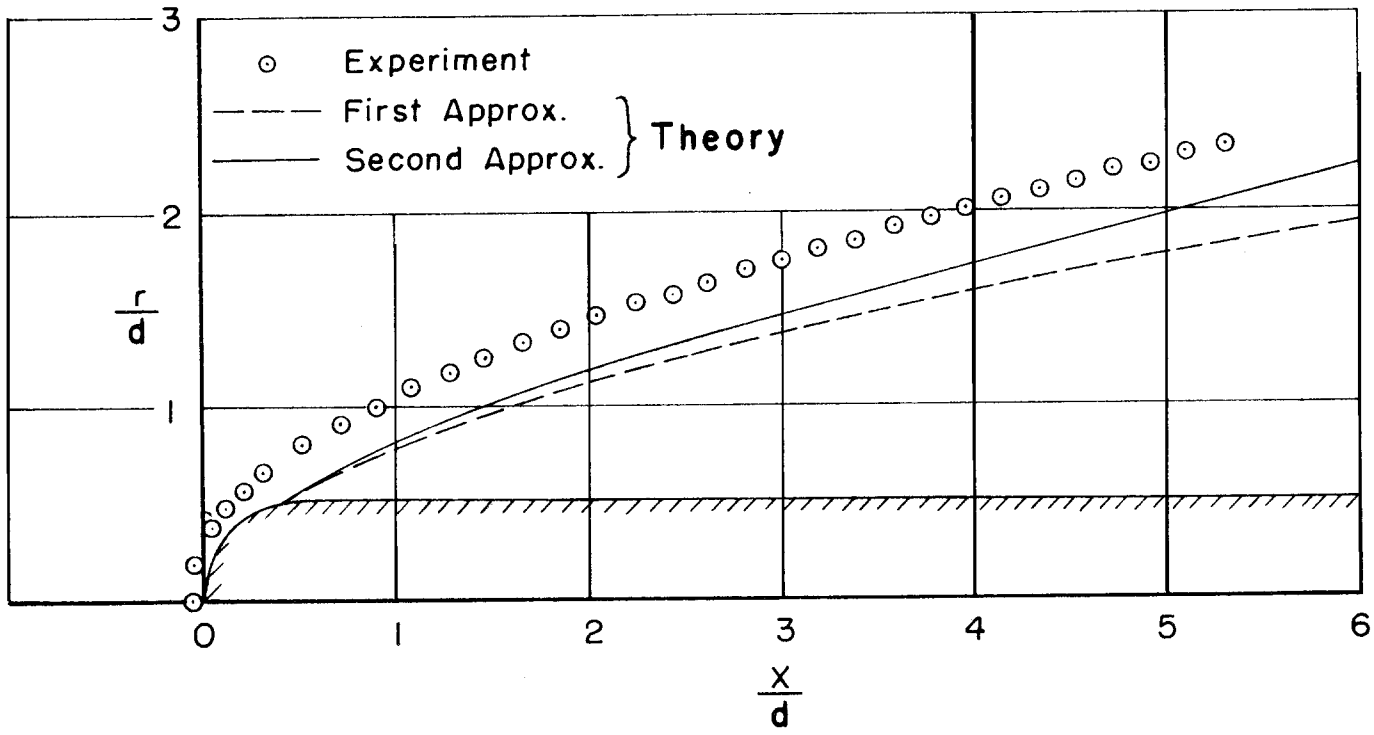


FIG. 17 – SHOCK SHAPE FOR HEMISPHERE-CYLINDER AT MACH NO. 7.7

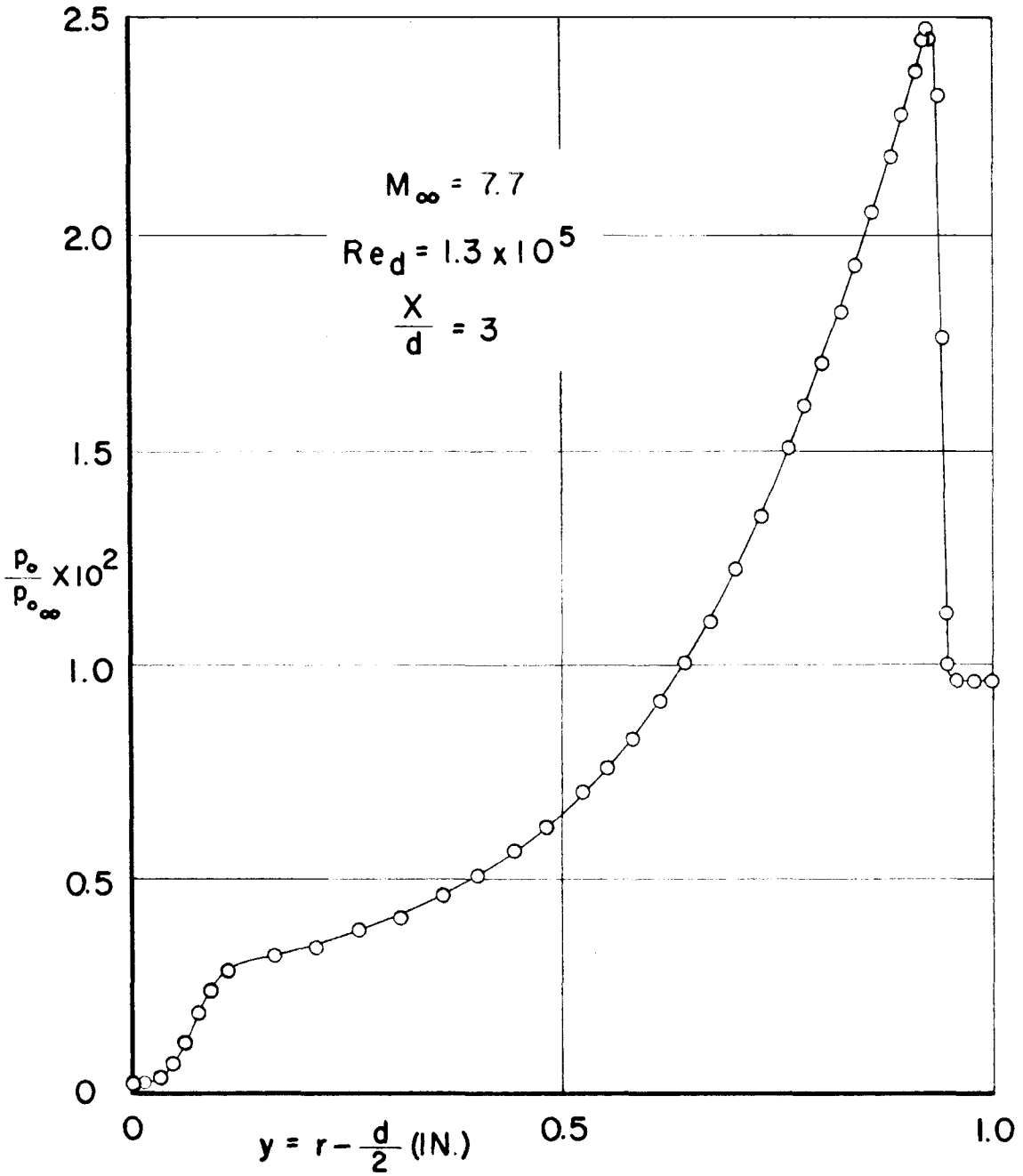


FIG. 18 — IMPACT PRESSURE PROFILE FOR HEMISPHERE – CYLINDER

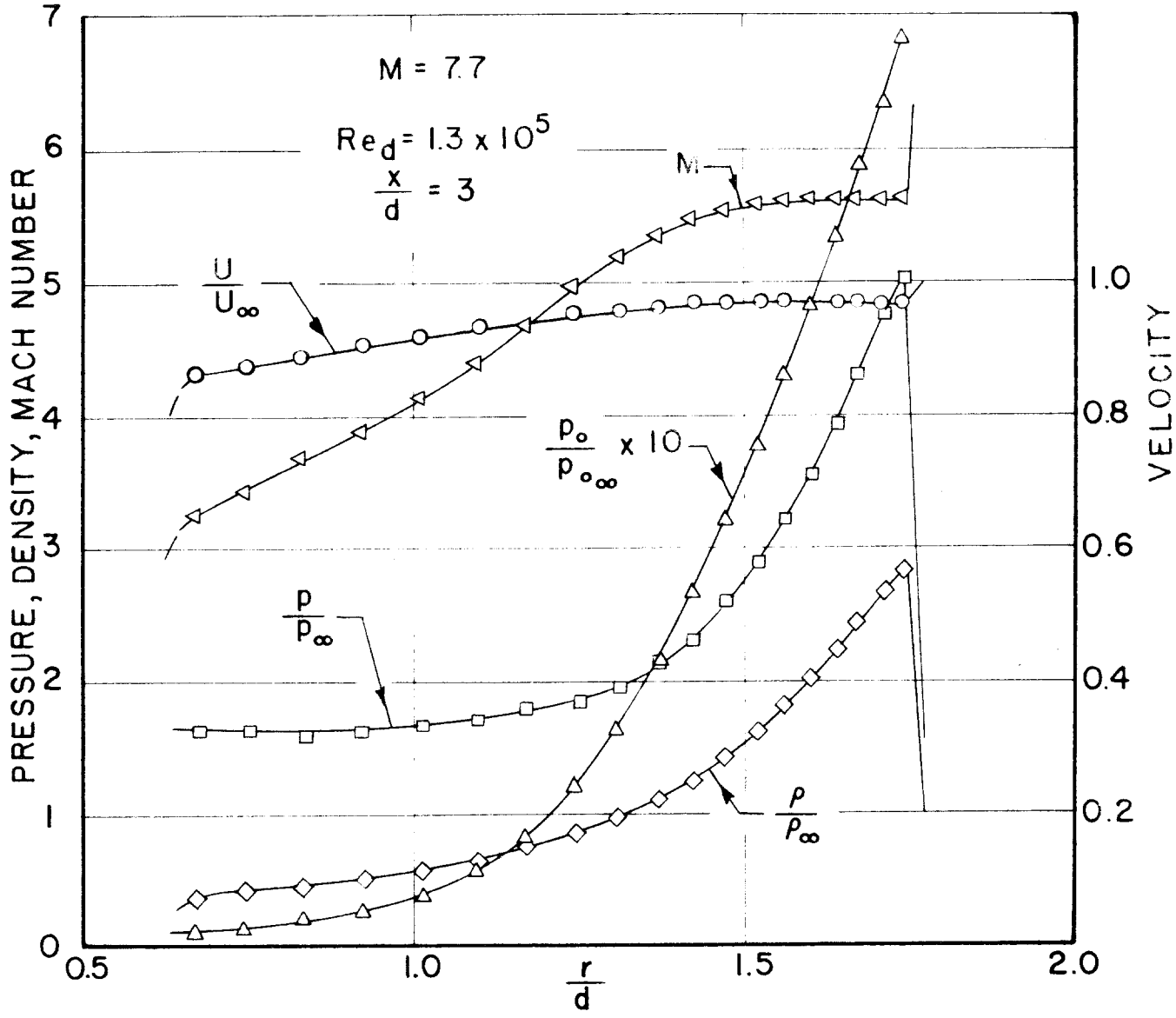


FIG. 19 — FLOW QUANTITY PROFILES FOR HEMISPHERE – CYLINDER

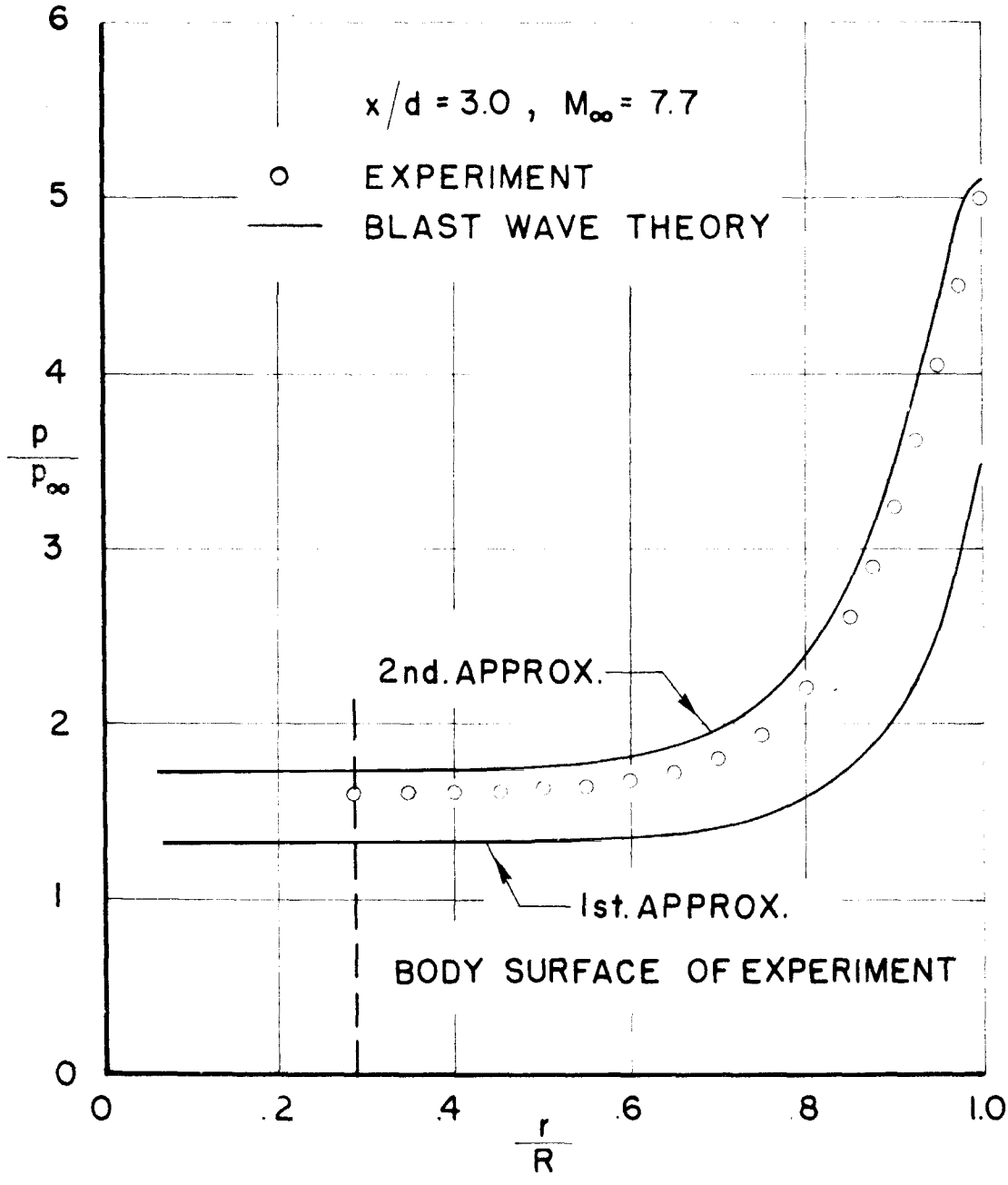


FIG.20 - STATIC PRESSURE DISTRIBUTION FOR HEMISPHERE - CYLINDER

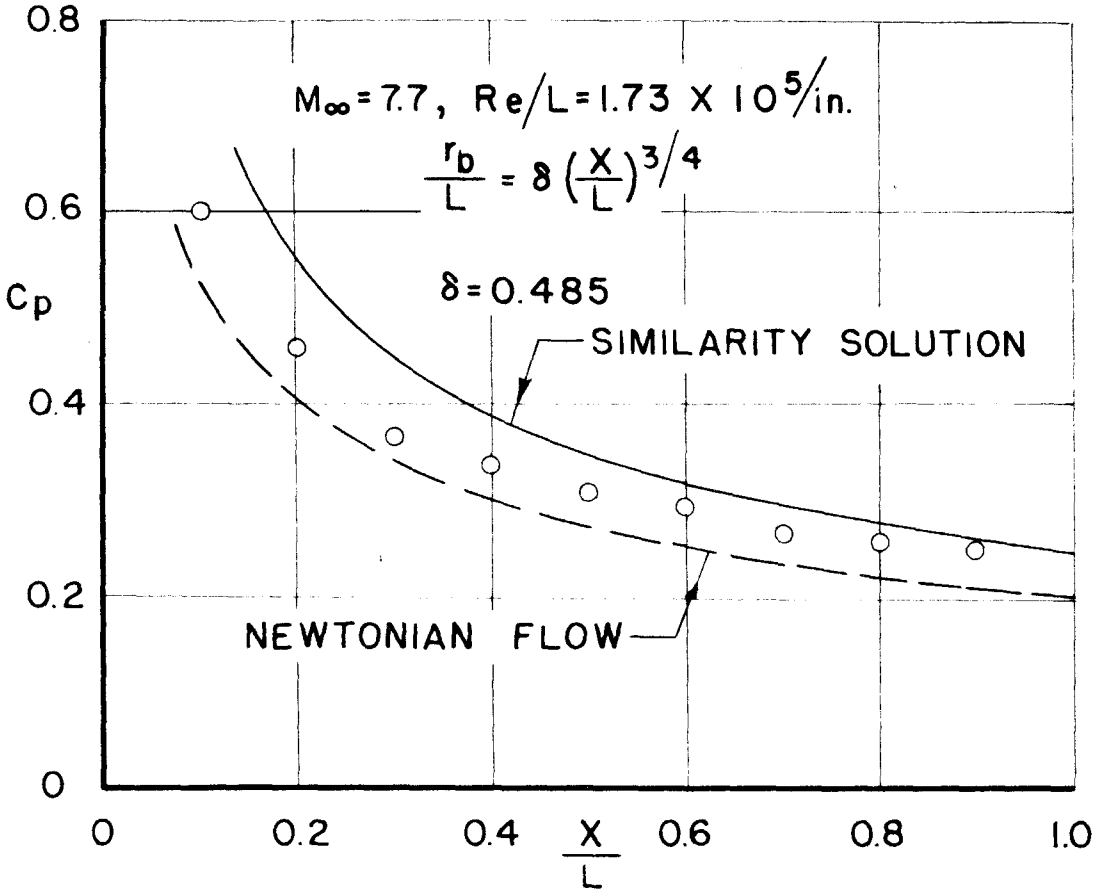


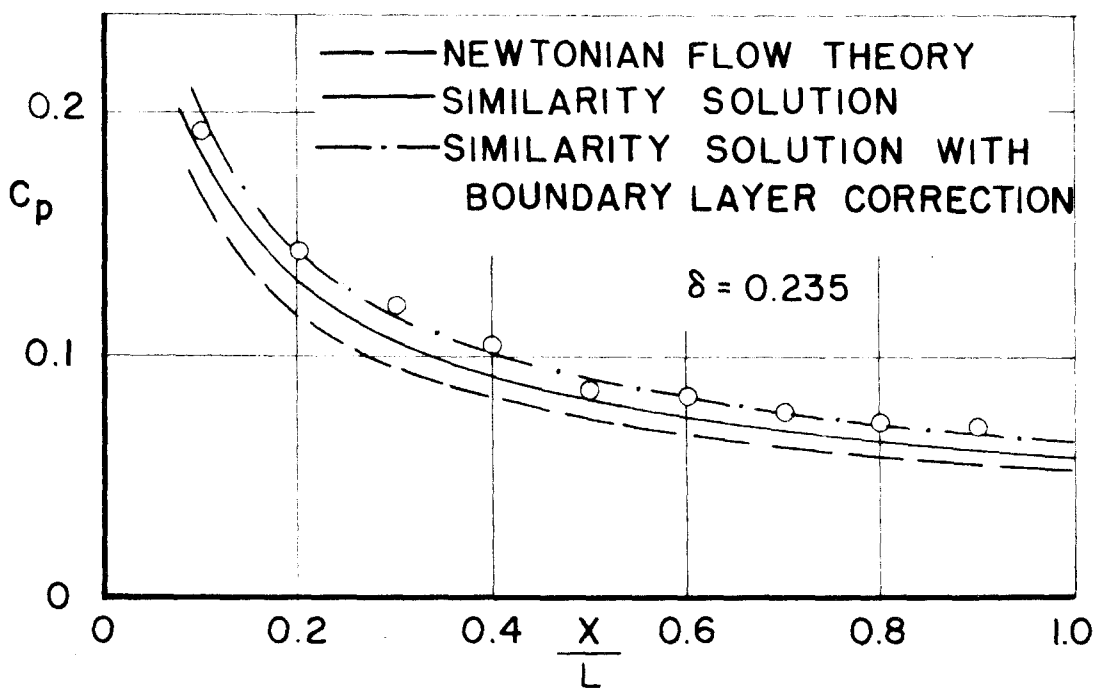


FIG. 21a — SURFACE PRESSURE DISTRIBUTION

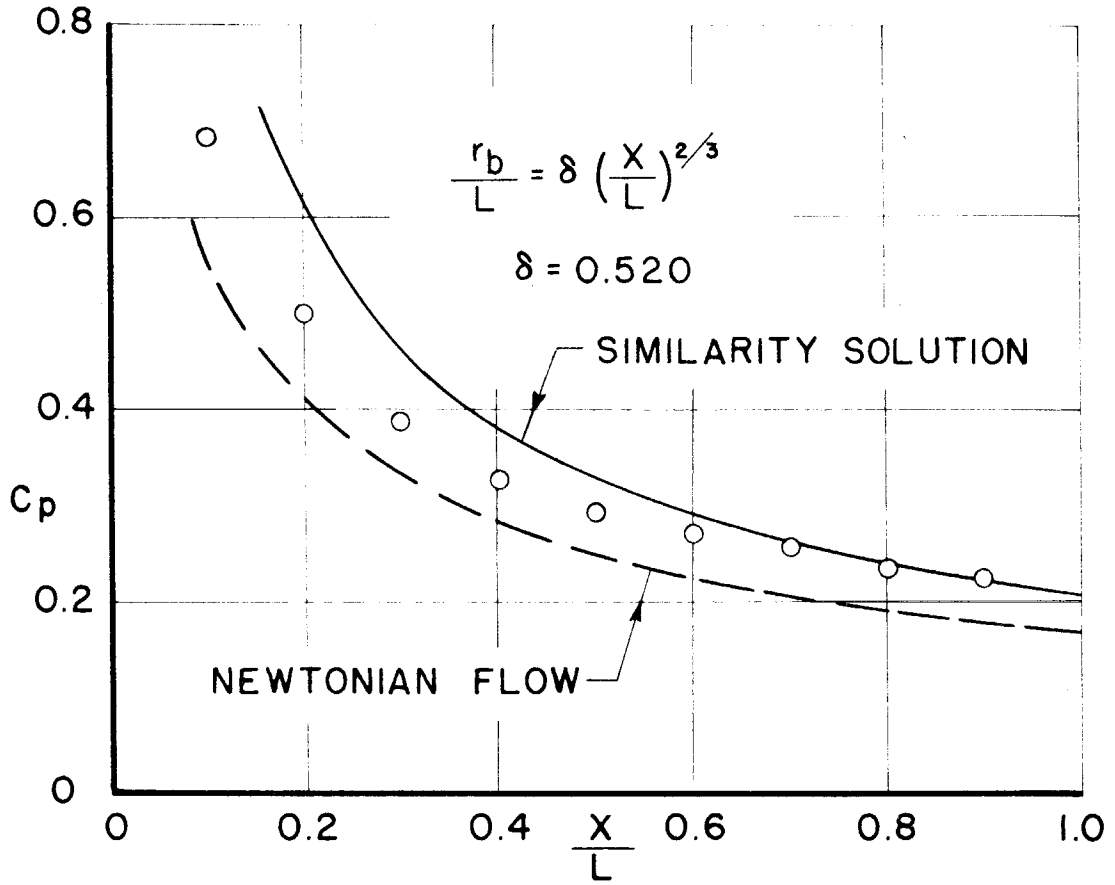


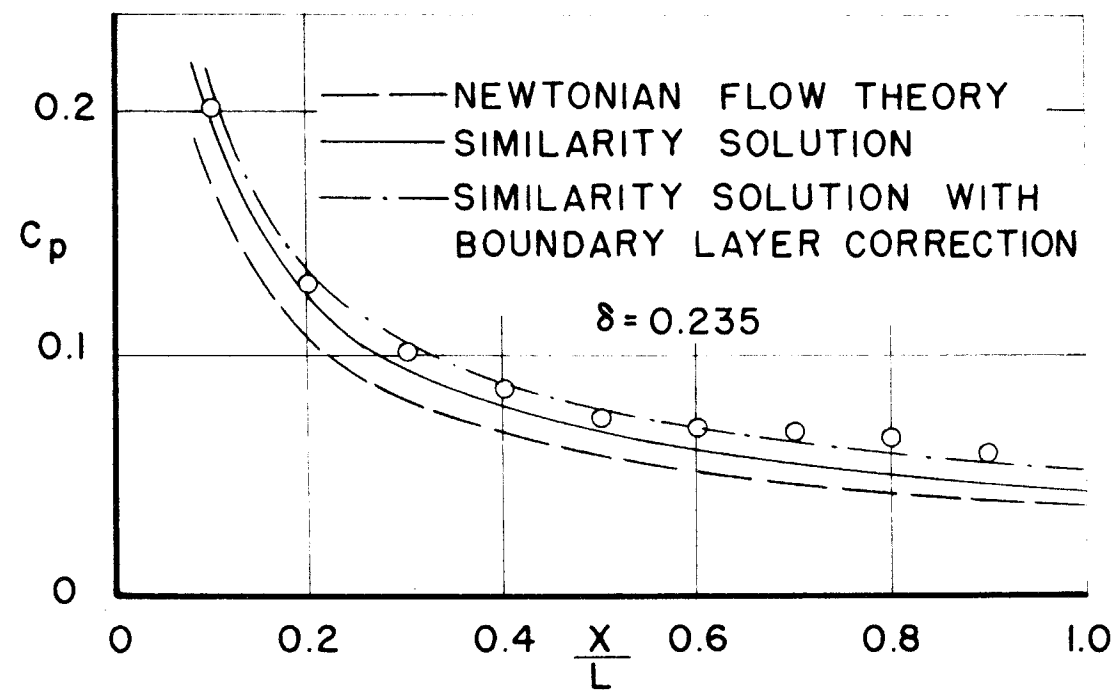


FIG. 21b — SURFACE PRESSURE DISTRIBUTION

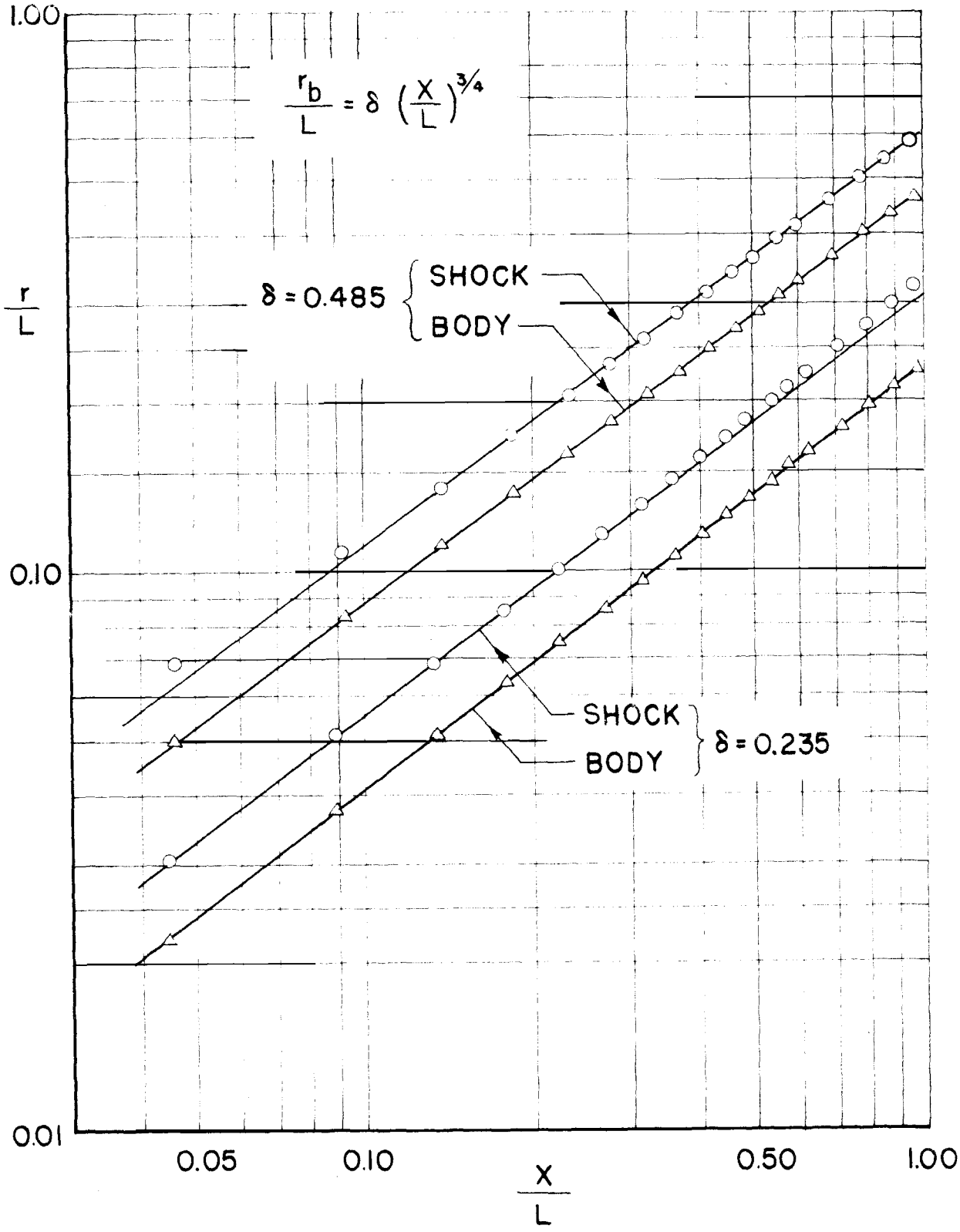


FIG. 22a - SHOCK WAVE LOCATION

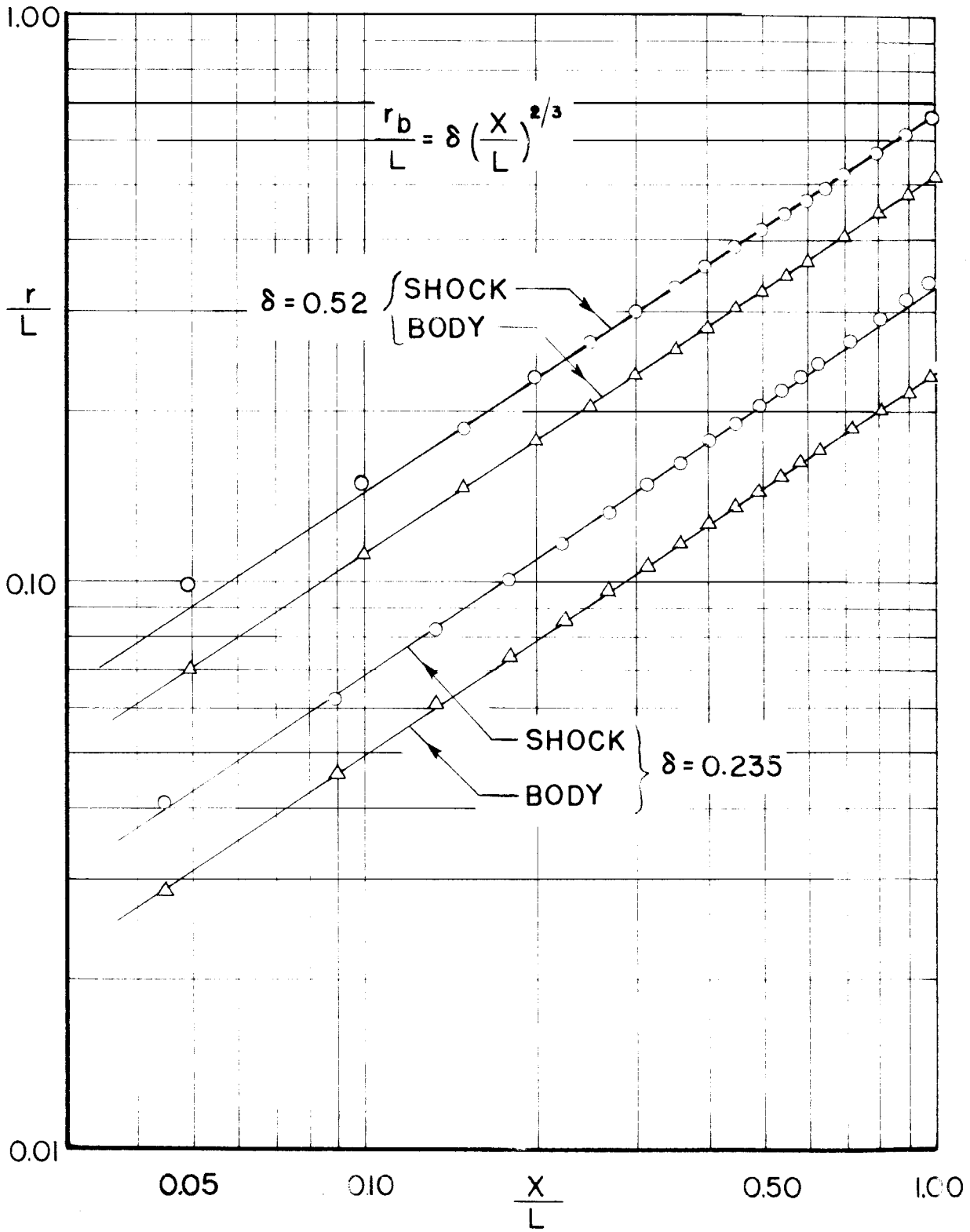


FIG. 22 b — SHOCK WAVE LOCATION

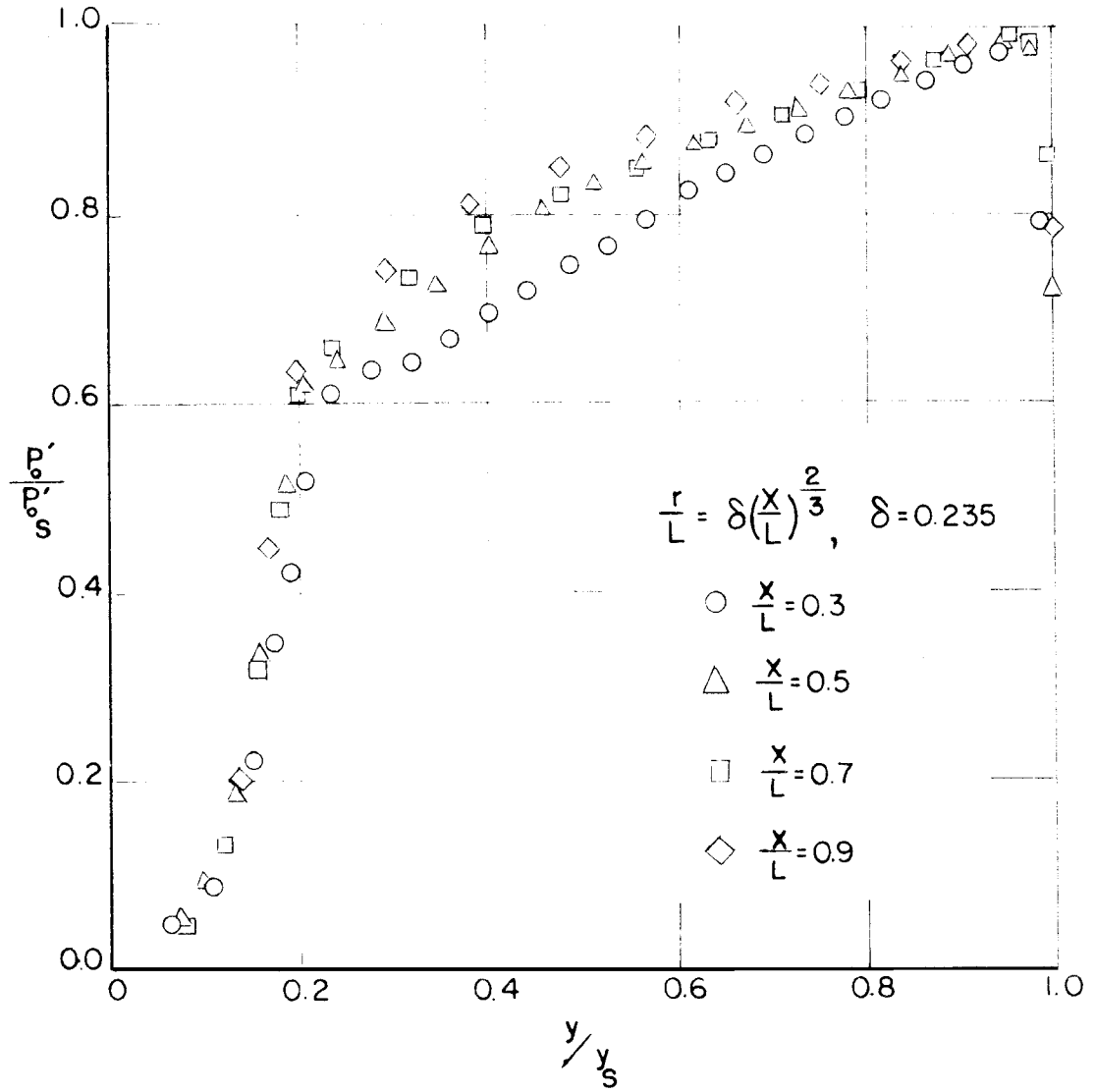


FIG. 23 — IMPACT PRESSURE PROFILES

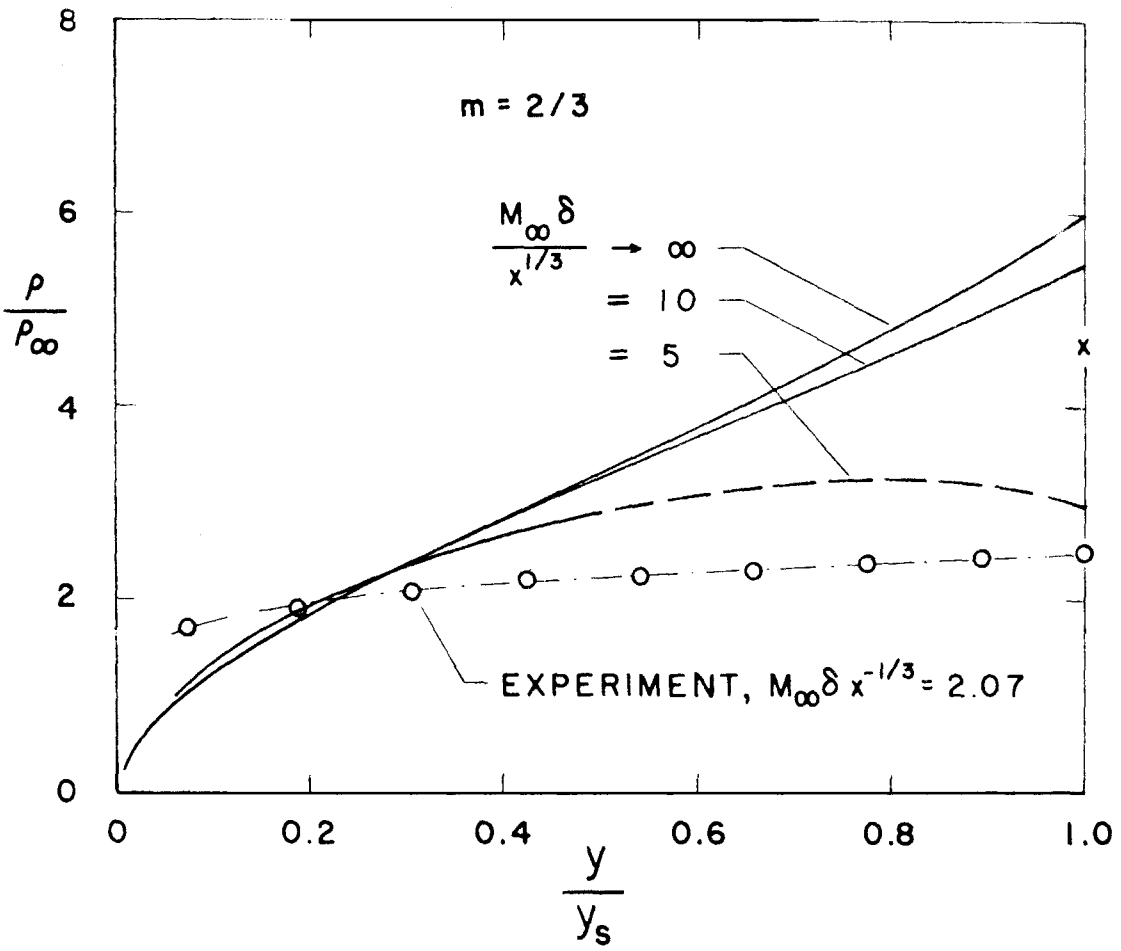


FIG. 24 - DENSITY PROFILE FROM SIMILARITY THEORY

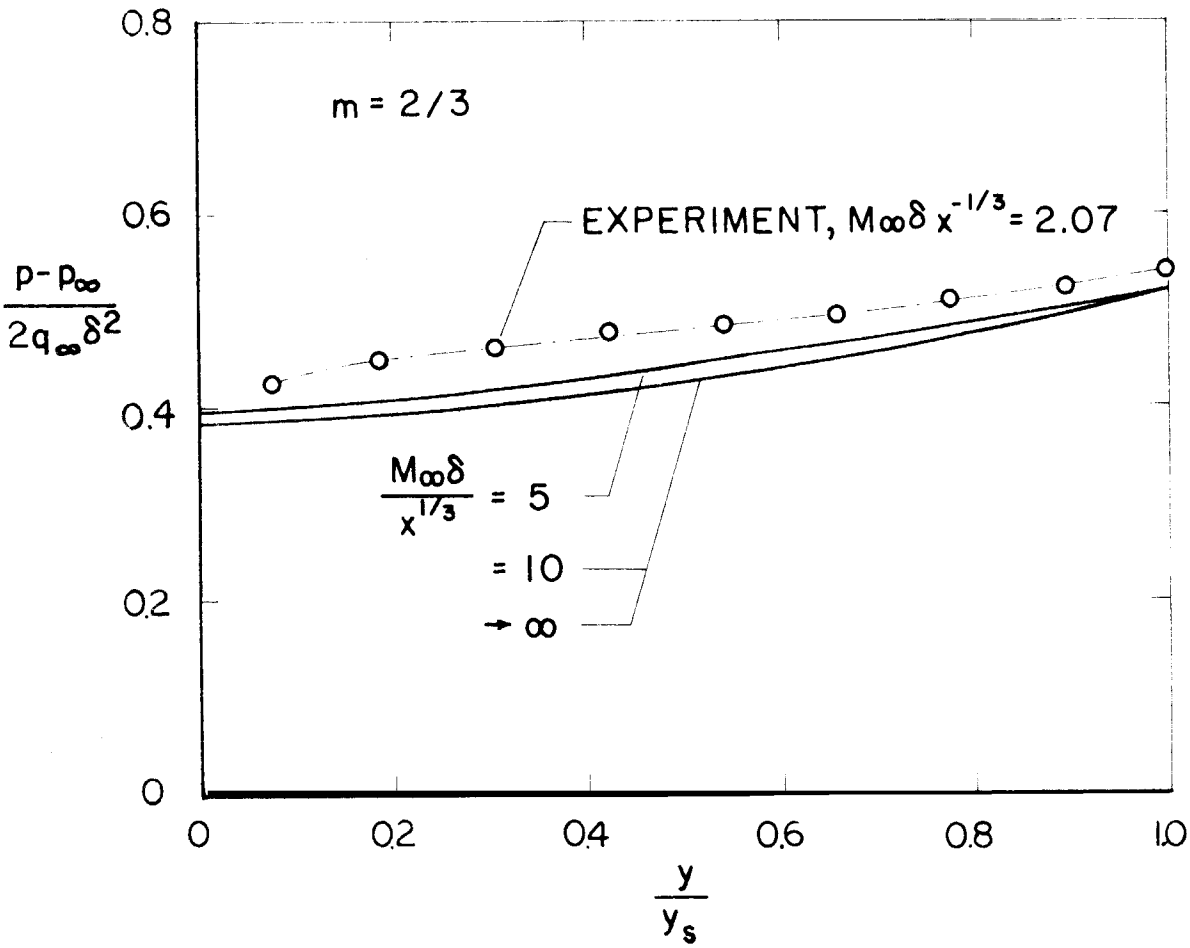


FIG. 25 - STATIC PRESSURE PROFILE FROM SIMILARITY THEORY

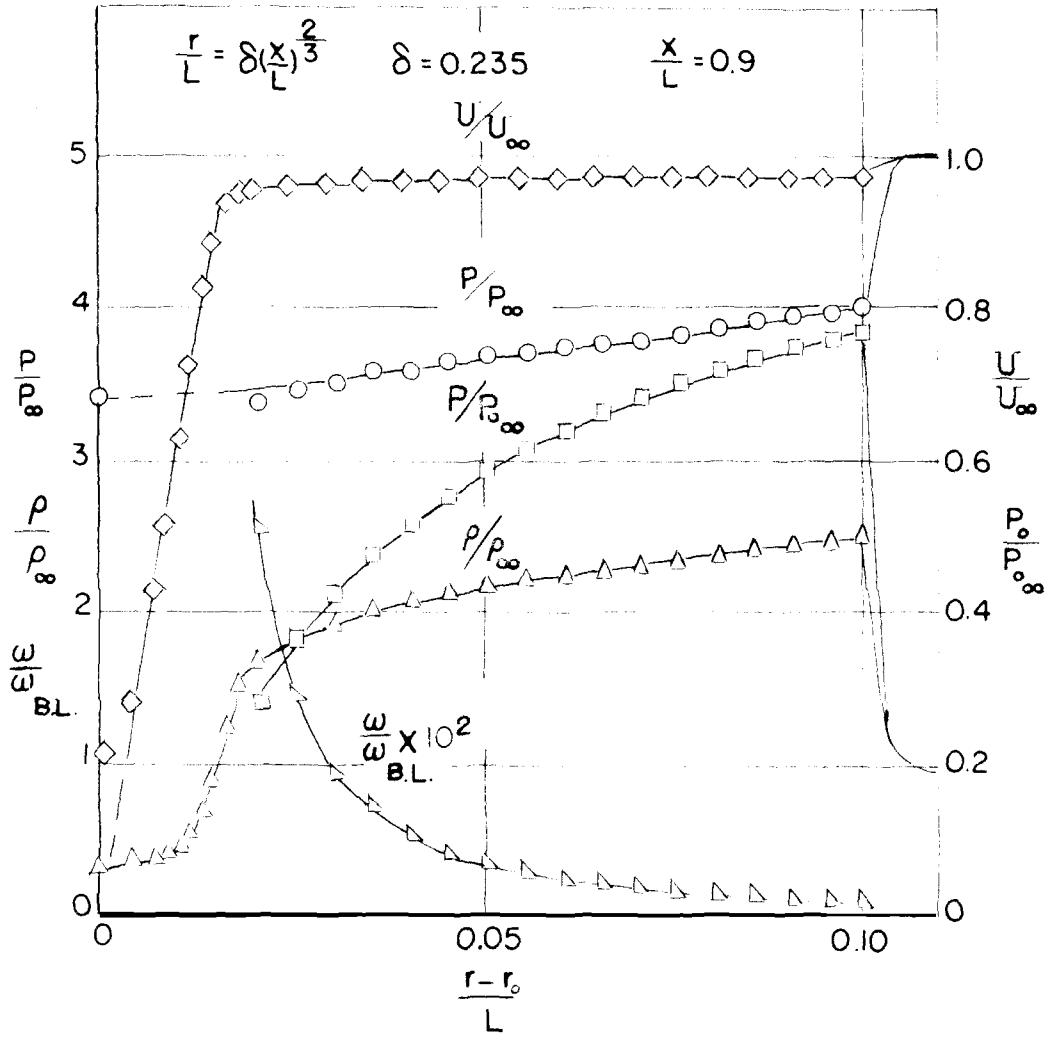


FIG. 26 — FLOW QUANTITY PROFILES

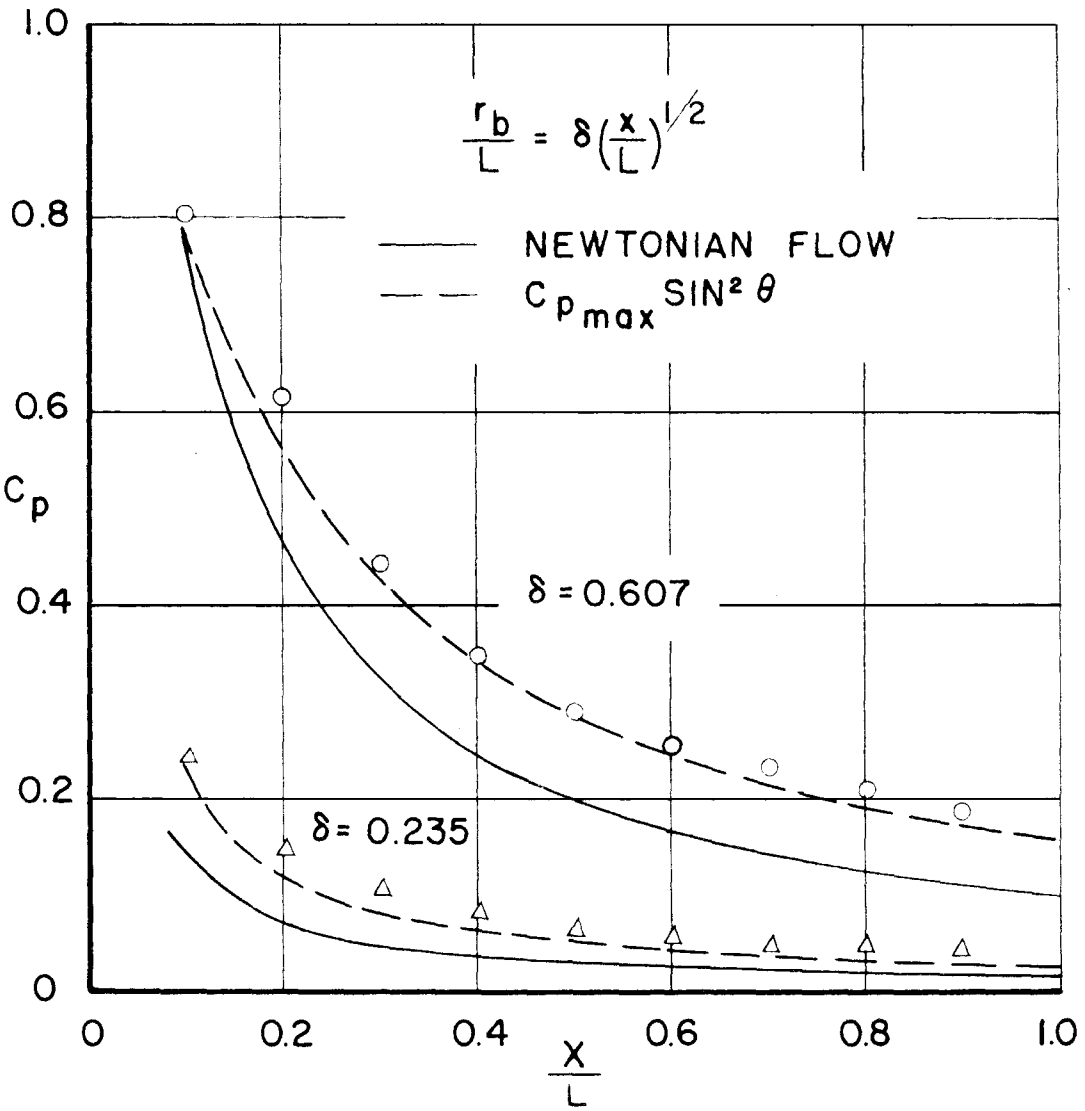


FIG. 27 — SURFACE PRESSURE DISTRIBUTION

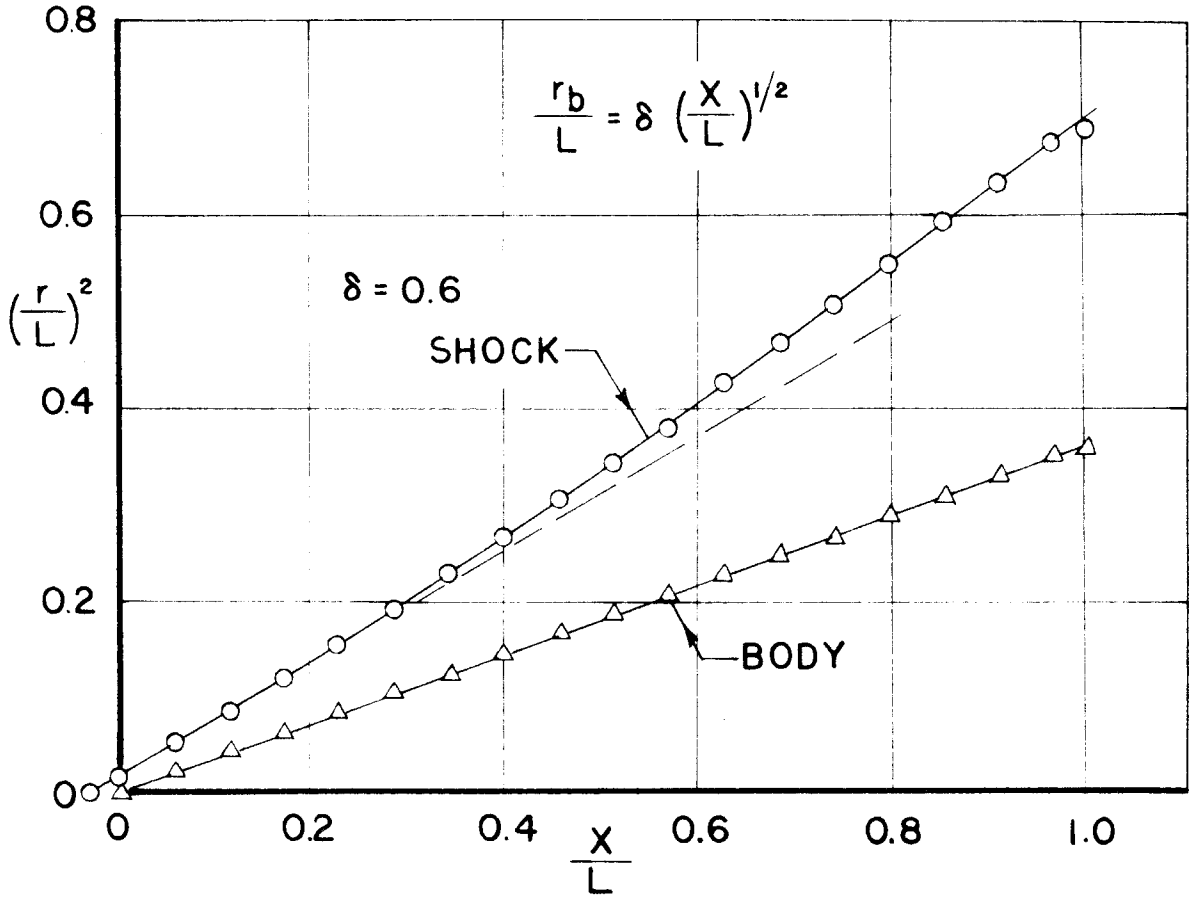


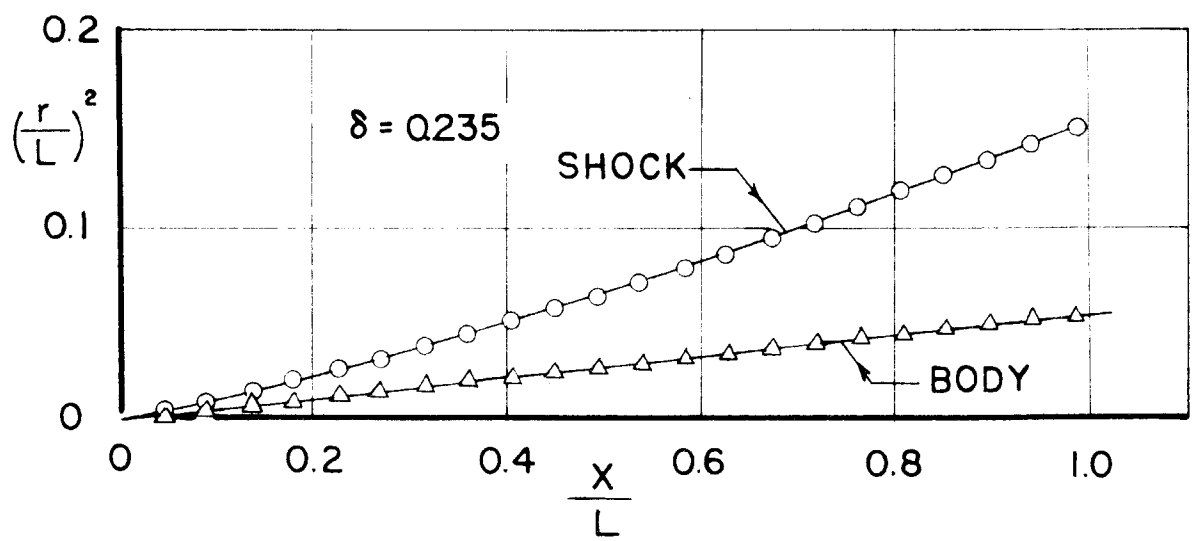


FIG. 28 — SHOCK WAVE LOCATION

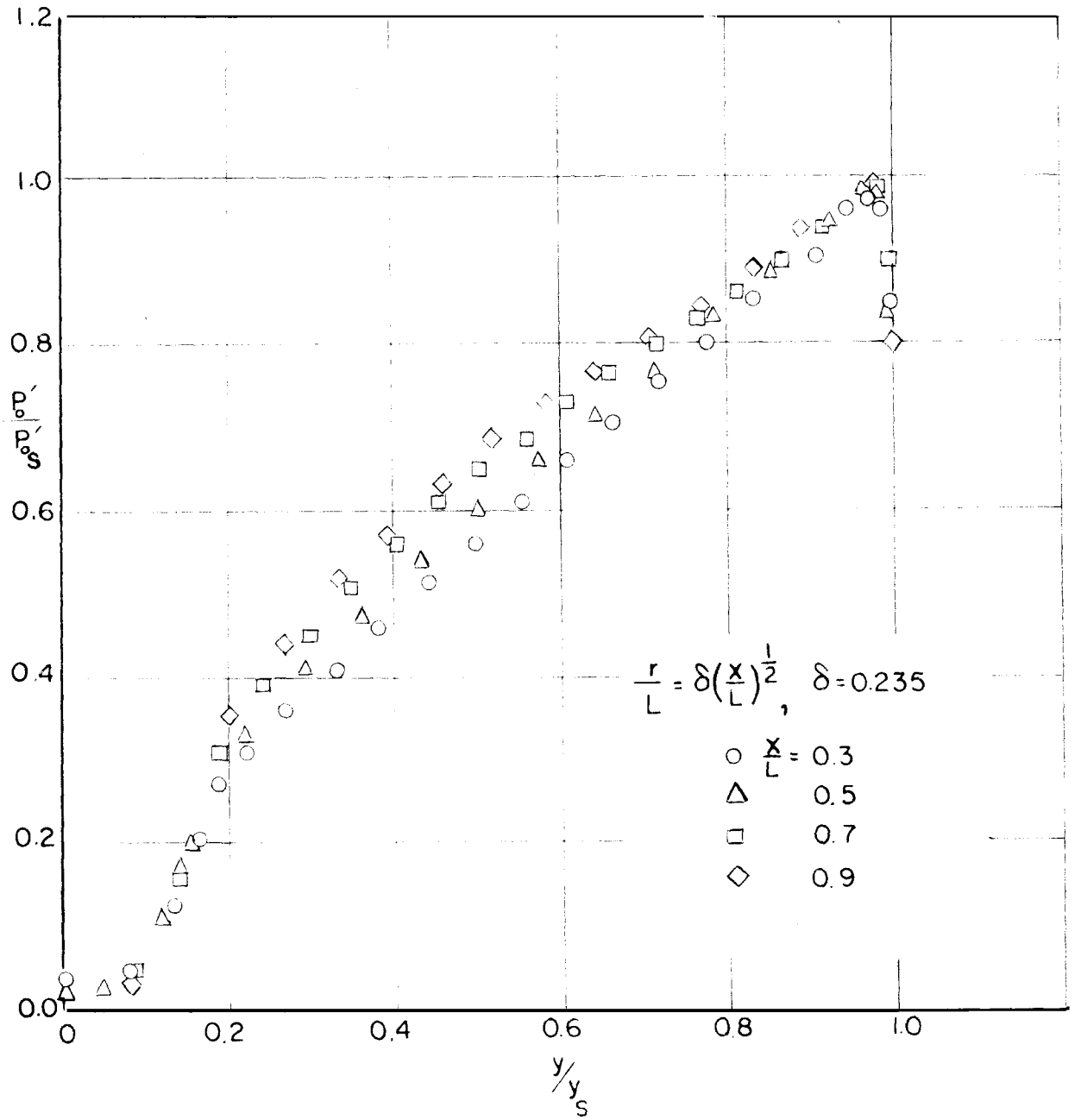


FIG. 29 — IMPACT PRESSURE PROFILES

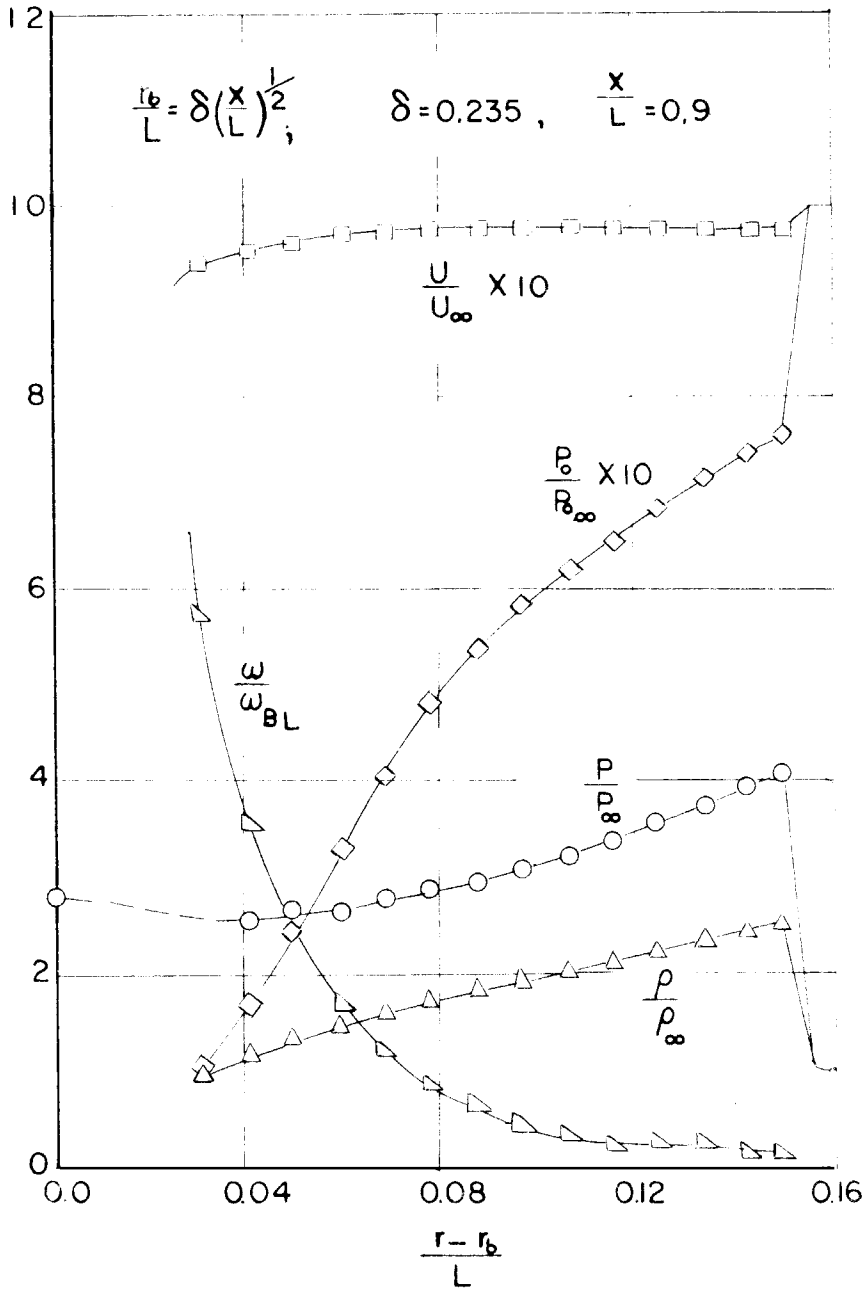


FIG. 30 — FLOW QUANTITY PROFILES

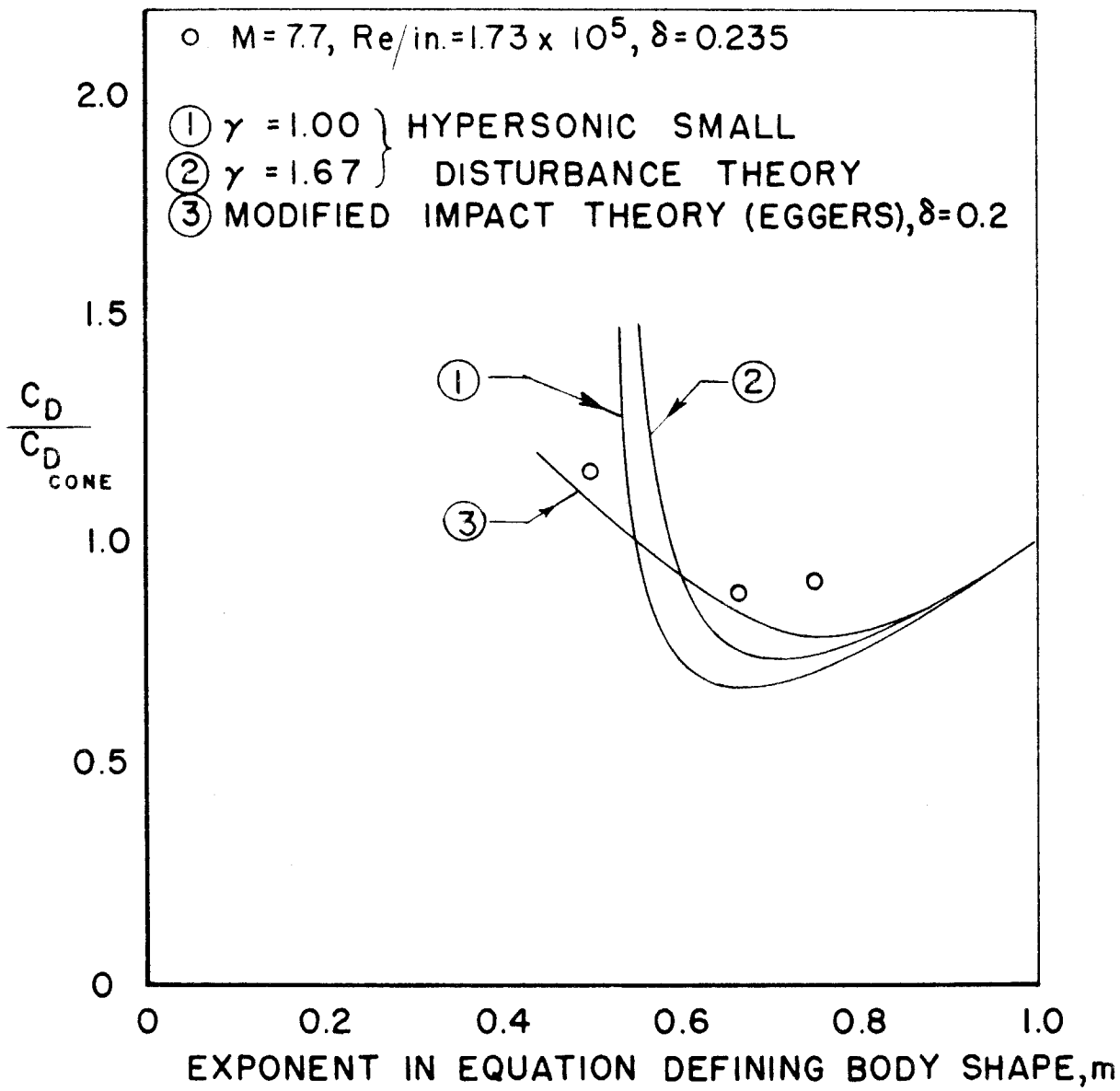


FIG. 31 — FOREDRAG COEFFICIENTS OF TEST BODIES